Stanford Geothermal Program
Interdisciplinary Research
in Engineering and Earth Sciences
Stanford University
Stanford, California

MATHEMATICAL MODELLING OF SINGLE-PHASE NONISOTHERMAL FLUID FLOW THROUGH POROUS MEDIA

by
Paul Gardiner Atkinson

May 1976

This research was carried out
under Research Grant GI-34925
by the National Science Foundation

This report was prepared originally as a dissertation submitted to the Department of Petroleum Engineering and the Committee on the Graduate Division of Stanford University in partial fulfillment of the requirements for the degree of Doctor of Philosophy.

ACKNOWLEDGEMENTS

The author would like to express sincere thanks to Dr. H. J. Ramey, Jr., Department of Petroleum Engineering, for his guidance and counsel as research advisor during this study. Dr. Ramey has given the author valuable insights into the reservoir engineering discipline, and an historical perspective of this field.

For his well-directed comments during the early stages of this work, the author is grateful to Dr. W. E. Brigham, Department of Petroleum Engineering. Thanks are due to Dr. F. G. Miller, Department of Petroleum Engineering, as well as to Dr. Brigham, for serving on the author's reading committee. In addition, the author is indebted to Dr. S. S. Marsden, Department of Petroleum Engineering, for his encouragement and their many candid conversations together.

The author wishes to express his deepest gratitude to his wife Carolyn for her support, encouragement, and prodding during their long and eventful years of undergraduate and graduate study together.

This research was carried out under Research Grant No. AER 78-03490-A03 by the National Science Foundation. The author is grateful for the financial assistance from the National Science Foundation and the Department of Petroleum Engineering which made this endeavor possible.

ABSTRACT

A series of mathematical models was developed to describe heat transfer in laboratory experiments using cylindrical cores in a Hassler-type coreholder. The models are general and can also be used to study behavior encountered in other laboratory arrangements. Analytical solutions were derived and the behavior of these solutions was studied to determine the interaction of the heat transfer mechanisms in laboratory cores.

The mathematical models were evaluated by comparison of calculated results with published experimental data. The three main conclusions resulting from the comparison are: (1) heat convection due to liquid flow, and heat losses from the core are important factors in the transport of energy for all times; (2) at early and intermediate times, the heat losses to the environment are transient in nature, while at long times they become steady (the transients were controlled by a film coefficient between the core and coreholder); and (3) during the early stages of hot or cold liquid injection, axial thermal conduction has a great effect on computed temperatures.

The mathematical models provide an understanding of heat transfer in laboratory cores which is important in designing experiments. For example, an experiment for determining the magnitude of the core-coreholder film coefficient

as a function of liquid mass velocity was planned. While the execution of such an experiment was outside the scope of this study, a description was included for future consideration.

The analysis of the behavior of the mathematical solutions was used to explain the sensitivity of heating and cooling thermal efficiencies to mass injection rate in laboratory experiments. As a result of this study, it now appears that heating and cooling thermal efficiency will not be sensitive to mass injection rate in field operations.

Finally, a new idea €or a dynamic displacement single-phase nonisothermal flow experiment was produced. Such an experiment could simplify the determination of the temperature effect on the absolute permeability of a porous medium, and permit determination under nonisothermal flowing conditions. The fundamental basis for this sort of experiment was described.

TABLE OF CONTENTS

Table of Contents, continued.

Table of Contents, continued.

Table of Contents, continued

APPENDICES

LIST OF FIGURES

FIGURE

List of Figures, continued.

List of Figures, continued.

List of Figures, continued.

List of Figures, continued.

LIST OF TABLES

1. INTRODUCTION

For a number of years there has been an interest in the injection of hot liquids into oil reservoirs in order to increase the recovery of oil. Recently there has been an interest in the injection of cold water into geothermal reservoir system in order to increase the effectiveness of energy extraction from them (Bodvarsson, 1974). These two processes are similar even though their goals are different. They are both concerned with nonisothermal fluid flow in porous media.

In both cases the reservoir engineer is concerned with two important questions: how will injectivity behave with time; and how will the producing wells respond to injection? The first question is concerned principally with fluid flow, and involves considerations of gravity override, fingering due to viscous instabilities and inhomogeneities in the reservoir, and finally, the effects of the changing temperature field on liquid mobility. The second question deals primarily with the movement of energy through the reservoir and surrounding formations in response to the nonisothermal fluid injection at a well. During hot liquid injection the goal is to heat the reservoir. Because injecting heat costs money, the operator would like to reduce heat losses from the reservoir to the surrounding nonproductive formation. We find the opposite situation in the case of heat scavenging by cold liquid injection into hot aquifers. Here heat transfer from surrounding formations to the aquifer is desirable because it increases the effectiveness of energy recovery from the earth.

A reservoir engineer has a number of procedures with which to forecast fluid behavior during nonisothermal fluid injection. These procedures are concerned with the use of field histories and pilot tests, laboratory scale physical models, and mathematical models. Mathematical models are formulated so as to incorporate the physical laws which are thought to be important in the process of interest. Solutions to these models are obtained using analytic, analog, or numerical techniques. These solutions are then related to the physical models at both the laboratory and field scales. The requirements of scaling laws (e.g., Geertsma, et al., 1956) are such that laboratory results often cannot be related to field behavior, although in some instances this can be done. It is thus usually necessary to interpret laboratory results in terms of mathematical models which incorporate the appropriate physical and phenomenological laws, and then to use these mathematical models to forecast or evaluate field behavior.

Thus, for example, relative permeabilities are one important set of reservoir properties needed to evaluate waterflooding projects. They can be determined by carrying out dynamic displacement experiments on sample cores of the reservoir. The data from these experiments can be analyzed using the mathematical model of Buckley and Leverett (1942) as solved by Welge (19521, Johnson, et al. (1959), and Jones (Ramey, 1971). This analysis produces relative permeability curves for the core samples which can then be used to forecast field performance (Craig, 1971). This interaction of physical and mathematical models is shown schematically in Fig. 1.1.

Fayers (1962) has shown that heat and mass transfer are only weakly coupled in the case of one-dimensional nonisothermal two-phase immiscible displacement in porous media. This coupling occurs primarily through the effect of temperature on fluid mobilities. This result has the implication that it is satisfactory to uncouple the mass and energy equations in one-dimensional nonisothermal fluid injection calculations. One can then solve the energy equation for temperature distribution as a function of time for the simplified case of single-phase flow. Then the mass balance equations for two-phase immiscible flow are solved using this temperature history to determine fluid mobilities. Thus, calculation of temperatures in one-dimensional single-phase nonisothermal liquid flow in porous media has direct utility in studying oil recovery by hot water injection. Furthermore, a complete understanding of the heat transfer phenomena affecting reservoir temperature behavior during the simplified case of one-dimensional liquid flow is essential to any attempt to calculate multi-dimensional multi-phase nonisothermal fluid flow.

Figure 1.1 Interaction of Physical and Mathematical Models

	SOLUTION OF THE PHYSICS	
REPRESENTATION OF THE PHYSICS — MATHEMATICALLY	ANALYTIC (Buckley and Leverett, Welge, etc.)	NUMERICAL (numerical simulators)
REPRESENTATION OF THE PHYSICS — PHYSICALLY	LABORATORY SCALE (dynamic displacement experiments)	FIELD-WIDE SCALE (waterflooding project)

This study has focussed on the development of analytic solutions to simplified mathematical models describing one-dimensional single-phase nonisothermal fluid injection into porous media. The specific objectives were:

1) to develop a series of simplified mathematical models of the single-phase nonisothermal liquid injection experiments of Arihara (1974);

2) to study the sensitivity of the behavior of these models to various important parameters; and

3) to examine the possibility of determining the effect of temperature on absolute permeability during nonisothermal fluid flow by carrying out a dynamic displacement experiment analogous to that described by Johnson, et al. (1959).

2. LITERATURE SURVEY

Both analytic and experimental studies of single-phase nonisothermal fluid flow in porous media appear in the literature. Dynamic displacement two-phase flow studies have also appeared. The following reviews studies which are pertinent to the stated objectives of this study.

2.1 Analytic Studies of Nonisothermal Single-phase Fluid Injection into Porous ""redia

A widely known mathematical study dealing with the injection of a hot liquid into a cold reservoir was presented by Lauwerier (1955). The basic mathematical model used by Lauwerier and numerous subsequent authors considers the constant rate injection of a constant temperature fluid into a uniform aquifer over- and underlain by a semi-infinite nonpermeable formation. Fluid flow within the aquifer is considered to be one-dimensional consistent with the flow geometry of interest. Steady flow of the constant density fluid is uncoupled from the unsteady heat flow caused by the hot fluid injection. Thus, the fluid flow field is given and unchanging, while the temperature field varies with time. Lauwerier developed a compact analytic expression for temperature propagation in the linear flow geometry. He neglected reservoir and surrounding formation thermal conductivities in the direction of fluid flow, and assumed uniform temperatures in the reservoir at any distance along it. This is equivalent to assuming infinite thermal conductivity in the reservoir in the direction perpendicular to fluid flow, and has been called the "Lauwerier assumption" by Prats (1969). Carslaw and Jaeger (1959, p. 396) have presented the solution to the same mathematical problem posed by Lauwerier. Their solution method is simpler than the one presented by Lauwerier.

In 1959 Marx and Langenheim presented a mathematical study of reservoir heating by hot fluid injection which was related to %he basic mathematical model used by Lauwerier. They used the Lauwerier assumption, and considered a radial flow system. Rather than solving for temperature distributions in the reservoir, they considered the total area of heated reservoir to be at constant temperature, and proceeded to develop an expression for the area heated as a function of time. Such an expression would be useful for determining the rate of growth of the heated area, and theoretical limits of heated area for different heat injection rates. Ramey (1959) extended the work of Marx and Langenheim to the case of variable heat injection rate, and observed that the solution was independent of flow geometry. Ramey also pointed out that the Marx and Langenheim type of solution should be more appropriate for the injection of saturated steam than for hot water injection, because heat losses would not necessarily cause the steam to cool, whereas they do cause water to cool.

Spillette (1965) presented a review of generalizations of the basic restrictive Lauwerier model, and compared them with an approximate numerical solution. Most of these generalizations have appeared in Russian publications. The various solutions differ mostly in the manner in which they relax assumptions about thermal conductivities in the system. While one intent of Spillette's paper was to demonstrate the advantages of an approximate numerical method for solving the energy balance equations, he also demonstrated the adequacy of using analytic solutions for practical hand calculations of hot fluid injection (Thomas, 1965).

An early general analytic solution for heat losses during hot fluid injection is due to Rubinstein (1959). He used the basic model of Lauwerier for radial flow geometry, and allowed for isotropic thermal conductivity in both the fluid reservoir and surrounding formation. The solution was in terms of heating efficiency, which is defined as the fraction of heat injected into the reservoir that still remains in it. Ramey (1964) determined that the heating efficiencies of the Lauwerier and Marx-Langenheim models were identical functions of dimensionless time even though the temperature distributions were different. He compared this result to that presented by Rubinstein, and concluded that the two simpler models gave pessimistic values of heating efficiency, particularly at early times.

According to Prats (1969), the most general analytic expression for hot liquid injection is that of Antimirov (1965). This model describes the arbitrary two-dimensional flow of a single-phase constant density fluid in the plane of a constant thickness homogeneous infinite aquifer of constant volumetric heat capacity. The rate and location of heat injection into the aquifer are arbitrary, and heat conduction can occur in all directions in both the reservoir and surrounding formation.

By making the Lauwerier assumption, Prats was able to develop an analytic expression for most of the general conditions used by Antimirov. Because he did not have to make assumptions about horizontal heat transfer mechanisms in the pay zone, Prats' results can be applied to any thermal recovery process, The general nature of Prats' work must make it a significant contribution to the evaluation of thermal recovery processes. Included in the paper are three conclusions particularly important to nonisothermal liquid injection into porous media. The first is that hot water injection has the highest heating efficiency of all the presently employed thermal recovery processes. The second conclusion is that once the Lauwerier assumption is made for hot water injection into a uniform thickness infinite aquifer of constant volumetric specific heat, the heating efficiency depends only on the net heat injected into the pay zone. Thus, if the same historv of net heat injection is applied to the simplified linear model originally proposed by Lauwerier, and into a uniform aquifer with arbitrary well location and two-dimensional planar flow geometry, both systems will have identical heating efficiencies. The Lauwerier assumption also leads to the corollary to the above result that the heating efficiency of hot water injection processes (or for any other processes for that matter) is independent of the horizontal thermal conductivity in both the injection interval and the adjacent formations.

There has also been an interest in the effects of injecting cold water into the earth. While the geometry and details of the fluid flow are complicated and area dependent, there are two limiting cases which are amenable to simplified mathematical modelling. The first of these is the case of single or multiple parallel planar fractures in which the fracture width is small compared to other significant length dimensions. Such fracture flow models have been discussed for the case of cold water injection by Rodvarsson (1969, 1972, 1974) and Gringarten, et al. (1975). The second limiting case occurs when the fluid flow is through a fine-grained porous medium such that the rock and fluid are locally in thermal equilibrium. Bodvarsson (1972, 1974) and Nathenson (1975) have examined this case for cold water injection when there is no heat conduction from the surrounding formation. Weinstein, et al. (1974), and Gringarten and Sauty (1975) have presented discussions of cold water injection into fine-grained porous media which include the effects of heat transfer from surrounding impermeable formations.

There were various motivations for these studies. Bodvarsson (1969) was interested in a periodically varying inlet temperature, which might correspond to the seasonal temperature variation of rainfall seepage into the ground. Bodvarsson (1974, 1974), Gringarten, et al. (1975), Gringarten and Sauty (1975), and Nathenson (1975) were concerned with temperature front behavior when injecting cold water into a hot system for purposes of both disposing of power plant effluents, and increasing energy recovery from the system. Weinstein, et al. (1974), were interested in the injection of cold water into a warm oil reservoir for purposes of waterflooding and pressure maintenance.

2.2 Experimental Studies of Nonisothermal Single-phase Liquid Injection into Porous Media

There were many laboratory and field experiments on hot fluid injection dating from the 1920s. Intense modern interest in this subject began in the late 1940s. The most important experimental study of hot fluid injection was the work of Wilman, et al. (1961). The injection of cold water, hot water, and steam was studied systematically for a variety of rocks, oils, and injection temperatures. Mechanisms for enhanced oil recovery due to steam injection were deduced. See Ramey (1968).

An interesting series of experimental investigation of hot liquid injection into a simulated reservoir system was offered by Malofeev (1958, 1959). According to Spillette (1965), this multidimensional linear flow physical model was designed so that the heat transfer effects that would be expected in the field were properly scaled. Malofeev reported on the results of a series of five experiments carried out at different heat injection rates.

Baker (1968) reported the results of experimental work similar to that of Malofeev. His scaled model simulated plane radial liquid flow. The experimental results were reported in terms of both temperature distributions and heating efficiencies, and were compared with various published mathematical models. Baker concluded that while there were relatively small temperature changes in a vertical line at a point in the flooded formation, this did not necessarily mean that the Lauwerier assumption was entirely satisfactory in calculating heating efficiencies. He also concluded that the various theories agreed among themselves only qualitatively, and even less so with experimental results. He was the first person to report of the dependence of experimentally determined heating efficiencies on liquid injection rate. Such a dependence was not indicated by any of the theories available at that time.

In 1969 Chappelear and Volek reported results from numerical and experimental investigations of the injection of hot liquids into a porous medium. They studied flow in a linear system, and allowed for both temperature and liquid flow variations across the formation. In addition to density changes, a liquid flow change should also be caused by liquid mobility variations in response to the temperature variation perpendicular to the main flow field. This would be primarily a result of the effect of temperature on liquid viscosity.

It would tend to cause flow channelling through the center of the injection interval due to reduced viscosity there. Chappelear and Volek did not consider gravity override or viscous instabilities that would be caused by an unfavorable mobility ratio. They also did not consider the possibility of a change of effective thermal conductivity of the formation parallel to the direction of fluid flow with mass flowrate. It was not possible to determine whether or not this would significantly affect their numerical results.

Chappelear and Volek concluded that while the Lauwerier theory did not accurately describe temperature profiles in a hot liquid injection system, it did give a good approximation to the average temperature in the injection interval everywhere, except near the leading edge of the heat front. They also concluded that the Lauwerier assumption is a poor approximation, and may lead to overestimation of the total heat loss by as much as 50%. This conclusion is not supported in the paper, even though it can be demonstrated to be valid for early times by an examination of Fig. 8 in Ramey (1964). A critical examination of Chappelear and Volek's paper suggests that their last conclusion may be valid at long times, but only for the case of a high ratio of cold temperature liquid viscosity to hot liquid temperature viscosity.

Ersoy (1969) reported results of an experimental and mathematical study of hot water injection into a linear flow system with radial heat losses into the surrounding insulating medium, He developed an interesting short time analytic solution to a mathematical model containing essentially the same assumptions used by Lauwerier. However, due to the restrictive nature of this solution he found that a finite difference numerical solution that included an effective thermal conductivity in the direction of fluid flow was more useful for examining the experimental results. He concluded that his experimental results also showed a sensitivity of heating efficiency to mass injection rate. On the basis of calculations made with his finite difference mathematical model, Ersoy concluded that this rate dependence of heating efficiency appeared to be caused by a sensitivity to mass flowrate of thermal conductivity in the injection interval.

In 1972 Crichlow presented the results of an experimental and numerical study of hot fluid injection into essentially the same physical system used by Ersoy. He also observed a sensitivity of heating efficiency to heat injection for hot liquid injection. On the basis of numerical experiments carried out with a finite difference mathematical model, he was unable to explain this sensitivity by hypothesizing a rate sensitive effective thermal conductivity parallel to the direction of liquid flow. However, Crichlow was able to explain the observed heating dependency on flowrate successfully by hypothesizing the presence of a rate sensitive film coefficient at the boundary between the porous medium and core holder. On the basis of matching computer calculations with experimental data, he deduced that this functional dependence was of the form:

$$h_f = a\,(w'')^b \tag{1.1}$$

where h_f is the film coefficient between the porous medium and the coreholder, w'' is the mass flowrate through the core per cross-sectional area to flow (also called mass velocity), and a and b are constants.

A study of nonisothermal fluid injection into consolidated porous media was presented by Arihara (1974). He presented the results of hot water, cold water, and steam injection into both naturally and artificially consolidated porous media. He concluded that there are no fundamental differences in energy transfer mechanisms between consolidated and unconsolidated porous media. Arihara appears to have been the first worker to report on cold liquid injection into a hot core. He proposed a definition of thermal efficiency for cold liquid injection directly analogous to that used in hot liquid injection (his p. 92):

$$E_{c,\text{Arihara}} \triangleq \frac{\text{Cumulative BTU Cooling Remaining in the Core}}{\text{Cumulative BTU Injected into the Core}} \tag{1.2}$$

In this expression, the term "cooling" refers to the opposite of heating. In the ideal limit of heat scavenging wherein all liquid injected is heated to reservoir temperature, the efficiency as defined by Arihara would go to zero. This is not consistent with the convention that the efficiency of idealized processes should approach 1. It would seem more reasonable to define cooling efficiency as:

$$E_{c,\text{proposed}} = \frac{\text{Heat Transfer from the Adjacent Media}}{\text{Cumulative Cooling Injected into the System}} \tag{1.3}$$

$$= 1 - E_{c,\text{Arihara}} \tag{1.4}$$

On the basis of his experimental results, Arihara concluded that both heating and cooling efficiencies are heat injection rate dependent. He presented heat transfer calculations which suggested that this rate dependency could be satisfactorily explained by a mass rate sensitive film coefficient between the core and the surrounding medium. Finally, he observed that whereas high heat injection rates were desirable for hot liquid injection, low injection rates were desirable for heat scavenging by cold liquid injection.

2.3 Dynamic Displacement Experiments in Porous Media

Johnson, Bossler, and Naumann (1959) proposed a dynamic displacement experiment for determining two-phase relative permeabilities in laboratory cores based on the pioneering study by Welge (1952). Previously the determination of relative permeabilities were made by a time-consuming sequence of steady-state experiments (Amyx, Bass, and Whiting, 1960, p. 184). A single experiment could only produce one datum point for each of the two phases. Johnson, et al., considered the injection of one fluid into a core containing a second fluid. They used the classic two-phase immiscible flow theory of Bucklet and Leverett (1942) in conjunction with the theory proposed by Welge (1952). This solution technique could produce individual two-phase relative permeability curves from a single dynamic displacement experiment. S. Jones of the Marathon Oil Company (Ramey, 1971) proposed a modification of the graphical solution technique of Johnson, et al., which was far easier to carry out than that of Johnson, et al.

The objectives of this study were concerned with developing simplified and convenient mathematical models of the nonisothermal liquid injection experiments of Arihara (1974). The preceding has discussed previous studies pertinent to the objectives of the study. The following two sections (3 and 4) discuss some simplified mathematical models of Arihara's experiments. The succeeding section (5) explores the idea of using nonisothermal dynamic displacement experiments to determine the variation with temperature of absolute permeability.

3. ONE-DIMENSIONAL MATHEMATICAL MODELS

The following discusses two simplified mathematical models of energy transport in the nonisothermal liquid injection experiments of Arihara (1974). First, the mathematical expressions are developed. Then, analytic solutions are derived and examined. Finally, the behavior of these models is compared quantitatively with the experiments of Arihara and qualitatively with the results of Crichlow (1972).

3.1 Introduction

The hot and cold water injection experiments of Arihara (1974) were carried out on consolidated sandstone cores mounted in a Hassler-type coreholder. The cores were slipped into a tightly-fitting viton sleeve which was placed in a stainless steel shell. The entire coreholder system was placed in an airbath. Overburden pressure was applied to the core by filling the annulus between the viton sleeve and steel shell with nitrogen gas at the appropriate pressure. The core had a diameter of 2 in., and was 2 ft long. The characteristics and dimensions that are relevant to this work are described in Appendix A (Table A.1) and sections 3.6.1 (Fig. 3.13) and 4.1 (Fig. 4.1). Other details of the coreholder system are described' in Arihara's report. Fig. 3.1 presents a schematic diagram of Arihara's equipment, and indicates idealized temperature behavior during a hot water

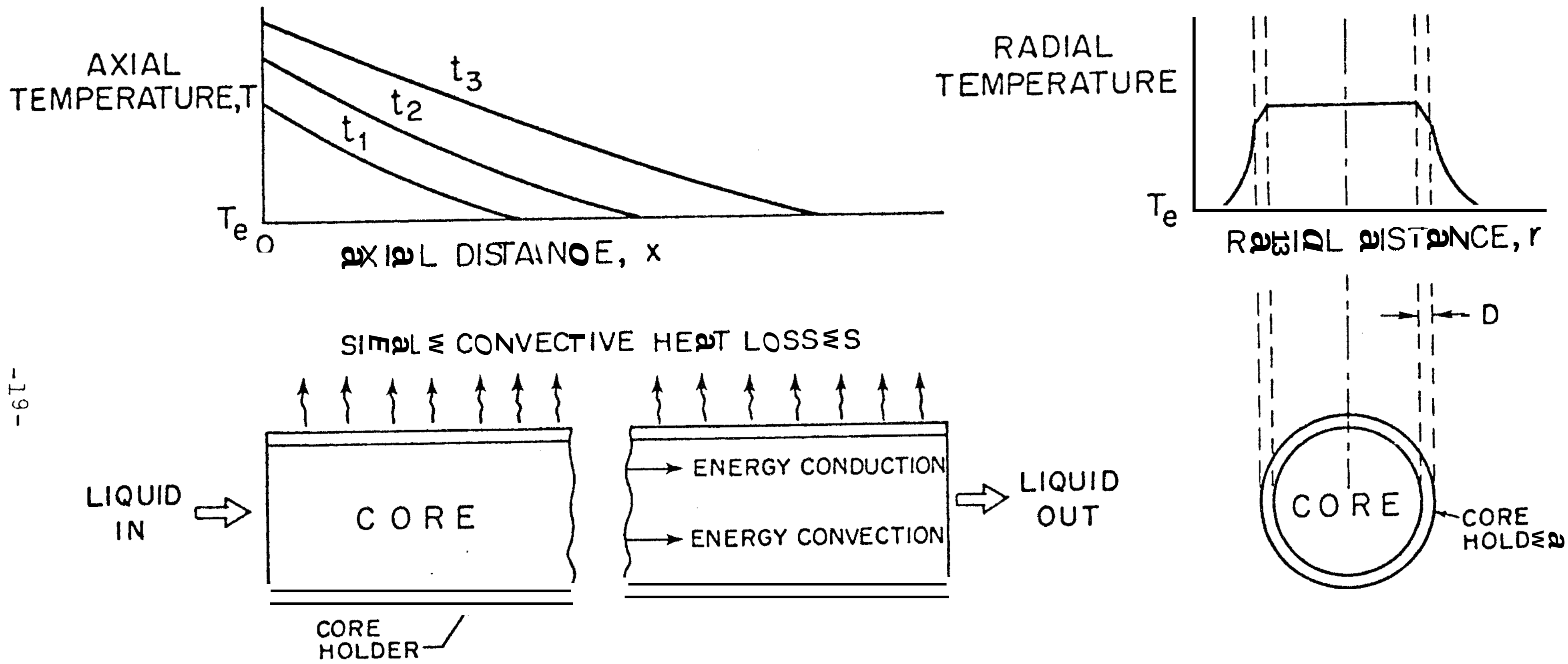

FIGURE 3.1. SCHEMATIC DIAGRAM OF THE EXPERIMENTAL EQUIPMENT OF ARIHARA, SHOWING IDEALIZED TEMPERATURE DURING HOT WATER INJECTION

injection experiment. Unless otherwise indicated, all discussions of heat transfer in this report are for the case of hot water injection into a cold core. The case of cold water injection into a warmer system could just as easily have been used. Heat transfer would simply be in the opposite direction, and theoretically, there are no qualitative differences.

Due to the nature of the coreholder design, the heat loss rate from the core to the outside air bath environment can, to a first approximation, be considered to be of a simple kind. In conjunction with the first assumption listed in the following, this approximation (No. 3) allows for the construction of mathematical models with only two independent variables: one in space and one in time.

This section describes two one-dimensional mathematical models of the heat transfer occurring during hot or cold liquid injection into a porous medium mounted in a coreholder such as was used by Arihara. Both of the models consider steady heat transfer between the core and airbath environment, and convective energy transfer due to liquid flow in the core. The first model (wave model) is described mathematically by a wave equation, and does not account for axial thermal conductivity in the core, However, it does allow for a variation of the overall heat loss coefficient from the coreholder with distance along the core, and a variation of mass injection rate with time. The second model (parabolic model) is described by a parabolic equation. This model accounts for the axial thermal conductivity in the direction of fluid flow, but requires that the thermal properties, mass injection rate, and overall heat loss coefficient be constant.

The various important assumptions required for the derivation of the two one-dimensional models are as follows. See also Appendix A. The assumptions are:

(1) The radial temperature distribution across the core is uniform at any axial distance along the core, x, and any time, t (shown schematically in Fig. 3.1). This is called the Lauwerier assumption (Prats, 1969). Thus, temperature in the core is a function of time and only one space coordinate: the distance, X, along the system. This is equivalent to assuming that the radial thermal conductivity in the core is infinite.

(2) There may be a constant effective axial thermal conductivity, λ_f, in the core due to conduction and dispersion mechanisms. There is no axial heat conduction in the coreholder system. If nonzero, the effective axial thermal conductivity, λ_f, increases as the mass flowrate in the core increases.

(3) Heat losses from the sides of the core through the coreholder system are steady and of the simple convective type, That is, locally the heat loss rate per unit length of core is given by:

$$\dot{Q}' = \bar{h}\, P\, (T - T_e) \tag{3.1}$$

where $\dot{Q}'$ is the instantaneous heat loss rate per unit length of core, and the other symbols are defined in the nomenclature section.

(4) The thermal properties of the fluid and rock matrix may vary with temperature for the wave model. Specifically, the heat of the water and rock matrix, C_w and C_{ma} respectively, may vary with temperature.

(5) The liquid is incompressible, and the rock matrix is incompressible and undeformable. Furthermore, both liquid and rock matrix have constant densities which do not depend on temperature. This assumption implies that the instantaneous mass flowrate at any cross-section perpendicular to flow is uniform throughout the core. This instantaneous mass flowrate is constant for the parabolic model, but may vary with time for the wave model.

(6) The fluid flow is one-dimensional and axial. Thus, convection cells are not set up, there are no viscous instabilities, there is no gravity override, and macroscopic fluid velocities are uniform across any cross-section perpendicular to fluid flow.

(7) There is local thermal equilibrium in the core between the liquid and the rock matrix, and hence sand grains are always at the local liquid temperature.

3.2 Derivation of the One-Dimensional Mathematical Models

Two one-dimensional mathematical models were developed. Each model incorporates a slightly different combination of the assumptions discussed in section 3.1. The first model is called the wave model because it is described by a wave equation. This model allows the mass injection rate to vary with time, the thermal properties of rock and liquid to vary with temperature, and the heat loss coefficient along the core to vary with distance. It does not consider axial thermal conduction in the core. The second model is called the parabolic model because it is described by a parabolic equation. It requires the assumption of constant mass injection rate, thermal properties, and heat loss coefficient. However, it does consider axial thermal conduction in the core.

3.2.1 Derivation of the Wave Model: Application of an energy balance to a cylindrical elemental volume of thickness, dx, cross-sectional area to fluid flow, A_C, and perimeter, P, in conjunction with the appropriate assumptions discussed in sections 3.1 and 3.2, yields the equation:

$$\left(\frac{w}{A_c}\right) \frac{\partial e_w}{\partial x} + \frac{\partial e_f'''}{\partial t} = - \left(\frac{\bar{h}P}{A_c}\right) (T-T_e) \tag{3.1}$$

The symbols in this equation are defined in the nomenclature section; however, e_w represents the specific energy of the liquid on a unit mass basis, whereas e_f''' represents the specific energy of the water-rock matrix composite on a unit volume basis. This property is given by the expression:

$$e_f''' = \phi e_w \rho_w + (1-\phi)\, e_{ma}\rho_{ma} \tag{3.2}$$

$$= \left[\phi C_w \rho_w + (1-\phi)\, C_{ma}\rho_{ma}\right](T-T_b) \tag{3.3}$$

$$= M_f \, (T-T_b) \qquad (3.4)$$

where M_f is the specific heat of the formation (liquid-rock matrix composite) on a unit volume basis. These expressions for e_f''' do not require that the various specific heats, C_w, C_{ma}, and M_f be constant with temperature.

Eq. 3.1 is a first order nonhomogeneous wave-equation of the form:

$$c_1 \frac{\partial e_w}{\partial x} + \frac{\partial e_f'''}{\partial t} = -c_2 \, (T-T_e) \qquad (3.5)$$

where

$$c_1 \triangleq w/A_c,$$
$$c_2 \triangleq \bar{h}P/A_c \qquad (3.6)$$

For the wave model e_w and e_f''' may be functions of temperature, w may be a function of time, and $(\bar{h}P)$ may be a function of distance along the core.

3.2.2 Derivation of the Parabolic Model: In conjunction with the appropriate assumptions discussed in sections 3.1 and 3.2, the application of an energy balance to the same elemental volume used in section 3.2.1 yields:

$$\left(\frac{wC_w}{A_c M_f}\right) \frac{\partial T}{\partial x} - \left(\frac{\lambda_f}{M_f}\right) \frac{\partial^2 T}{\partial x^2} + \left(\frac{\bar{h}P}{A_c M_f}\right) (T-T_e) + \frac{\partial T}{\partial t} = 0 \qquad (3.7)$$

where the symbols are defined in the nomenclature section. This is a nonhomogeneous, linear, second-order parabolic equation of the form:

$$\alpha \frac{\partial T}{\partial x} - \beta \frac{\partial^2 T}{\partial x^2} + \gamma (T-T_e) + \frac{\partial T}{\partial t} = 0 \qquad (3.8)$$

where:

$$\alpha \triangleq (wC_w/A_c M_f),$$

$$\beta \triangleq (\lambda_f/M_f), \text{ and} \qquad (3.9)$$

$$\gamma \triangleq (\bar{h}P/A_c M_f)$$

For this model, all of the symbols in the definitions of α, β, and γ must be constants.

3.3 Analytic Solutions to the One-Dimensional Mathematical Models

The following describes the derivation of analytic solutions to the wave and parabolic models. The wave equation is solved using the method of characteristics. This solution is valid for injection temperature and mass flowrate variable with time, thermal properties variable with temperature, and heat loss coefficient variable with distance along the core. The parabolic equation is solved using the Laplace transformation technique. This solution requires constant injection temperature, mass flowrate, thermal properties, and heat loss coefficient.

3.3.1 Initial and Boundary Conditions: The same initial and boundary conditions may be used for both models. These are for $T(x,t)$ in the domain $x \geq 0$, and $t \geq 0$. They are:

$$T(x,0) = T_e, \; x \geq 0;$$

$$T(0,t) = T_i(t), \; t>0; \text{ and} \tag{3.10}$$

$$\lim_{x \to \infty} \frac{T}{x} = 0, \; t \; 0$$

Even though the core has a finite length, expressing the right-hand boundary condition for $x \to \infty$ is reasonable, and consistent with experimental results. This is the same as saying that there are no important end effects at the right-hand end of the core.

3.3.2 Solution to the Wave Equation Using the Method of Characteristics: The wave equation model is described by Eq. 3.5 with definitions (3.6). Because e_f''' and e_w are single-valued functions of temperature, T, one can write:

$$\frac{\partial e_w}{\partial x} = \frac{de_w}{de_f'''} \cdot \frac{\partial e_f'''}{\partial x} \tag{3.11}$$

Substituting this into the wave equation (3.5), we obtain:

$$\left(c_1 \frac{de_w}{de_f'''}\right) \frac{\partial e_f'''}{\partial x} + \frac{\partial e_f'''}{\partial t} = - c_2 (T-T_e) \tag{3.12}$$

where de_w/de_f''' s a single-valued function of temperature. Because the temperature in the system is a function of the two independent variables distance and time, T(x,t), the total differential of e_f''' m y be written:

$$de_f''' = \left(\frac{\partial e_f'''}{\partial t}\right)_x dt + \left(\frac{\partial e_f'''}{\partial x}\right)_t dx \qquad (3.13)$$

Dividing by dt, and rearranging, gives:

$$\frac{dx}{dt}\left(\frac{\partial e_f'''}{\partial x}\right)_t + \left(\frac{\partial e_f'''}{\partial t}\right)_x = \frac{de_f'''}{dt} \qquad (3.14)$$

Comparing Eqs. 3.5 and 3.14, it can be seen that the characteristic line in the x-t plane is given by:

$$\frac{dx}{dt} - c_1 \frac{de_w}{de_f'''} \qquad (3.15)$$

and that the formation volumetric specific energy, e_f''', of a fictitious particle following this characteristic must satisfy:

$$\frac{de_f'''}{dt} = - c_2 (T-T_e) \qquad (3.16)$$

Thus, a fictitious particle injected into the core at $x=0$ with temperature T_i will decay in temperature according to Eq. 3.16 and will move with a velocity given by Eq. 3.15. This velocity will, in general, be less than the macroscopic fluid velocity.

The fact that e_f''' is a single-valued function of temperature can be used to convert Eq. 3.16 into a more convenient form:

$$\frac{de_f'''}{dt} = \frac{de_f'''}{dT} \cdot \frac{dT}{dt} = M_f \frac{dT}{dt} \tag{3.17}$$

Thus, Eq. 3.16 becomes:

$$\frac{dT}{dt} = -\frac{c_2}{M_f} \cdot (T-T_e) \tag{3.18}$$

where the formation volumetric specific heat, M_f, may be a function of temperature for this model.

For constant thermal properties and constant injection temperature, the characteristics solution simplifies to:

$$\left(\frac{T-T_e}{T_i-T_e}\right) = \exp\left(-\frac{\bar{h}P}{wC_w} \cdot x\right) \cdot H\left(\frac{\bar{h}P}{\hat{A}_c M_f} \cdot t - \frac{\bar{h}P}{w\hat{C}_w} \cdot x\right) \tag{3.19}$$

or:

$$T_D = \exp(-x_{DW}) \cdot H(t_{DW} - x_{DW}) \tag{3.20}$$

where:

$$H(\xi) \triangleq \begin{cases} 1, & \xi \geq 0 \\ 0, & \xi < 0 \end{cases} \tag{3.21}$$

and the dimensionless variables T_{DW}, x_{DW}, and t_{DW} are defined **by:**

$$T_D \triangleq (T-T_e)/(T_i-T_e),$$

$$x_{DW} \triangleq (P\bar{h})x/(wC_w), \text{ and} \tag{3.22}$$

$$t_{DW} \triangleq (\bar{h}P)t/(A_c M_f)$$

Arihara (1974, p. 60) developed a solution to this same problem with constant thermal properties and injection rate using the Laplace transform technique. While his method was for the case of injection temperature varying as a function of time, it simplifies to Eqs. 3.20 to 3.22 if injection temperature is constant.

3.3.3 Solution to the Parabolic Model Using the Laplace Transform Method: The mathematical problem is:

$$\alpha \frac{\partial T}{\partial x} - \beta \frac{\partial^2 T}{\partial x^2} + \gamma (T-T_e) + \frac{\partial T}{\partial t} = 0,$$

$$x>0, \ t>0; \qquad (3.8)$$

$$T(0,t) = T_i, \ t>0;$$

$$\lim_{x\to\infty} \frac{\partial T}{\partial x} = 0, \ t>0, \text{ and} \qquad (3.10)$$

$$T(x,0) = T_e, \ x>0$$

The solution considers T_i constant. Solutions for T_i, a function of time, can be obtained by either explicit superposition of the constant T_i solution, or by using Duhamel's integral.

It is convenient to recast the problem into nondimensional form by defining:

$$T_D \triangleq (T-T_e)/(T_i-T_e);$$

$$x_{DP} \triangleq (\frac{\alpha}{\beta})\ x = (\frac{wC_w}{A_c\lambda_f})\ x$$

$$t_{DP} \triangleq (\frac{\alpha^2}{\beta})\ t = (\frac{wC_w}{A_c})^2 \cdot \frac{1}{M_f\lambda_f} \cdot t \qquad (3.23)$$

$$c_P \triangleq (\frac{\beta\gamma}{\alpha^2}) = \frac{\lambda_f A_c \bar{h} P}{(wC_w)^2}$$

Eq. 3.8 becomes:

$$\frac{\partial T_d}{\partial x_{DP}} - \frac{\partial^2 T_D}{\partial x_{DP}^2} + c_P T_D + \frac{\partial T_D}{\partial t_{DP}} = \qquad x_{DP}>0,\ t_{DP}>0 \qquad (3.24)$$

and the conditions, Eq. 3.8, become:

$$T_D\ (0,t_{DP}) = 1,\ t_{DP}>0;$$

$$\lim_{x_{DP}\to\infty} \frac{\partial T_D}{\partial x_{DP}} \quad 0,\ t_{DP}>0;\ \text{and} \qquad (3.25)$$

$$T_D\ (x_{DP},0) = 0,\ x_{DP}>0$$

The solution to this problem is characterized by the single parameter c_P.

Taking the Laplace transform of Eqs. 3.24, 3.25 gives:

$$\frac{\partial \bar{T}_D}{\partial x_{DP}} - \frac{\partial^2 \bar{T}_D}{\partial x_{DP}^2} + (c_P+S)\ \bar{T}_D = 0; \qquad (3.26$$

$$\bar{T}_D\ (0) = \frac{1}{S}$$

$$\lim_{x_{DP}\to\infty} \frac{\partial \bar{T}_D}{\partial x_{DP}} = 0 \tag{3.27}$$

where the Laplace transform of T_D, $L\{T_D\}$ is given by $\bar{T}_D$. The solution to Eqs. 3.26, 3.27 is given by:

$$\bar{T}_D = \frac{1}{s} \exp \{\frac{x_{DP}}{2} - \sqrt{\zeta+s}\, x_{DP}\} \tag{3.28}$$

where $\zeta \triangleq \frac{1}{4} + c_P$.

This can be inverted as follows:

$$T_D = L^{-1} \left\{ \frac{1}{s} \exp\left[\frac{x_{DP}}{2} - \overline{\quad s}\ x \quad \right] \right\} \tag{3.29}$$

$$= \exp \{\frac{x_{DP}}{2} - \zeta t\}\ L^{-1} \left\{ \frac{1}{(s-\zeta)} \exp \left[-\sqrt{s}\, x_{DP}\right]\right\} \tag{3.30}$$

$$= \exp (\frac{x_{DP}}{2} - \zeta t) \cdot \frac{1}{2} \left\{ e^{x_{DP}\sqrt{\zeta}} \operatorname{erfc} (\frac{x_{DP}}{2\sqrt{t_{DP}}} + \sqrt{\zeta t_{DP}}) + e^{-x_{DP}\sqrt{\zeta}} \operatorname{erfc} (\frac{x_{DP}}{2\sqrt{t_{DP}}} - \sqrt{\zeta t_{DP}}) \right\} \tag{3.31}$$

$$= \frac{1}{2} \left\{ \exp \left[- \frac{x_{DP}}{2} (-1+\sqrt{1+4c_P})\right] \cdot \operatorname{erfc}\left[\frac{x_{DP}}{2\sqrt{t_{DP}}} - \frac{\sqrt{(1+4c_P)t_{DP}}}{2} \right] + \exp \left[\frac{x_{DP}}{2} (1+\sqrt{1+4c_P})\right] \cdot \operatorname{erfc}\left[\frac{x_{DP}}{2\sqrt{t_{DP}}} + \frac{\sqrt{(1+4c_P)t_{DP}}}{2} \right]\right\} \tag{3.32}$$

The Laplace transform inversion in Eq. 3.30 is given as No. 88 by Roberts and Kaufmann (1966, p. 244). The solution, Eq. 3.32, has been previously presented by Penberthy and Ramey (1966).

3.4 Behavior of the One-Dimensional Analytic Solutions for Constant Injection Temperature

The following discusses the behavior of the constant injection temperature analytic solutions to the wave and parabolic models. The wave equation solution is discussed in section 3.4.1, while the parabolic equation is discussed in section 3.4.2.

3.4.1 Wave Equation: The solution consists of following the temperature decay of a fictitious particle as it moves along the characteristic:

$$\frac{dx}{dt} = c_1 \frac{de_w}{de_f} \qquad (3.15)$$

This is directly analogous to solutions that appear in both the frontal advance theory of Buckley and Leverett (1942) and in the theory of chromatographic transport (Acrivos, 1956). Such solutions describe the rate of advance, dx/dt, of an entity (which may be purely mathematical) in terms of a differential of the flowing concentration with respect to the bulk concentration of some quantity related to the entity. In the case of single-phase nonisothermal flow in porous media, this is the differential of flowing energy concentration, e_w, with respect to bulk energy concentration on a unit volume basis, e_f.''' In Buckley-Leverett frontal advance theory, it is the differential of flowing fluid concentration with respect to bulk fluid concentration.

The behavior of such solutions depends on the nature of the relationship between the flowing and bulk concentration. If a graph of flowing versus bulk concentration is concave down (curve A in Fig. 3.2.a), then an initial step function increase in injection temperature (shock) will tend to disperse because lower temperatures will advance more rapidly. This is shown schematically in Fig. 3.2.b for the case of no heat losses. If the relationship in Fig. 3.2.a is a straight line (curve B), then all temperatures across the initial shock will advance with the same velocity and the shock will remain (see Fig. 3.2.c). If flowing versus bulk concentration is concave up (curve C in Fig. 3.2.a), then in the absence of dissipative phenomena the initial shock will also tend to remain (Fig. 3.2.C). This shock will move at a velocity which is directly proportional to the slope of curve B in Fig. 3.2.a. This is directly analogous to the formation of a sharp saturation front in the frontal advance theory of Buckley and Leverett, which in turn is closely related mathematically to the formation of shocks in high speed compressible fluid flow described by hyperbolic equations (Fayers, 1962; Courant and Friedriechs, 1948, Ch. II).

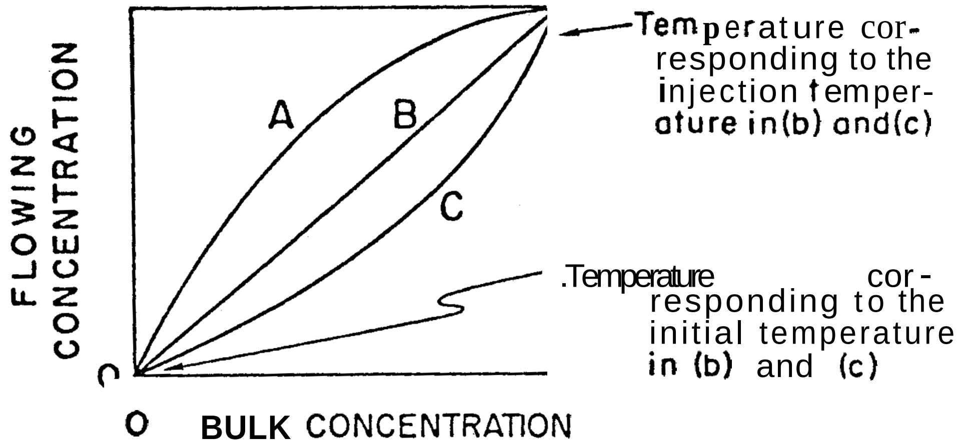

a. Relationship between flowing and bulk concentration.

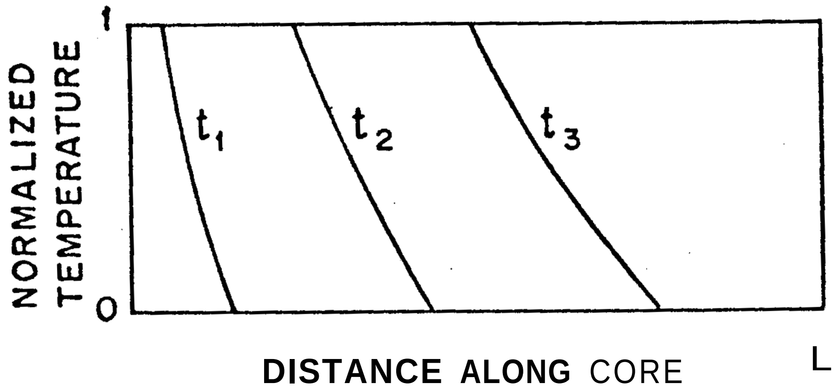

b: Temperature vs Distance for curve A

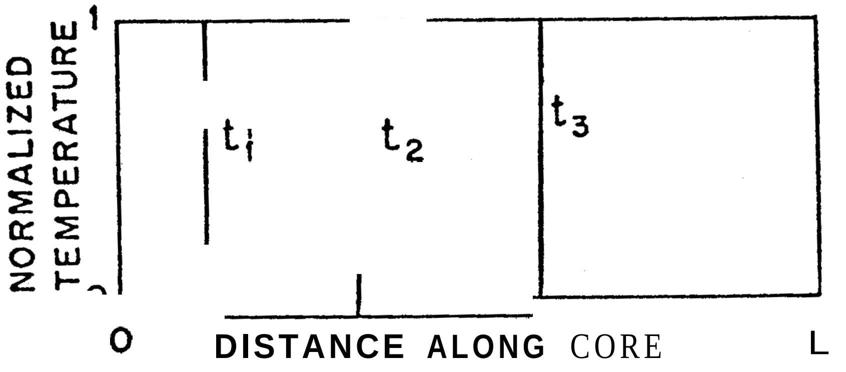

c. Temperature vs Distance for curve 8 and C in (A) above

3.2. Temperatures Computed from the Wave Equation Mathematical Model (Step Function Increase in Temperature and No Heat Losses)

The computational procedure used to evaluate the characteristics solution is described in Appendix B. This procedure can consider thermal properties variable with temperature, mass injection rate variable with time, and heat loss coefficient variable with distance along the core. The formation of thermal shocks was not a problem, and hence not incorporated into the calculational procedure.

Calculations of the relationship between the flowing energy concentration (that of water) and bulk energy concentration (that of the water-matrix continuum) indicate that it is approximately linear. This can be seen from Fig. A.2 in Appendix A, which shows only a slow variation of de_w/de_f with temperature for various porosities. The computed temperature behavior of variable thermal property cases for 22% porosity over a temperature range from 70 to 150°F differed negligibly from those calculated using average (constant) thermal properties. It was concluded that the effect of variable thermal properties was negligible, and the use of constant thermal properties was satisfactory for the physical conditions of interest. This conclusion is valid for both the constant and variable injection temperature cases, but may require modification for lower porosities and higher temperature ranges.

Temperature calculations using the variation of mass injection rate reported by Arihara were also made and compared to those obtained using a constant (average) flowrate. The differences in calculated temperature were insignificant relative to experimental errors inherent in such experiments, It was concluded that for the experimental conditions of interest, an average mass injection rate could be assumed for the mathematical models. This conclusion is not surprising, because the mass injection rates in the experiments of Arihara did not vary greatly from an average value.

The conclusion of the adequacy of assuming both constant thermal properties and constant mass injection rate simplifies the analytic solution considerably. The characteristics in the x-t plane become parallel straight lines, and the decay of temperature above external temperature becomes exponential with both distance and time along these characteristics. For the case of constant injection temperature, $T_D(0,t) = 1$, the solution has already been presented (Eq. 3.20) as:

$$T_D\,(x_{DW},t_{DW}) = \exp\,(-x_{DW}) \cdot H\,(t_{DW}-x_{DW}) \qquad (3.20)$$

This behaves simply as a sharp front which moves down the core, remaining in an unchanging exponential decay behind the front (see Fig. 3.3). The rate of decline of temperature with distance depends on the factor $(\bar{h}P)/(wC_w)$. Thus, either a high $(\bar{h}P)$, or a low (wC_w) can cause T_D to fall to essentially zero by the end of the core. Physically, this occurs if all of the injected heat is lost to the environment before it can reach the outlet end of the core.

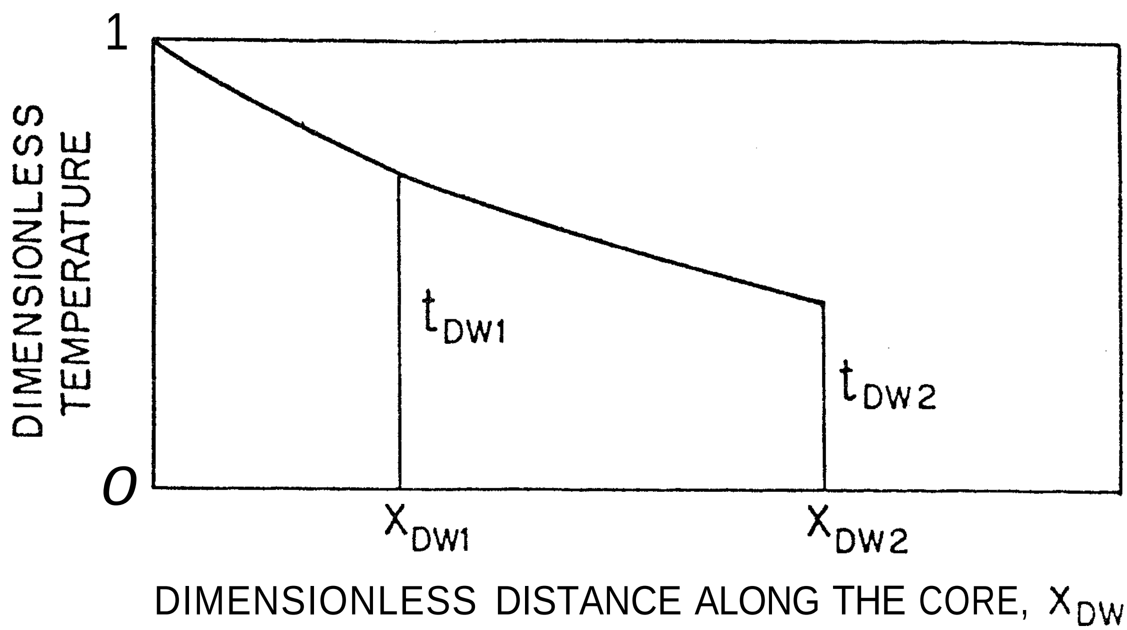

FIGURE 3.3. BEHAVIOR OF THE CONSTANT INJECTION TEMPERATURE WAVE EQUATION SOLUTIOIJ FOR CONSTANT MASS INJECTION RATE AND CONSTANT THERMAL PROPERTIES.

It can be seen from an examination of Fig. 3.3 that the heating efficiency of a process described by Eq. 3.20 depends initially <u>only</u> on the dimensionless time, t_{DW}, and at longer times on the dimensionless length of the system. Heating efficiency is defined as:

$$E_h = \frac{\text{Heat Remaining in the Core}}{\text{Net Heat Injected into the Core}} \tag{3.33}$$

The solution (Eq. 3.20) suggests that if steady state temperature profiles for experiments such as those of Arihara are graphed as $\log_{10}(|T-T_e|)$ versus distance, feet, then they might be expected to form straight lines with a negative slope of $(\bar{h}P)/(2.303\ wC_w)$. This can be used to obtain experimentally determined values of $\bar{h}$ if w and C_w are known. If such a graph does not produce a straight line, then it can be concluded that the assumptions of the wave equation model are being violated, and the source of this violation would have to be found. A comparison of these theoretical steady state conclusions with experimental results of Arihara is made in section 3.6.1.

On the basis of the above analysis, the following experiment would be of possible interest: measurement of steady state temperature profiles at various mass injection rates, while maintaining constant heat loss characteristics external to the core. In this case one would obtain a series of values for $\bar{h}$ versus w. It can be hypothesized that $\bar{h}$ depends on w in the following manner:

$$\bar{h} = 1/\left[R_i + r_o/(r_{so}h_e) + 1/h_f\right] \qquad (3.34)$$

$$= 1/\left[R_{int} + (r_o/r_{so})/h_e + (1/a)\,(w'')^{-m}\right] \qquad (3.35)$$

where:

R_{int} = internal thermal resistance in the coreholder system due to conduction through it (see section 4.1, Eq. 4.1)

h_f = film coefficient between the core and coreholder system, depending on w via the relation $h_f = a\,(w'')^m$ (Crichlow, 1972; Colburn, 1931)

w'' = w/A_c, mass flowrate through the core per unit bulk cross-sectional area to flow (mass velocity), lb/(min-ft2)

r_o = outside radius of the core

r_{so} = outside radius of the steel shell

h_e = film coefficient between the outside of the steel shell and the external environment.

If the relationship between h_f and w'' can indeed be represented by the indicated expression, then the parameters a and m can in principle be obtained by graphing the log of $1/\bar{h} - r_o/(r_{so}h_e) - R_{int}$ versus the log of w''. Such a graph would have a slope of $(-m)$ and an intercept of $(1/a)$ at $w''=1$.

Because it is difficult to measure h_e independent of $\bar{h}$, its value must be estimated using available correlations.

Since an inaccuracy in the value of h_e may destroy the accuracy of the evaluated parameters a and m, the sensitivity of this method to the value of h_e was evaluated for physical and experimental parameters such as those reported by Arihara and Crichlow. The results of these calculations are presented in Appendix C. These calculations suggest that an accurate value of h_e is needed to produce the desired straight line on log-log paper. This value of h_e can, however, be obtained by graphing the data for various values of h_e and selecting the straight line as lying between the concave up and concave down parametric curves. Furthermore, the desired straight line becomes more sensitive to the estimated value of h_e when $h_f > h_e$.

3.4.2 Parabolic Equation: The parabolic solution, Eq. 3.32, has been previously discussed by Penberthy and Ramey (1966), but was applied to a different physical system. The parameter c_p tends to be much less than 1.0 (on the order of 0.05) for physical systems of interest. Penberthy and Ramey presented graphs of this solution in terms of nondimensional variables. Their results were presented for dimensionless lengths of only up to 7.0, while the dimensionless lengths of interest for the experimental results of Arihara range to as much as 160.

Fig. 3.4 presents calculated temperature behavior for a hypothetical constant injection temperature experiment with physical parameters comparable to those of Arihara (experiment HWI-B-1). Results are presented for 15, 45, and

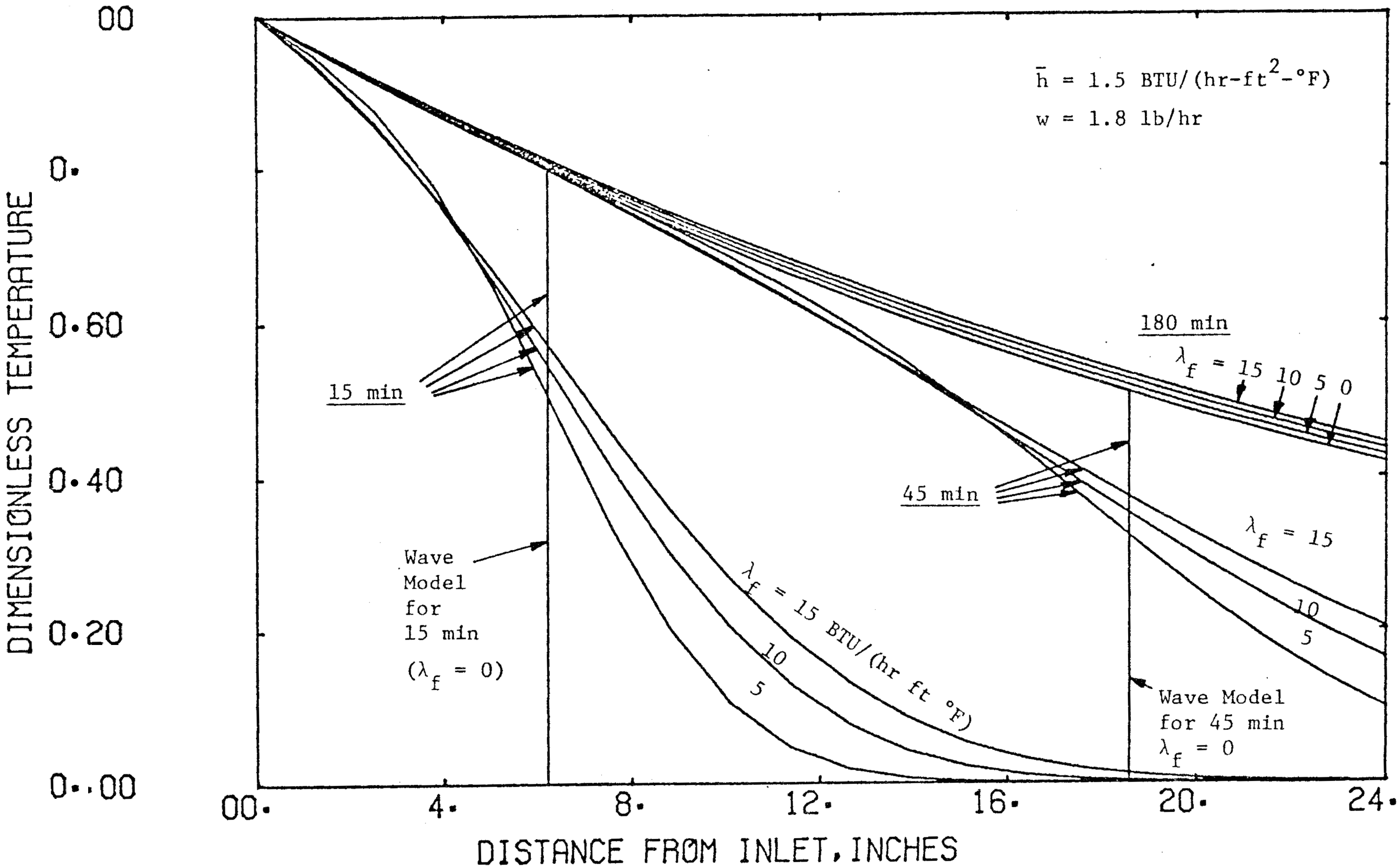

FIGURE 3.4. CALCULATED TEMPERATURES AT 15, 45, and 180 MINUTES FOR CONSTANT INJECTION TEMPERATURE AND CONDITIONS COMPARABLE TO THE HWI-B-1 EXPERIMENT OF ARIHARA

180 minutes, and for effective axial thermal conductivities of 5, 10, and 15 BTU/(hr-ft-^{o}F). The behavior of the wave equation (zero axial thermal conductivity) using the same overall heat loss coefficient of 1.5 BTU/(hr-ft^{2}-^{o}F) is also presented. It can be seen that the effect of axial thermal conductivity is to eliminate discontinuous temperature profiles, and that higher axial thermal conductivities cause smoother temperature profiles. This is directly analogous to the effect that capillary pressure has in eliminating shock discontinuities in Suckley-Leverett frontal advance theory.

Many calculations were made for temperature profiles for experimental conditions comparable to those of Arihara. Results indicate that an effective axial thermal conductivity significantly reduces the tendency to form sharp temperature fronts. Fig. 3.5 presents results of such calculations for conditions different from those in Fig. 3.4. This observed effect of λ_f is important even at higher mass injection rates, because λ_f increases with mass injection rate (Adivarahan, et al., 1962). For example, while a value of 1.0 BTU/(hr-ft-^{o}F) wculd lead to a sharper temperature profile in Fig. 3.4, such a value is unrealistically low. Based on the results of Adivarahan, et al., and a mass flowrate of about 80 lb/(hr-ft2) (which is 1.33 lb/(min-ft2)), one would expect a λ_f of between 8 and 20 for an experiment such as that shown in Fig. 3.4, and between 1 and 7 for the experiment in Fig. 3.5.

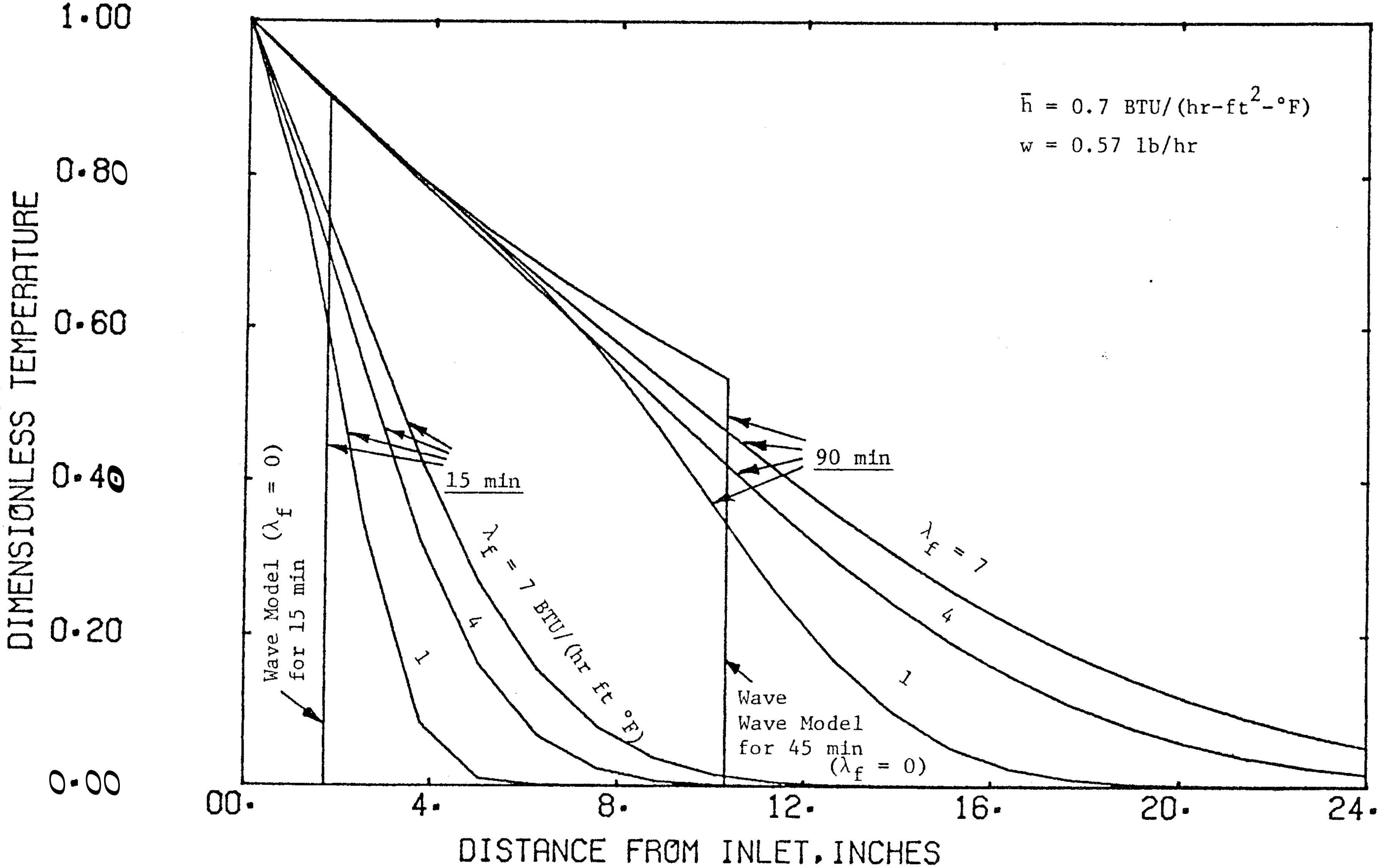

FIGURE 3.5. CALCULATED TEMPERATURES AT 15 AND 90 MINUTES FOR CONSTANT INJECTION TEMPERATURE AND EXPERIMENTAL CONDITIONS COMPARABLE TO THE HWI-S-1 EXPERIMENT OF ARIHARA

This range of values of axial thermal conductivity can lead to measurably different temperature profiles at early times during constant temperature fluid injection. This suggests the possibility of attempting to design an experiment which could use this difference to determine values of λ_f. This possibility was not pursued further in this work, because the parabolic mathematical model upon which it is based was not found to be valid for the experimental configuration of interest.

The steady state form of the parabolic solution is:

$$T_D = \exp\left\{-(x_{DP}/2)\,(-1+\sqrt{1+4c_P})\right\} \tag{3.36}$$

For $c_P<1$, this can be approximated by:

$$T_D = \exp\left\{-x \quad (1-c_P+2c_P^{\,2} - \ldots)\right\} \tag{3.37}$$

$$\left\{ \quad {}_{DW}\,(1-c_P)\right\}, \text{ if } c_P \ll 1 \tag{3.38}$$

This is the same as the steady state wave equation solution, Eq. 3.20, except for the lower order modifying terms as powers of c_P. Thus, use of the steady state form of the wave equation on experimental data affected by axial heat conduction actually produces a value of $\bar{h}\,(1-c_P)\,(P/wC_w)$ instead of $\bar{h}\,(P/wC_w)$. If (P/wC_w) is known, and c_P can be estimated, a more accurate estimate of $\bar{h}$ can be obtained. However, the correction for axial thermal conduction effects will tend to be small when c_p<<1. These effects were neglected in the remainder of this report.

Examination of Figs. 3.4 and 3.5 indicates that heating processes described by the parabolic model depend on the parameter c_p as well as on time. This is indicated by the fact that the area under the temperature profiles for a specified time depend on the axial thermal conductivity, λ_f. Thus, for fixed other physical parameters, the heating efficiency, E_h, depends on the value of axial thermal conductivity in the core, as well as on time. This result is in contrast with the conclusion of Prats (1969) that heating efficiencies are independent of thermal conductivity in the direction of fluid flow if the Lauwerier assumption is made. It should be noted that the character of heat losses from the two systems (the parabolic model presented here and the more general model of Prats) is different. In Prats' model, heat is lost into a semi-infinite medium, whereas in the parabolic model it is simply lost across a temperature difference to a uniform external environment.

3.5 Behavior of the Analytic Solutions for Time-Dependent Injection Temperature

The results that will be discussed in this section are based on injection temperature variation similar to that reported by Arihara (1974). This variation consisted of a rapid change in the injection temperature at early times, followed by an approach to constant temperature at long times. Such a variation can be approximated by suitable modification of the exponential function. Fig. 3.6 presents a graph of the injection temperature history for run HWI-B-1 of Arihara, and compares it to a particular analytic approximation due to Arihara. This analytic approximation was used to calculate hypothetical temperature profiles, examining the effect of different physical and computational parameters. It was not used for calculations which were compared to experimental results. Such calculations used linear interpolation on the experimental data.

Two basic cases were examined. In the first there was a discontinuity between the initial core temperature and the initial injection temperature. Initial core and initial injection temperature were the same for the second case.

A number of numerical experiments were carried out using the method of characteristics procedure described in Appendix B. As has already been stated, these experiments indicated that for experimental conditions such as those of Arihara, it was sufficient to use an average (constant) mass injection rate, and to consider the system to have constant thermal properties. The wave equation solution to this simplified case of constant thermal properties and mass injection rate reduces to a simple form described in section 3.3.2. The superposition algorithm described in Appendix B was used to generate temperature profiles for both the simplified wave equation solution and the parabolic equation solution.

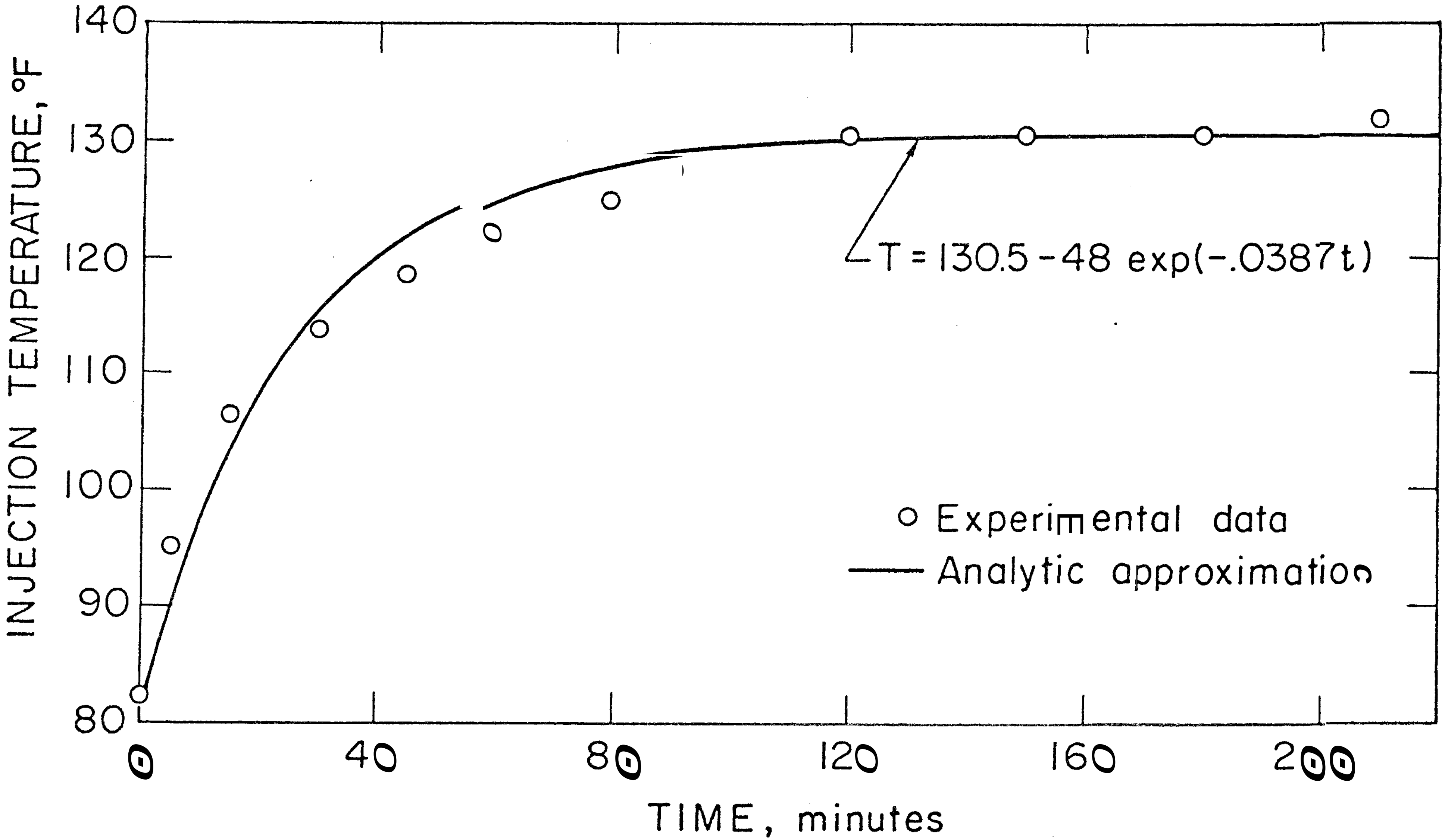

FIGURE 3.6. INJECTION TEMPERATURE vs TIME FOR EXPERIMENT HWI-B-1 OF ARIHARA

Fig. 3.7 presents calculations showing temperature profiles resulting when the analytic injection temperature history of Fig. 3.6 is applied to a hypothetical core with experimental conditions similar to those of run HWI-B-1 of Arihara. Four cases are presented for each time: one for zero axial thermal conductivity (the wave equation model), and three cases which include the effects of axial thermal conductivity values of 5, 10, and 15 BTU/(hr-ft-^{o}F). It can be seen that axial thermal conductivity does have an effect on the temperatures near the leading edge of the front, but that this effect becomes small behind the initial front. Thus, diffusion processes smooth the shock inherent in the wave equation solution, and cause early injection temperatures to advance rapidly through the core. However, these processes do not change the basic shape of the wave equation solution behind the front. This observation will become important when variable injection temperature calculations for both the wave and parabolic equation models are compared to the experimental results of Arihara in section 3.6.3 below.

Calculations using both different experimental conditions and continuity of initial core and initial injection temperature further demonstrated the above conclusions. Fig. 3.8, for example, presents calculations for the same conditions as Fig. 3.7, but with the initial injection temperature equal to the initial core temperature.

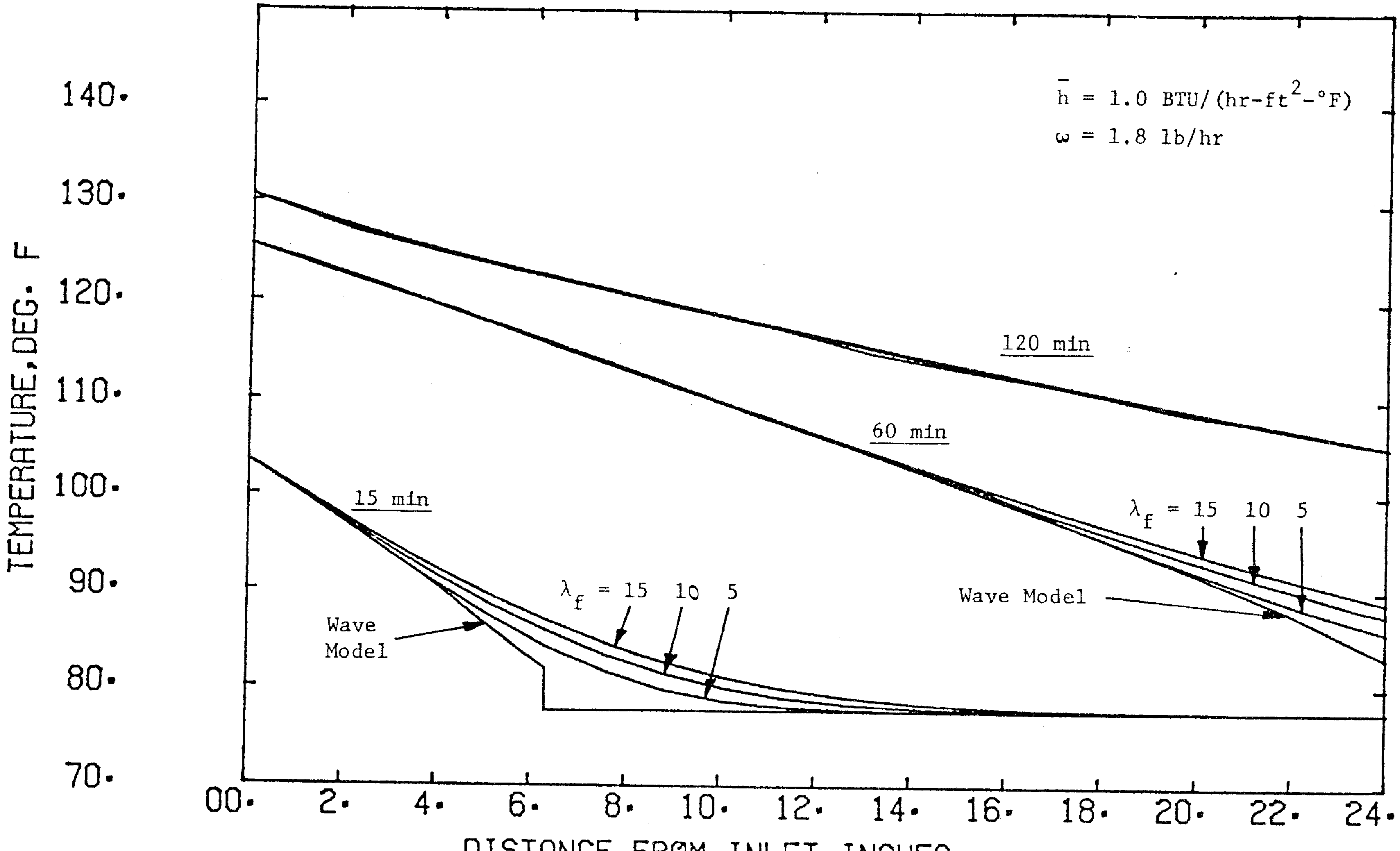

FIGURE 3.7. CALCULATED TEMPERATURES FOR EXPERIMENTAL CONDITIONS CORRESPONDING TO EXPERIMENT HWI-B-1 OF ARIHARA, AND THE ANALYTIC INJECTION TEMPERATURE HISTORY OF FIG. 3.6

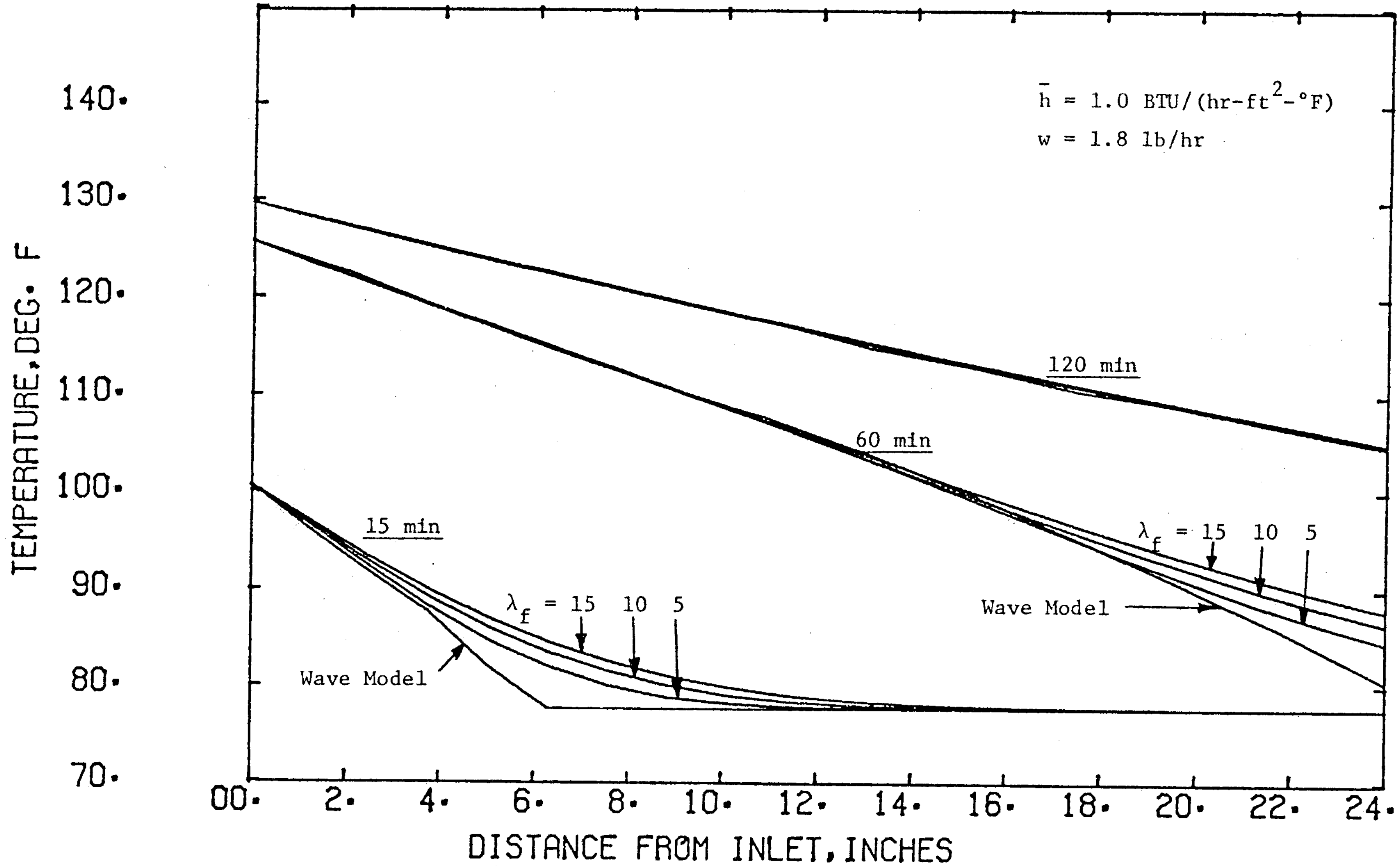

FIGURE 3.8. CALCULATED TEMPERATURES FOR ESSENTIALLY THE SAME CONDITIONS AS FIG. 3.7 EXCEPT THAT INITIAL INJECTION TEMPERATURE EQUALS THE EXTERNAL TEMPERATURE

It is convenient at this point to define terminology which will be used throughout the rest of this report. Three periods of time were observed during which Arihara's experimental data showed different characteristics. The first period is called the "early-time" period, and is defined as that period during which the injection temperature was changing rapidly. The second period is called the "medium-time" period, and occurs when the injection temperature was changing slowly, or approaching a constant value. The last period was the "long-time" period, and was characterized by steady temperatures throughout the core. While these terms are imprecise, they do serve a useful purpose for discussing the experimental data.

3.6 Comparison with Published Experimental Results

The behavior of the one-dimensional mathematical models can be compared with published experimental results of three different types. The first comparison may be made with the long-time temperature profiles for the hot and cold water injection experiments of Arihara (1974). The second comparison may be made with the conclusions of Crichlow (1972, pp. 82-88) concerning the effect of axial thermal conductivity on temperature profile behavior for the case of constant injection temperature. The conclusions of Crichlow with which the comparison is made are based on numerical experiments carried out with a finite-difference mathematical model. The third comparison may be made with the transient temperature behavior for the variable injection temperature experiments of Arihara that were mentioned in the preceding. Each of these comparisons is discussed in detail below.

3.6.1 Long-Time, Steady-State Results: Analysis presented in section 3.4.1 indicates that normalized steady-state temperature profiles should decay exponentially with distance. The hot and cold liquid injection experiments of Arihara tended to approach constant injection temperature a long times. It would thus be expected that a graph of $\ell n\,(|T-T_e|)$ versus distance for these long-time temperature vs. distance data should produce a straight line. Figs. 3.9 to 3.12 present such graphs for the long-time results of Arihara. It can be seen that many of the sets of data do fall on straight lines, but others do not (see Table 3.1).

There are two interpretations which explain satisfactorily why the data points do not fall on straight lines for most cases. An examination of the reported transient experimental data for two of the anomalous cases (CWI-S-1 and CWI-B-1) reveals one cause. The injection temperature was not constant for a long enough time for the entire profile to become steady.

The second interpretation is aimed at explaining why many of the hot water injection profiles were semi-log straight at the downstream end of the core, but increased in slope near the upstream end. The only apparently satisfactory explanation for this behavior found to date is the hypothesis that heat was being conducted through the mass of metal in the brass inlet plug and cap, and then along the steel shell, from which

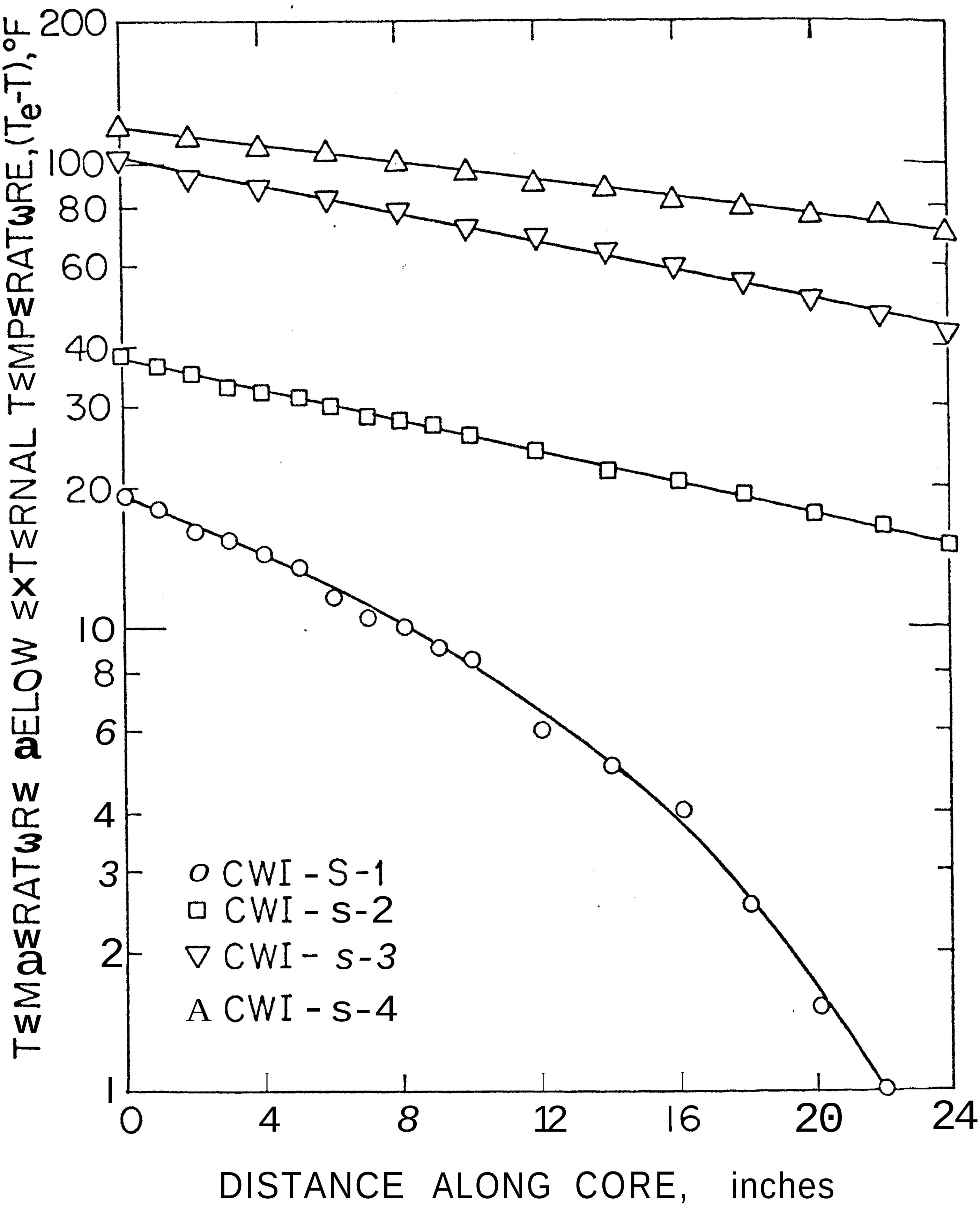

FIGURE 3.3. GRAPH OF LOG_{10} (T_e-T) VS. DISTANCE ALONG THE CORE FOR LONG TIME TEMPERATURES IN THE COLD WATER INJECTION EXPERIMENTS OF ARIHARA (CWI-S SERIES)

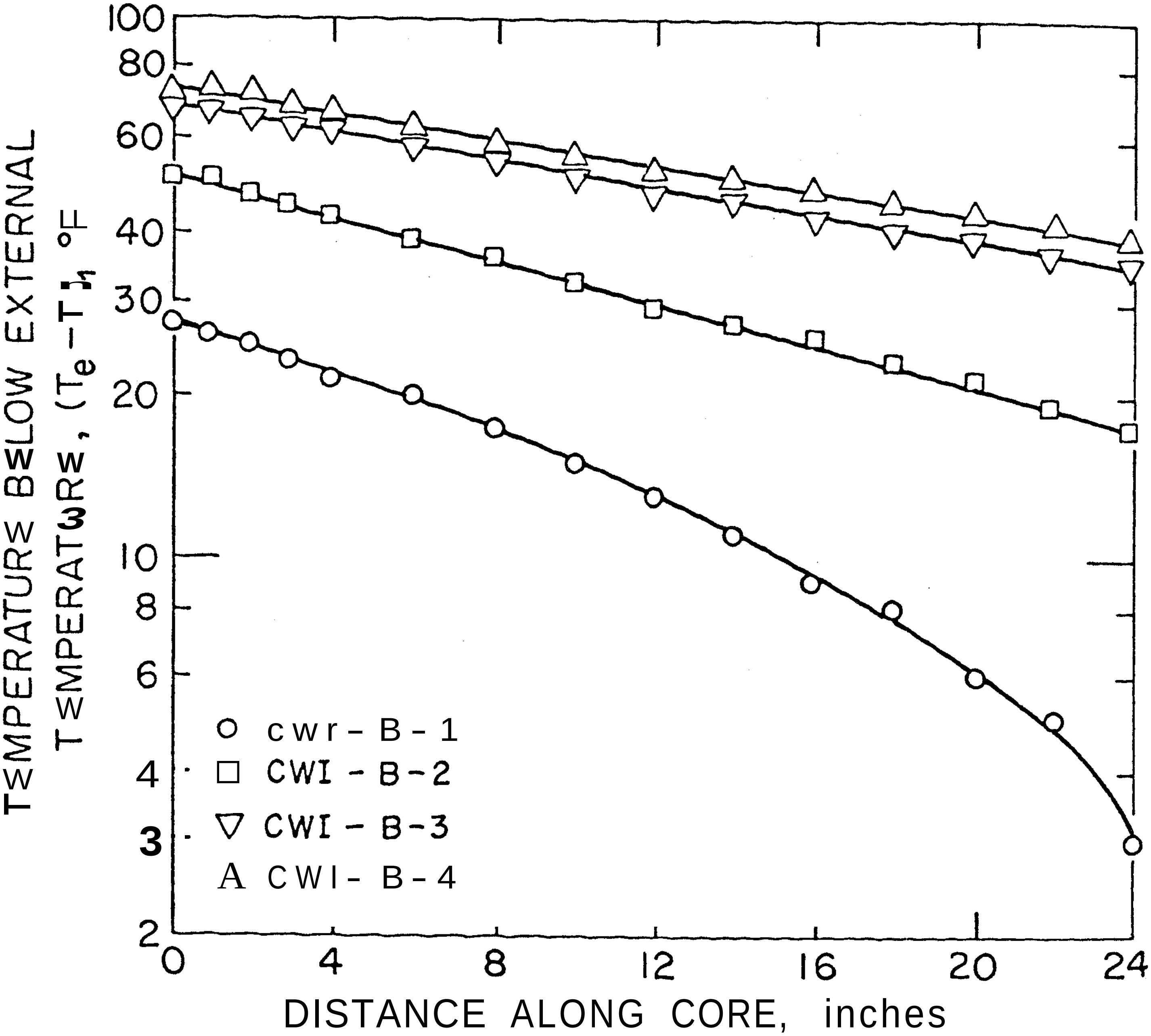

FIGURE 3.10. GRAPH OF LOG_{10} (T_e − T) VS DISTANCE ALONG THE CORE FOR LONG TIME TEMPERATURES IN THE COLD WATER INJECTION EXPERIMENTS OF ARIHARA (CWI-B SERIES)

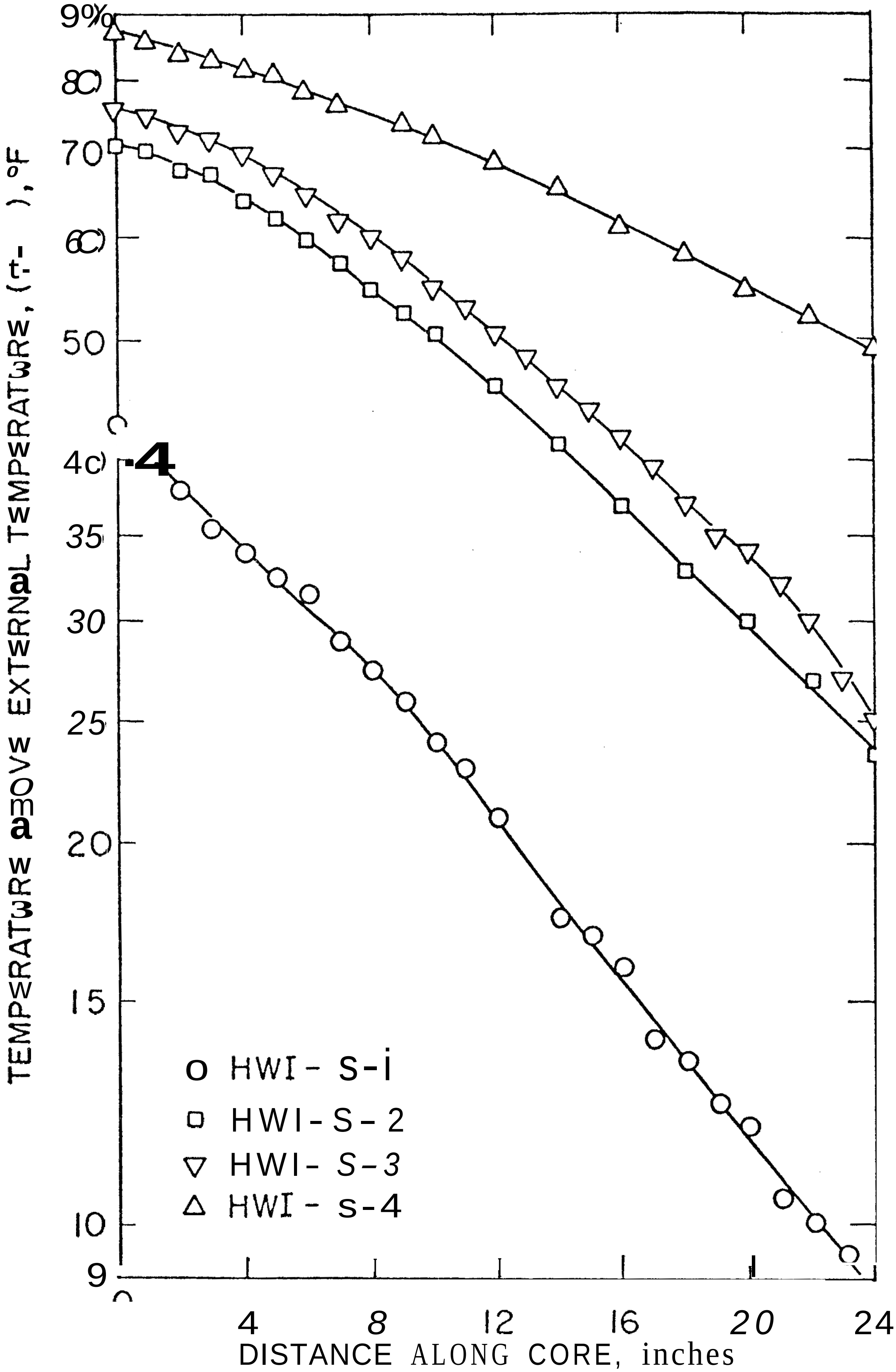

3.11 GRAPH OF LOG_{10} $(T-T_e)$ VS. DISTANCE ALONG THE CORE FOR LONG TIME TEMPERATURES IN THE HOT WATER INJECTION EXPERIMENTS OF ARIHARA (HWI-S SERIES)

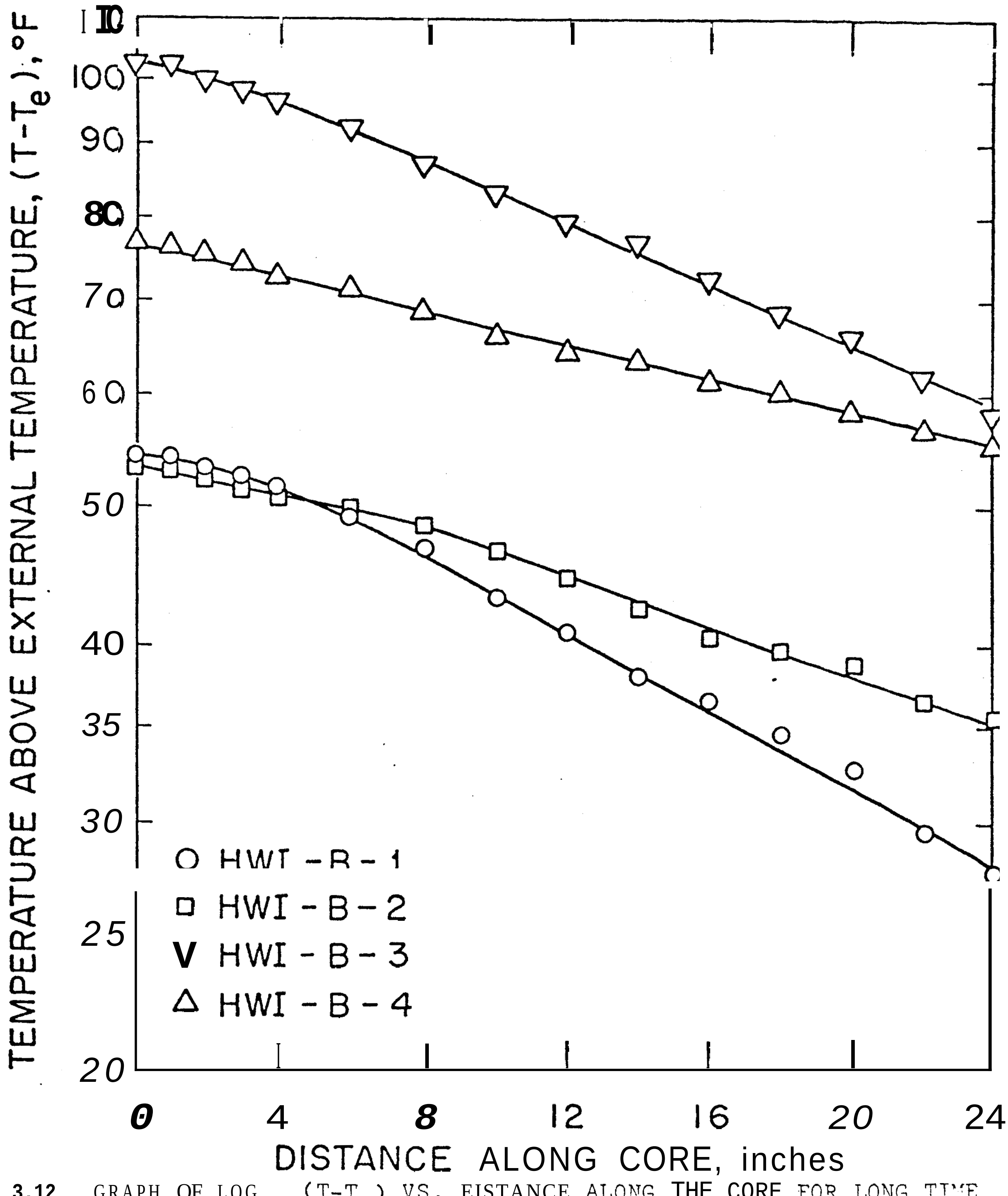

3.12 GRAPH OF LOG_{10} $(T-T_e)$ VS. EISTANCE ALONG THE CORE FOR LONG TIME TEMPERATURES IN THE HOT WATER INJECTION EXPERIYEYTS OF ARIHARA (HWI-B SERIES)

RUN	STRAIGHT LINE ON SEMI-LOG GRAPH?	EXPLANATION IF NO	AVERAGE MASS INJECTION RATE		$\bar{h}$ BASED ON REAL OR ESTIMATED STRAIGHT LINE, BTU/(hr-ft^2-°F)	VALUES OF $\bar{h}$ REPORTED BY ARIHARA	
			w lb/hr	w'' lb/min-ft^2		THEORETICAL VALUE BASED ON CORRELATIONS	APPROXIMATE ANALYSIS OF DATA
CWI-S-1	NO	1	0.97	0.74	1.81	2.00	2.08
CWI-S-2	YES		1.86	1.42	1.68	2.06	2.28
CWI-S-3	YES		2.88	2.20	2.38	2.23	2.44
CWI-S-4	YES		3.93	3.00	1.98	2.22	2.40
CWI-B-1	NO	1	1.38	1.06	1.80	2.12	2.45
CWI-B-2	YES		2.12	1.62	2.23	2.24	2.48
CWI-B-3	YES		2.92	2.23	1.85	2.23	2.38
CWI-B-4	YES		3.31	2.53	2.04	2.25	2.40
HWI-S-1	two lines	2 ?	0.57	0.44	0.76/0.96 ?	0.89	0.69
HWI-S-2	NO	2	0.82	0.63	1.04	1.04	0.83
HWI-S-3	NO	3	0.96	0.73	------	1.06	1.00
HWI-S-4	two lines	2 ?	2.10	1.62	0.93/1.37 ?	1.17	1.17
HWI-B-1	NO	2	1.80	1.38	1.31	1.06	1.25
HWI-B-2	NO	2	2.60	2.0	1.25	1.09	1.25
HWI-B-3	NO	2	2.20	1.68	1.22	1.21	1.25
HWI-B-4	YES		4.50	3.44	1.42	1.18	1.44

Explanations: 1. Steady state conditions not reached. Temperatures were still propagating down the core.
2. Thermal shielding by heat transfer along the outside of the coreholder system.
3. Original Experimental Data unclear.

TABLE 3.1 SUMMARY OF THE ANALYSIS OF LONG TIME EXPERIMENTAL TEMPERATURES REPORTED BY ARIHARA it was lost to the environment (see Fig. 3.13.a). If conduction along the steel shell raised the temperature of the shell for a distance down the coreholder, it would have the effect of shielding the core from heat losses by increasing the effective external temperature. The effect of thermal shielding would be to lower the apparent heat loss coefficient from the core to the environment, This hypothesis is consistent with the behavior of the observed anomalous temperature profiles.

The original experimental temperature charts can be examined to determine the flowing liquid temperatures a short distance upstream from the inlet brass plug. In some of the hot water injection cases, this temperature was significantly higher than the temperature at the entrance to the core. For example, in the HWI-B-1 experiment, the long-time upstream flowing liquid temperature outside the coreholder was 100°F higher than the long-time core inlet temperature. This is large compared to a maximum temperature drop along the core of 30°F, and a maximum temperature difference between the core and the external environment of 55°F.

The distance down the steel shell for which such thermal shielding might be significant was estimated with the use of thin rod theory (Carslaw and Jaeger, 1959, p. 133; Kreith, 1973, p. 56). This approximate analysis can be made by examining the decline of steady dimensionless temperature profiles along the infinitely long cylindrical thin rod indicated in Fig. 3.13.b. These profiles can be described (Kreith, 1973, Eq. 2-37, p. 57) by the equation:

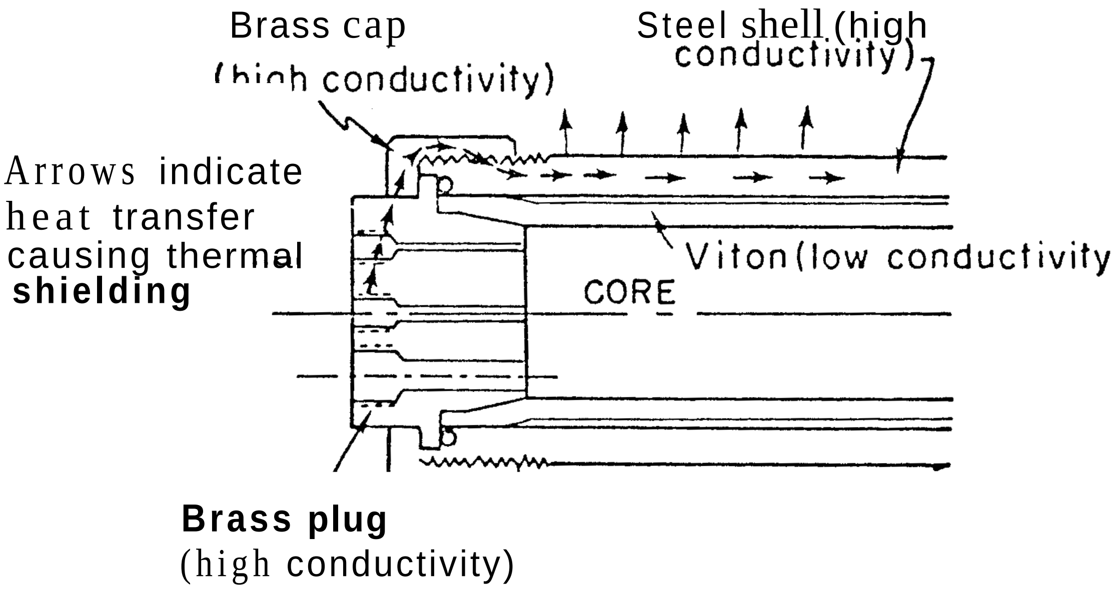

3.13a SCHEMATIC OF THE COREHOLDER SYSTEM SHOWING THE HYPOTHESIZED CAUSE OF THERMAL SHIELDING NEAR THE INLET

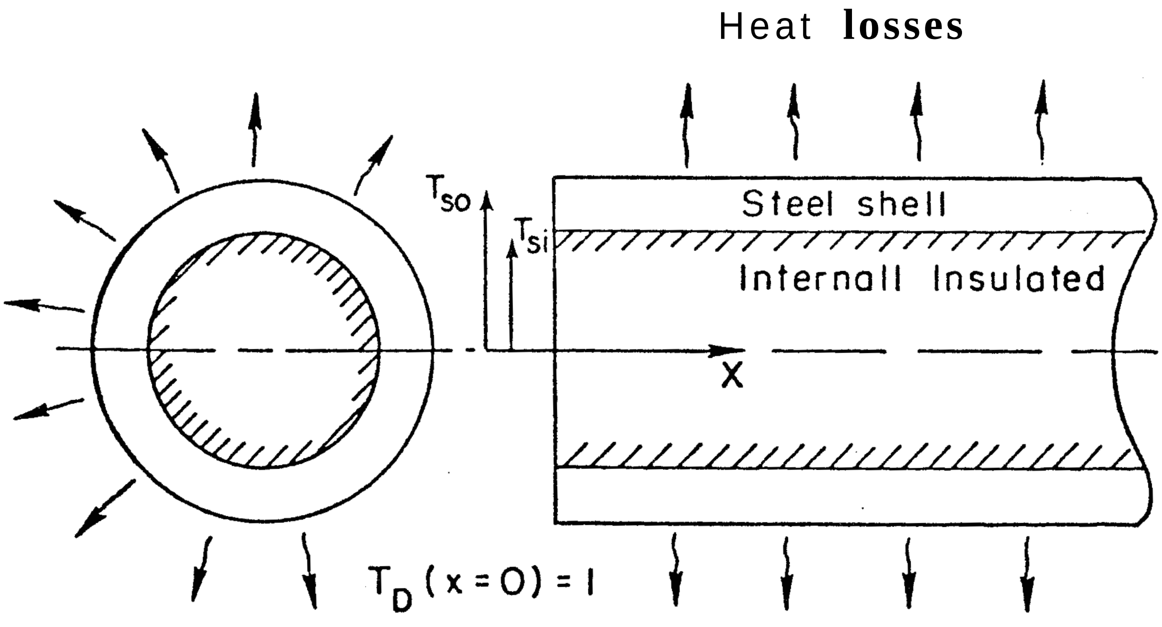

3.13b SCHEMATIC OF THE PHYSICAL SYSTEM CORRESPONDING TO THE SIMPLIFIED MATHEYATICAL MODEL OF THERMAL SHIELDING

$$\frac{d^2T}{dx^2} - m^2 (T-T_e) = 0 \tag{3.39}$$

where $m^2 \triangleq (h_e P)/(\lambda_{ss} A_{cs})$,

h_e = film coefficient between the steel shell and the external environment

P = perimeter from which convective heat losses are occurring

λ_s = thermal conductivity in the steel shell

A_{cs} = cross-sectional area through which conduction is occurring

For the case of an infinitely long rod, the solution in terms of dimensionless temperature, T_D, is:

$$T_D = \exp(-mx) \tag{3.40}$$

This solution was evaluated for parameters corresponding to the experimental conditions of Arihara. The results for h_e=1 and 5 BTU/(hr-ft2-°F) are presented in Fig. 3.14. It can be deduced from this figure that for the hot water injection experiments of Arihara wherein conduction through the brass inlet plug to the steel shell was probably substantial, thermal shielding along the steel shell could occur for distances which are on the order of inches or greater.

A more detailed analysis of the shape of the temperature profile along the core in the presence of thermal shielding was not made, even though this would not have been difficult.

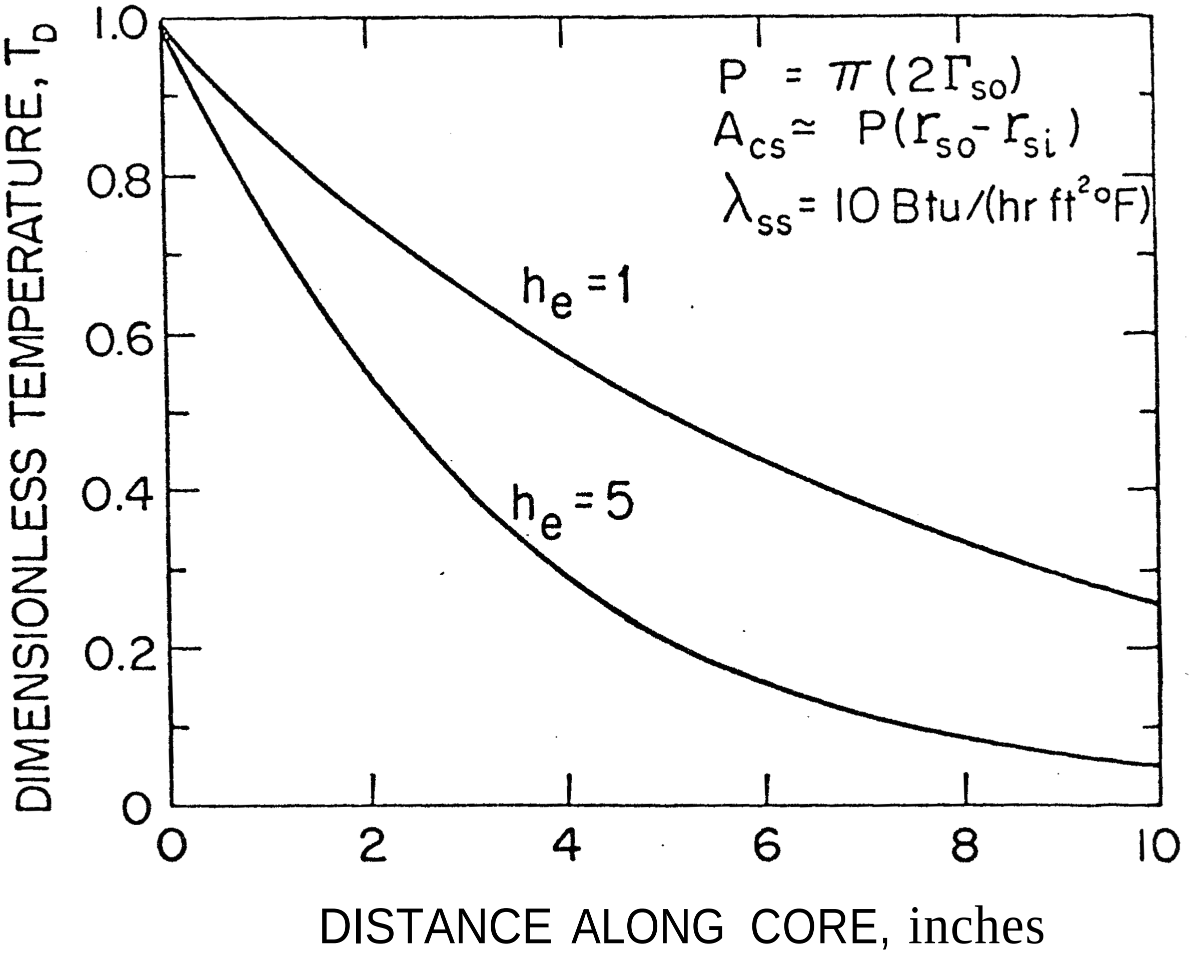

3.14 CALCULATED DIMENSIONLESS TEMPERATURES ALONG THE STEEL SHELL IF IT WERE VERY LONG AND INSULATED FROM THE CORE

Such analysis could demonstrate whether the temperature profiles in the shielded region would be expected to be semi-log straight lines. If this did occur, then the appearance of the two distinct semi-log straight lines in the experiments HWI-S-1 and HWI-S-4 might be explained.

Table 3.1 presents a summary of the results of analyzing the long-time temperature profiles of Arihara. Included in this table are values of $\bar{h}$ based on actual or estimated semi-log straight lines in Figs. 3.9 through 3.12, and values of $\bar{h}$ reported by Arihara. He reported both theoretical values based on existing correlations (Table 2, p. 81, and Table 3, p. 99 of Arihara), and experimentally determined values based on an approximate analysis of the data that assumed cartesian straight line temperature profiles (Table 1, p. 72 of Arihara).

Values of $\bar{h}$ for the cold water injection experiments based on semi-log straight lines in Figs. 3.9 and 3.10 tend to be about 10-20% less than the theoretical values reported by Arihara. This may be due to the fact that the values of h_f that Arihara used were 5 to 10 times larger than would have been forecast using the correlations between h_f and w" reported by Crichlow (1972, p. 100). The results of Colburn (1931; also presented by Jakob, 1957, pp. 553-557) indicate that h_f tends to increase as the grain size decreases for unconsolidated systems. Arihara (1974, p. 142) used two consolidated porous mediums with permeabilities that were substantially smaller than those of the unconsolidated porous mediums of Crichlow (1972, p. 179) (400 mD or less for Arihara as compared to 6.6 D for Crichlow). The porous mediums of Arihara would thus have much smaller pore sizes than those of Crichlow. Thus, it would be reasonable to expect higher values of h_f in the experiments of Arihara than in those of Crichlow, but it is not clear that they should be 5 to 10 times as large.

Arihara's cold water injection experiments had an estimated external film coefficient, h_e, of around 3.5 BTU/(hr-ft^2-^{o}F) (his Table 3, p. 99). This was larger than the value of h_e of roughly unity reported for the hot water injection experiments. An estimation of the value of $\bar{h}$ for the case with the higher external film coefficient would tend to be more sensitive to errors in estimating h_f than for the case with a lower h_e. This is because the overall thermal resistance of a circuit of greatly varying resistances in series will tend to be dominated by the largest one. In this case, this may be that at the external surface. This observation is consistent with the hypothesis that Arihara's estimated values of h_f are probably too high. This statement is based on the observation that while the cold water experiments usually had lower values of $\bar{h}$ than Arihara's theoretical calculations (as would be caused by over-estimating h_f), the hot water experiments usually had values of $\bar{h}$ close to those forecast by Arihara (as would occur if $\bar{h}$ were dominated by the lower h_e).

The overall heat transfer coefficient in the experiments of Arihara seemed to increase slightly with liquid injection rate. Fig. 3.15 presents values of $\bar{h}$ determined using the semi-log straight line analysis, as a function of w". This graph is similar to Fig. 23 of Arihara, which presents values of $\bar{h}$ found using an approximate method. Fig. 3.15 shows more scatter in the results than does Fig. 23 of Arihara. Because of this scatter, no attempt was made to analyze the nature of the functional dependence of $\bar{h}$ on w" further.

3.6.2 Constant Injection Temperature Results: In section 3.4, it was concluded that the addition of an effective axial thermal conductivity, λ_f, to the one-dimensional mathematical model had a major effect on the character of transient temperature profiles. Furthermore, changing the value of λ_f over a range of reasonable values for the mass flowrates of interest had an important effect on the shape of the computed temperature profiles.

This conclusion is not consistent with Crichlow's observation (1972, p. 83) that there was only a slight effect of λ_f on temperature distributions for flowrates of experimental interest (the range of flowrates reported by Crichlow falls within those reported by Arihara). This observation of Crichlow's is based upon a series of calculations using a finite-difference mathematical model. The physical model studied by Crichlow had external boundary conditions different from those of Arihara. The Arihara conditions involved transient radial

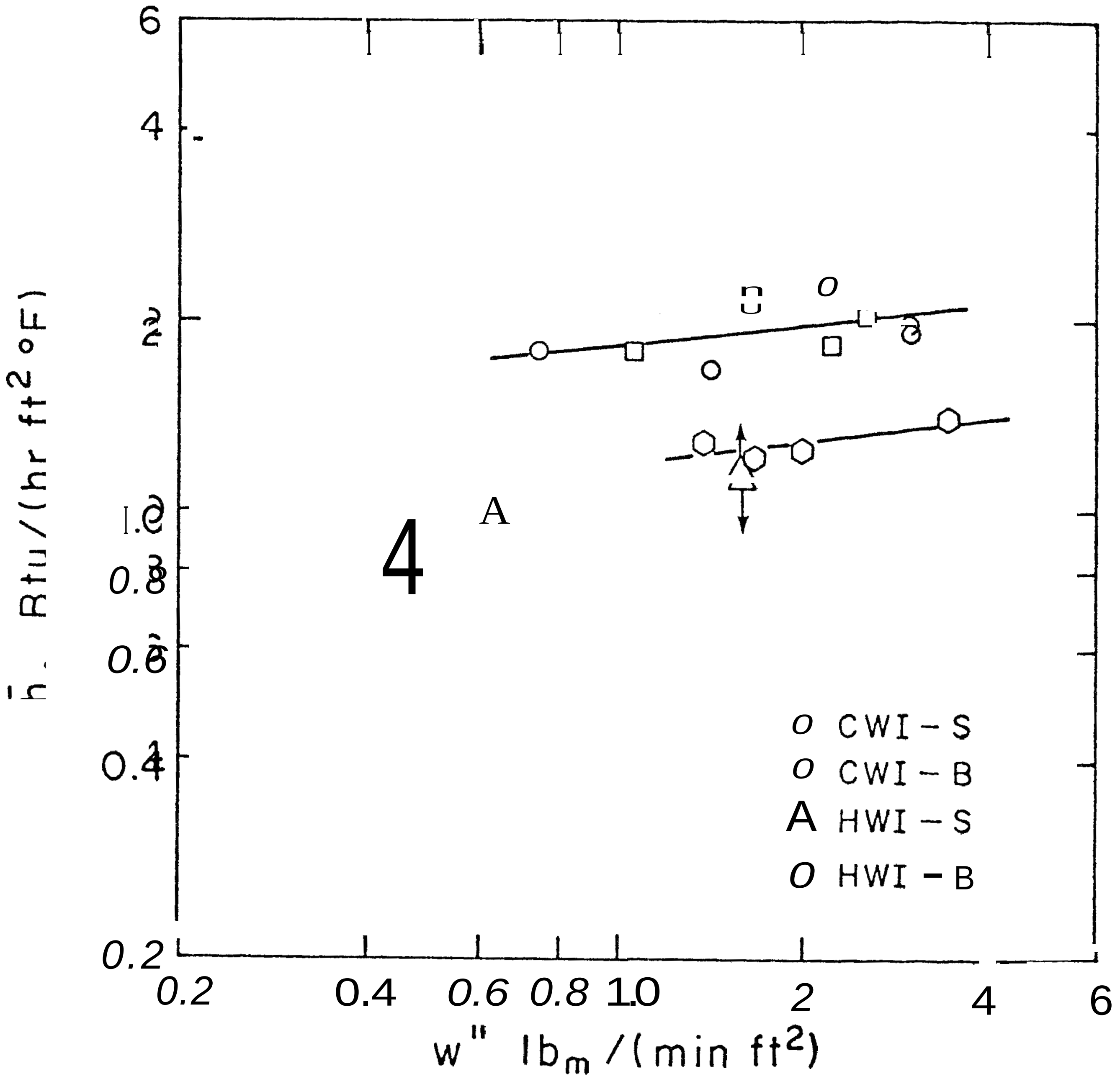

FIGURE 3.15. GRAPH OF $\overline{h}$, BTU/(hr-ft^2-°F), OBTAINED FROM THE SEMI-LOG STRAIGHT LINE ANALYSIS VS MASS INJECTION RATE PER UNIT CROSS-SECTIONAL AREA, w'', lb/(min-ft2), FOR THE SINGLE-PHASE NONISOTHERMAL FLUID INJECTION EXPERIMENTS OF ARIHARA

heat loss through a thick, low-conductivity medium which surrounded the core. However, the difference between the Crichlow and Arihara systems would not be expected to affect overall conclusions about the effect of axial thermal conductivity on temperature profiles. Crichlow's calculations examined the effect of varying λ_f on temperature profiles for a range of mass injection rates. These calculations showed a significant effect for flowrates lower than could be obtained in the laboratory (Crichlow, 1972, Figs. 28 and 29), and little effect at higher flowrates (his Fig. 30).

In order to attempt to rationalize the disagreement between the results of Crichlow and those reported herein, an approximate analysis was made to determine the conduction lengths that would be expected for the physical conditions of interest. Such an analysis can be made easily for the limiting case of Eq. 3.39 when $\bar{h} = 0$, and can give an indication of the length dimensions in the system over which axial conduction effects will be important. These calculations are directly analogous to mixing-length calculations as applied to miscible displacement phenomena in porous media (Brigham, 1974). The calculations confirmed Crichlow's observation that conduction dominates the flow behavior over length dimensions of the length of the core for mass flowrates lower than could be obtained in the laboratory. However, the calculations indicated that while conduction does not dominate the heat transfer at the flowrates of interest over these length dimensions, it is important enough to have at least a second order effect on the conduction length. Finally, the values of axial thermal conductivity used by Crichlow for his higher mass injection rate cases were much lower than would be expected, based on the results of Adivarahan, et al. (1962).

3.6.3 Time-Dependent Injection Temperature Results: A series of calculations were made in an attempt to reproduce the transient temperature behavior of the hot and cold water injection experiments of Arihara. In every case, the simulated physical dimensions, average thermal properties, average mass injection rate, and injection temperature history corresponded closely to the reported experimental results. Only the overall heat transfer coefficient, $\bar{h}$, and the axial thermal conductivity, λ_f, were allowed to vary.

The first set of calculations simulated the HWI-B-1 experiment. Fig. 3.16 presents the calculated temperature profiles using $\bar{h}$ = 1.25 BTU/(hr-ft^2-$^\circ$F) at three times, and for two cases of axial thermal conductivity $\lambda_f = 0$ and 10 BTU/(hr-ft-$^\circ$F). The measured experimental temperature data are also presented. The comparison of calculated long-time temperature profiles with the measured results is reasonable considering the presence of anomalous behavior as discussed in section 3.6.1. However, the profiles calculated at earlier times do not compare very well with the measured profiles. Fig. 3.17 presents calculations for all of the same parameters as Fig. 3.16, except for a value of

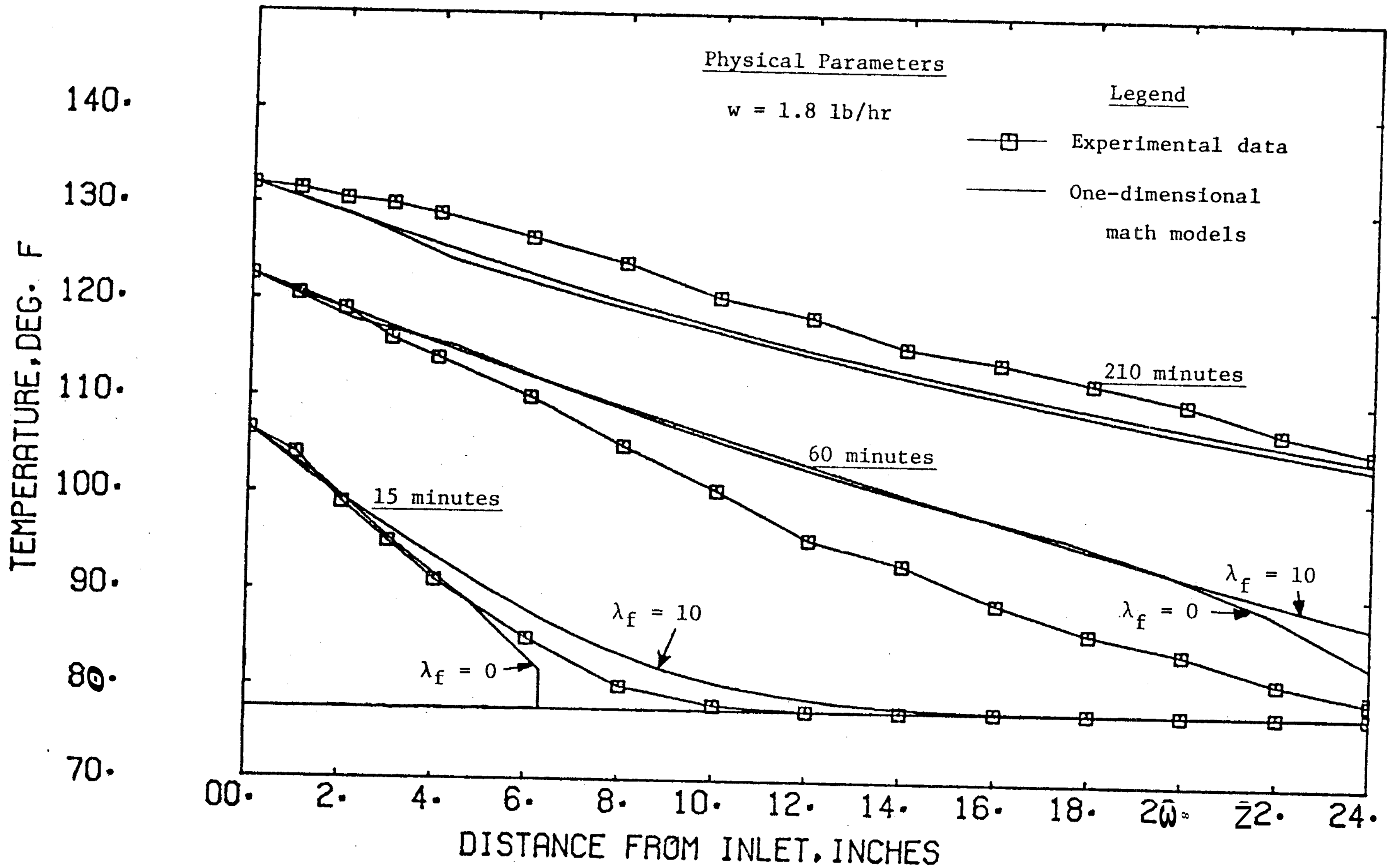

FIGURE 3.16. CALCULATED AND EXPERIMENTAL TEMPERATURES FOR EXPERIMENT HWI-B-1 OF ARIHARA, $\overline{h}$ = 1.25 BTU/(hr-ft^2-°F)

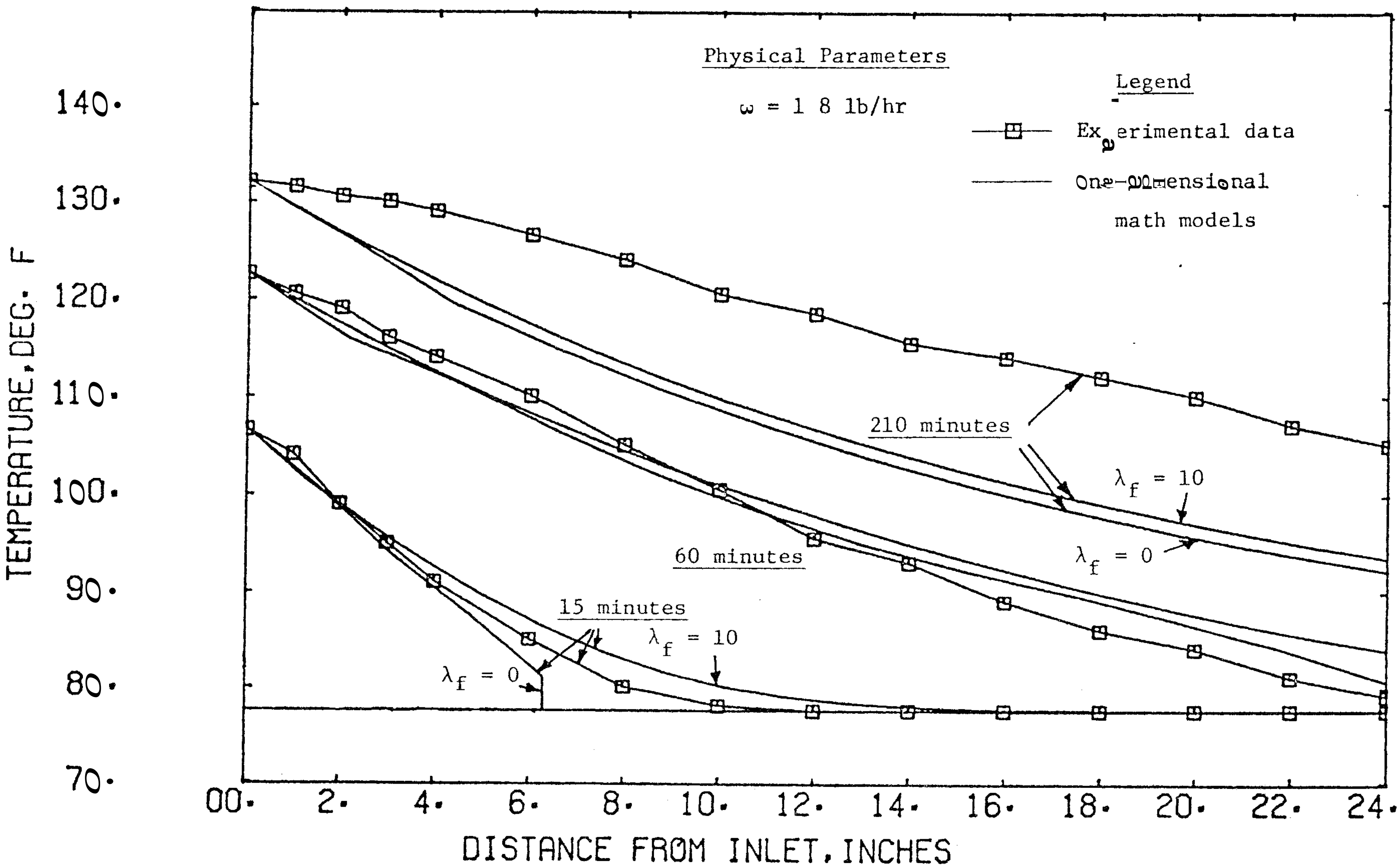

FIGURE 3.17. CALCULATED AND EXPERIMENTAL TEMPERATURES FOR EXPERIMENT HWI-B-1 OF ARIHARA, $\bar{h}$ = 2.25 BTU/(hr-ft^2-°F)

$\bar{h}$ = 2.0 BTU/(hr-ft^2-$^\circ$F). In this case, the comparison of calculated early-time profiles with those measured is much better than before. However, the long-time calculated profiles are much lower than the measured values. Figs. 3.16 and 3.17 seem to suggest that the transient temperature profiles are affected by a heat loss coefficient larger than that controlling the steady-state behavior. This is not surprising.

This observation was found to be substantially correct for all of the single-phase experiments of Arihara that were examined. Fig. 3.18, for example, compares calculated and experimental temperature profiles for the CWI-B-2 experiment. The long time profiles in this experiment agreed with the theoretically forecast results of section 3.4 (see also 3.6.1), and hence a good value of $\bar{h}$ = 2.23 BTU/(hr-ft^2-$^\circ$F) (see Table 3.1) could be obtained for the overall heat transfer coefficient. Fig. 3.18 presents calculations for this value of $\bar{h}$, for the cases of λ_f = 0 and 10 BTU/(hr-ft-$^\circ$F). Fig. 3.19 compares measured profiles with calculations for the same conditions as the previous figure, except for a value of $\bar{h}$ = 4 BTU/(hr-ft^2-$^\circ$F). The correspondence of calculated behavior with measured behavior can be seen in Fig. 3.18 for long times, and in Fig. 3.19 for shorter times. Figs. 3.20 and 3.21 present similar results for an experiment of Arihara that was run on a different porous medium (CWI-S-2).

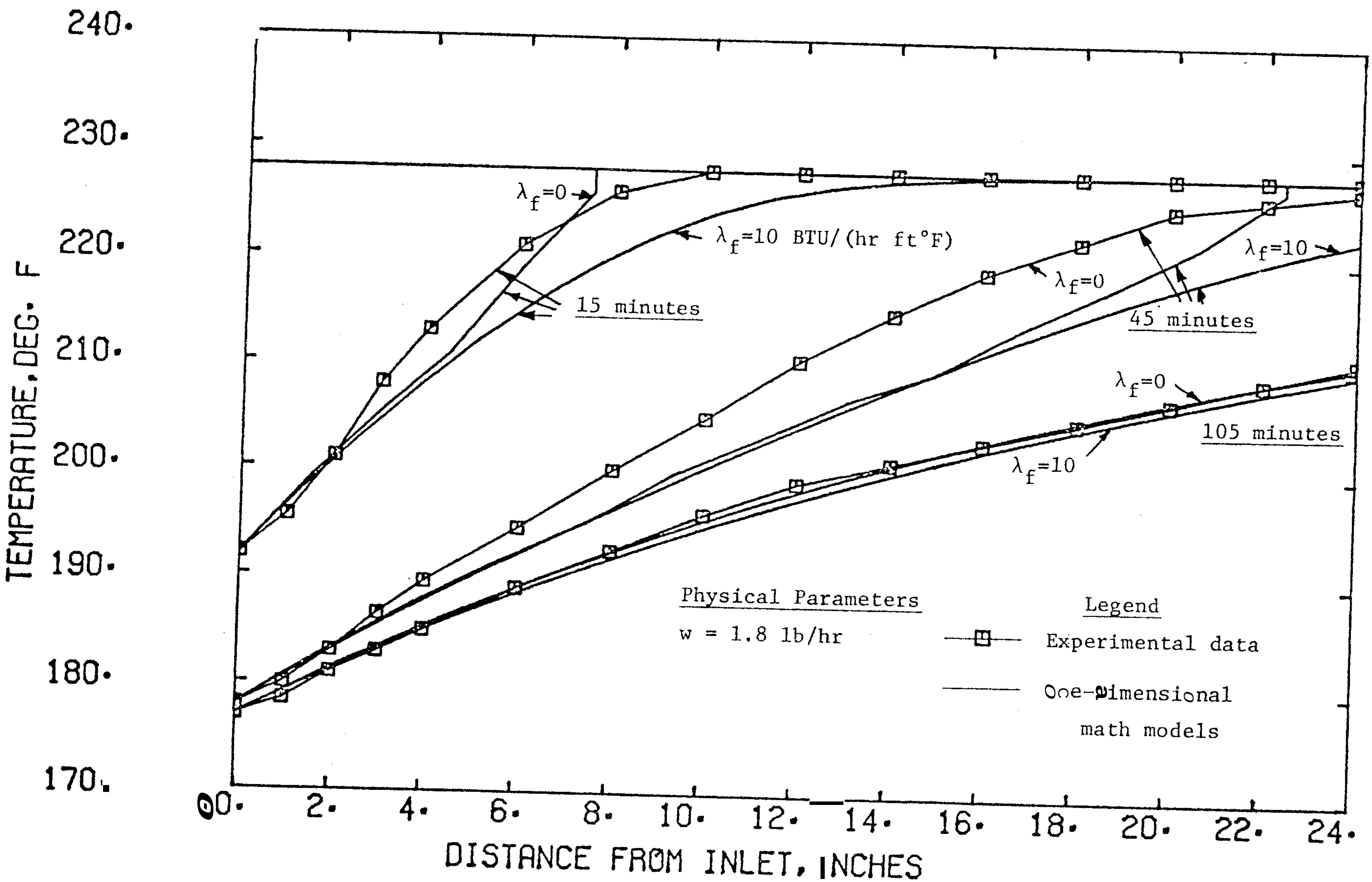

FIGURE 3.18. CALCULATED AND EXPERIMENTAL TEMPERATURES FOR EXPERIMENT CWI-B-2 OF ARIHARA, $\overline{h}$ = 2.23 BTU/(hr-ft^2-°F)

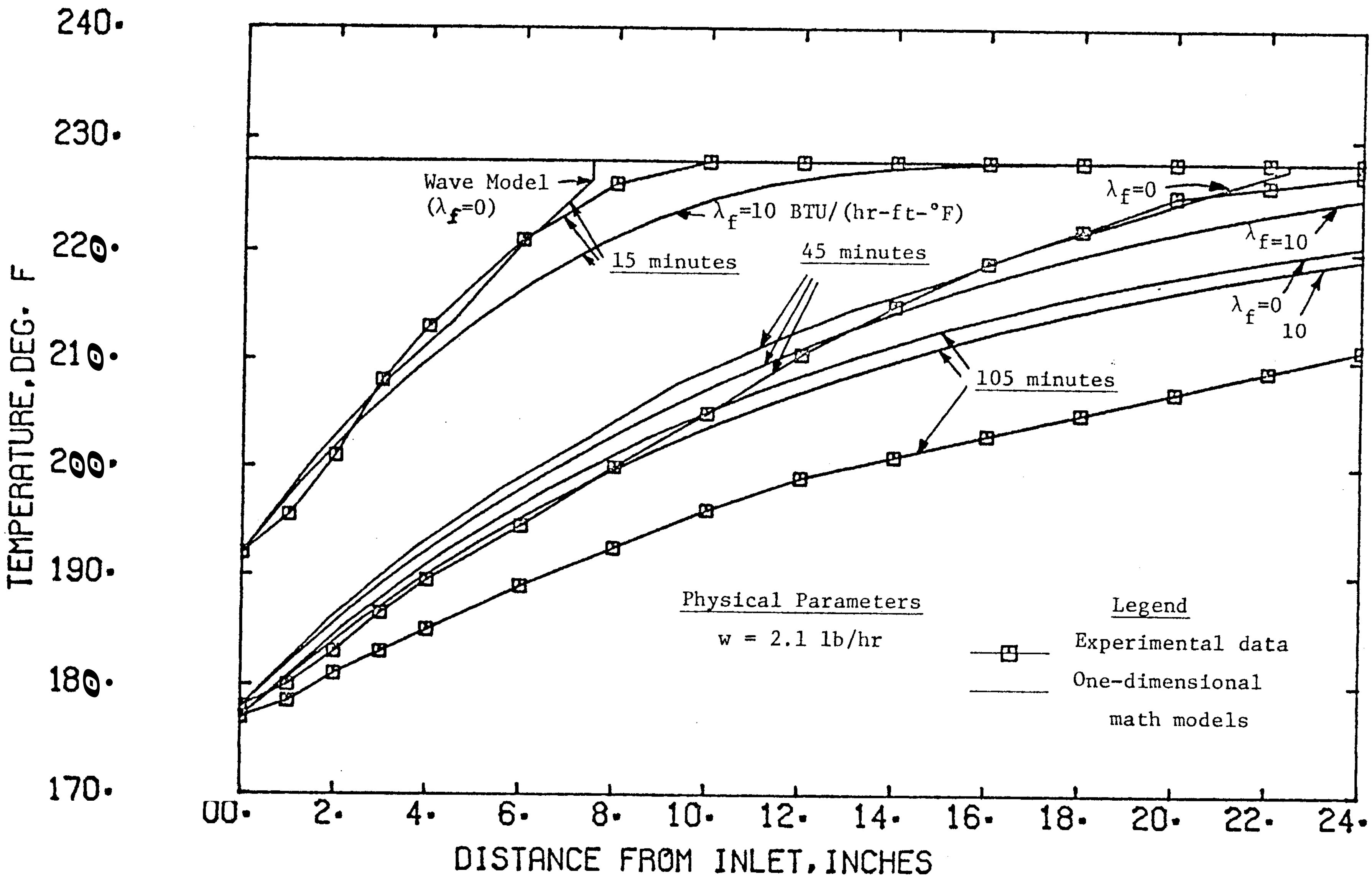

FIGURE 3.19. CALCULATED AND EXPERIMENTAL TEMPERATURES FOR EXPERIMENT CWI-B-2 OF ARIHARA, h = 4.0 BTU/(hr-ft^2-°F)

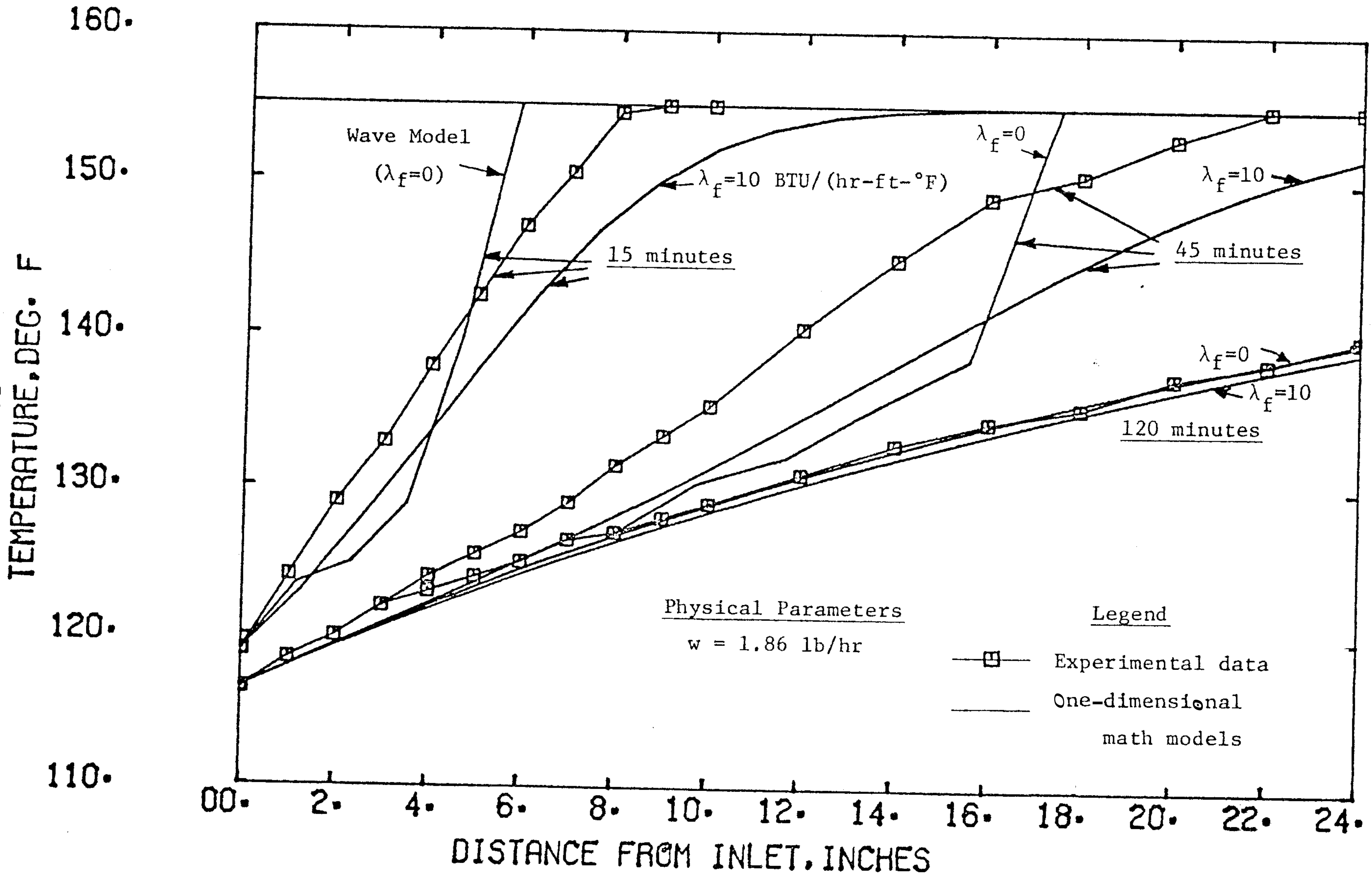

FIGURE 3.20. CALCULATED AND EXPERIMENTAL TEMPERATURES FOR EXPERIMENT CWI-S-2 OF ARIHARA, $\bar{h}$ = 3.5 BTU/(hr-ft^2-°F)

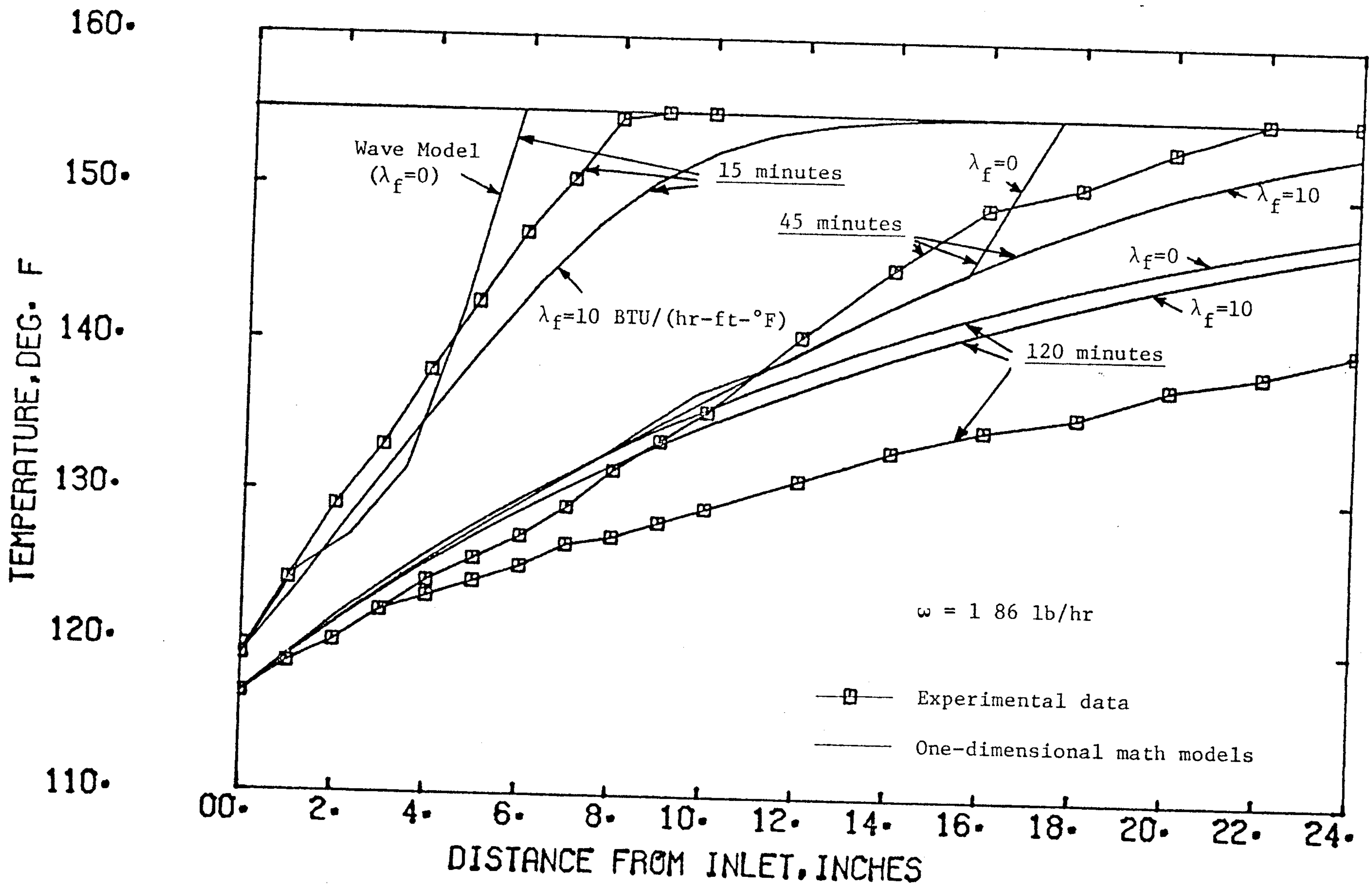

FIGURE 3.21. CALCULATED AND EXPERIMENTAL TEMPERATURES FOR EXPERIMENT CWI-S-2 OF ARIHARA, $\overline{h}$ = 3.5 BTU/(hr-ft^2-°F)

The effect upon calculated temperature profile behavior caused by changing the parameters $\bar{h}$ and λ_f can be seen from Figs. 3.16 to 3.21. The value of $\bar{h}$ affects the overall temperature level in the system, while λ_f has an important effect only near the leading edge of the early temperature fronts. It does not seem possible to reproduce the experimental results of Arihara accurately by varying $\bar{h}$ and λ_f. The appearance of an effective overall heat transfer coefficient which is higher during the transients than at steady state suggests that other heat transfer mechanisms than those contained in the mathematical model are important. In particular, the heat losses from the core may have initial transients which affect the early-time behavior. This suggestion was made by Arihara (1974, pp. 63, 82), and is consistent with the experimental results. It is discussed further in the next section.

3.7 Conclusions about the One-Dimensional Models

The results of calculations based on the one-dimensional mathematical models, and their comparison with published experimental results, can be summarized in the following conclusions:

1) Thermal properties and mass injection rates can be considered to be constant under the experimental conditions of Arihara.

2) The steady state temperature profiles reported by Arihara agree with the theoretical results developed in section

3.4, except when thermal shielding due to conduction along the coreholder occurs. These profiles depend slightly upon the effective axial thermal conductivity of the core.

3) An experiment consisting of measuring a series of steady-state temperature profiles at different mass injection rates has been proposed. This experiment seems to offer the possibility of determining the internal film coefficient, h_f, between the core and the coreholder, as well as the external film coefficient, h_e, between the coreholder and environment.

4) Axial thermal conductivity has a significant effect upon transient temperature profiles resulting from a constant injection temperature for experimental conditions reported by Crichlow and Arihara. This effect is smaller for the case of variable injection temperature. In this latter case, the effect is felt primarily at the leading edge of the temperature front.

5) The one-dimensional mathematical model cannot reproduce the experimental transient temperature profiles accurately in the variable injection temperature experiments reported by Arihara over the full range of time. The early-time behavior appears to be controlled by an effective heat transfer coefficient which is larger than that controlling the long-time behavior.

6) It is proposed that the transient behavior of Arihara's experiments was affected by transient radial heat transfer through the coreholder system.

7) The heating efficiency of a process described by the wave model initially depends only on time. After the temperature front has reached the outlet end of the core, the heating efficiency also depends on the length of the core. The heating efficiency of a process described by the parabolic model depends on axial thermal conductivity as well as on time at early times before the temperature front reaches the outlet end of the core. The heating efficiency of this model is similar to that of the wave model at long times.

4. PSEUDO TWO-DIMENSIONAL MODELS USING THE LUMPED PARAMETER APPROXIMATION

4.1 Introduction

One of the weakest assumptions in the one-dimensional mathematical models is the consideration of heat losses through the coreholder as being steady. The possibility of transients through the coreholder is discussed in quantitative terms in Appendix A (No. 3). The existence of transients is strongly indicated by an inability to match calculations using the one-dimensional solutions to the experimental results of Arihara (see section 3.6.3).

A mathematical model which incorporates the radial transients through the coreholder system can be formulated. However, this model is not amenable to straightforward analytic solution. It is possible to simplify the analytic solution to this model if the transient heat losses are considered to be of a simple form. This form considers the transients as being caused only by the heat capacity of the viton sleeve surrounding the core. An examination of the diffusivities of the various coreholder components in Table A.I indicates that this is reasonable, because viton appears to have the lowest thermal diffusivity of all the coreholder components. The thermal capacity of the viton is considered to be concentrated at the inside boundary of the viton sleeve. Heat losses through the rest of the coreholder system are still considered to be steady; that is, directly proportional to the temperature difference between the inside boundary of the viton and the external airbath. As heat travels from the core to the coreholder, it first heats the viton, and then passes through the coreholder system to the external environment. Initially, all heat losses from the core heat the viton. As the viton warms, heat begins to transfer to the external environment. Finally, at long times after the viton has completely heated, all heat losses from the core pass through the coreholder system to the external environment.

This is commonly called a lumped-parameter approach. The resulting heat transfer model of the transients through the coreholder is depicted in terms of an analogous thermal circuit representation in Fig. 4.1. The thermal resistances, R, are all based on the core perimeter, and are given by:

$R_f = 1/h_f$ = thermal resistance due to the film coefficient between the core and the viton

$R_v = r_o \ln (r_{vo}/r_o)/\lambda_v$ = thermal resistance across the viton

$R_A = r_o \ln (r_{si}/r_{vo})/\lambda_A$ = thermal resistance across the annulus

$R_{ss} = r_o \ln (r_{so}/r_{si})/\lambda_{ss}$ = thermal resistance across the steel shell

$R_e = r_o/(r_{so} h_e)$ = thermal resistance at the outside surface of the steel shell due to an external film coefficient

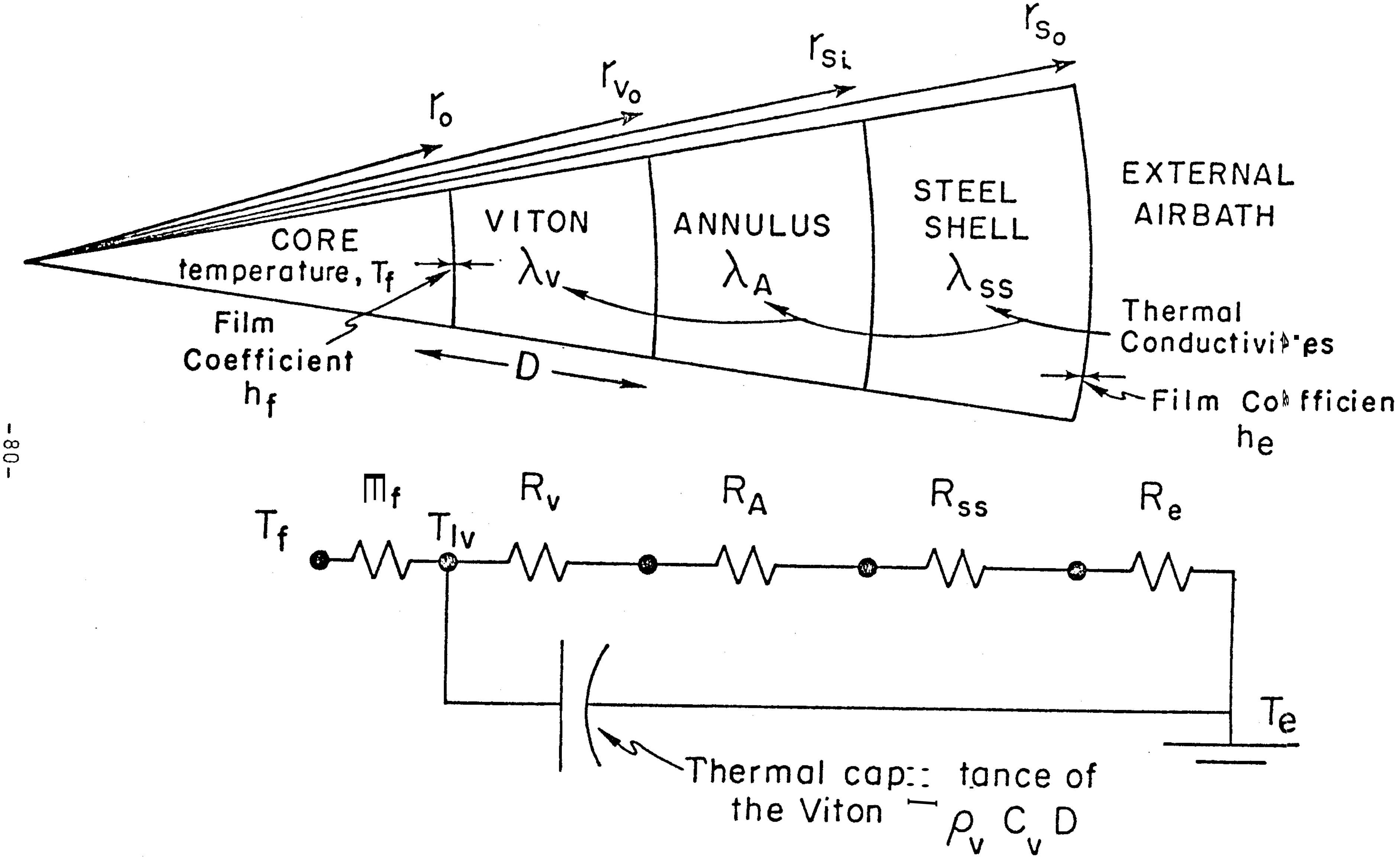

FIGURE 4.1. SCHEMATIC OF THE COREHOLDER COMPONENTS, AND A THERMAL CIRCUIT REPRESENTATION OF HEAT LOSSES THROUGH THESE COMPONENTS

where the symbols are indicated in Fig. 4.1, and are defined in the Nomenclature section. These expressions for thermal resistance are for heat transfer rate per unit area of the core exposed to heat losses. Thus, the heat loss rate to the external environment per unit exposed surface area of core is $\dot{Q}''$, and is given by:

$$\dot{Q}'' = \frac{(T_{\ell v}-T_e)}{R_f+R_v+R_A+R_{ss}+R_e} = \frac{(T_{\ell v}-T_e)}{R_f+R_{int}+R_e} \tag{4.1}$$

where:

$T_{\ell v}$ = lumped temperature of the viton

$R_{int} = R_v + R_A + R_{ss}$ = internal thermal resistance due to conduction through the coreholder system.

If the thickness of the viton, D, is small with respect to r_o, then the viton can be approximated as a plane instead of a cylinder. In this case, its thermal capacitance is $\rho_v C_v D$, where heat transfer is again in terms of the unit area (peripheral) of the core exposed to heat losses. Thus, if the rate of change of temperature in the viton is dT/dt, then the instantaneous rate of heat transfer per unit exposed surface area of the core required to heat the viton is: $\rho_v C_v D(dT/dt)$.

4.2 The Lumped Parameter Assumption

This assumption can be justified when the thermal resistance at the surface of a body is large compared to its internal thermal resistance to heat conduction. If this is the case, the temperature in the body should be uniform, and its behavior is largely dominated by the surface resistances. This can be expressed quantitatively in terms of the Riot dimensionless number, which is a measure of the conductance at the surface to the conductance in the body:

$$Bi \triangleq \frac{hL}{\lambda} \tag{4.2}$$

where L is a characteristic length of the system, and h and λ are defined in the Nomenclature section. The lumped parameter assumption is good when:

$$Bi \leq 0.1 \qquad \text{(Kreith, 1973, p. 140).}$$

Considering only the viton sleeve in the coreholder system, Biot numbers can be calculated based on either the internal film coefficient, h_f, or the external film coefficient, h_e. Values of the Biot number based on h_f values of from 5 to 10 BTU/(hr-ft^2-^{o}F) are in the range of 0.8 to 1.6. Using values of h_e of from 1 to 2 BTU/(hr-ft^2-^{o}F), one obtains Biot numbers ranging from 0.15 to 0.30.

Based on these simple Biot number calculations, it would appear that the lumped parameter approach might not give very good results. However, because of the significant simplification in the overall analytic problem resulting from making this approximation, its adequacy was further investigated. Appendix D compares the behavior of the simplified lumped parameter model of heat losses through the coreholder system with an analytic solution which accounts for transients in a single viton layer. The calculations presented in this Appendix suggest that while the lumped parameter model cannot reproduce the transient heat losses from the core accurately, it does give an approximate representation of these losses over the range of time of interest.

4.3 Mathematical Model

The physical system and assumptions required for the two-dimensional mathematical model are essentially the same as those used for the parabolic model in section 3. However, axial thermal conduction is neglected, and transient heat losses through the coreholder are considered in the same manner discussed above and in Appendix D. This mathematical model is hereafter referred to as the "pseudo two-dimensional model," because it does not fully account for heat' flow in two dimensions.

The equation describing local heat losses through the lumped thermal capacitance of the viton insulator is presented in Appendix D (Eq. D.11), and is:

$$\eta \frac{\partial T_{\ell v}}{\partial t} + T_{\ell v} = \delta + \zeta T_f \tag{4.3}$$

where:

$$\eta \triangleq \frac{\rho_v C_v D}{h_f + h_e}$$
$$\delta \triangleq \frac{h_e T_e}{h_f + h_e} \tag{4.4}$$
$$\zeta \triangleq \frac{h_f}{h_f + h_e}$$

and the symbols are defined in the Nomenclature section. The equation describing the interaction of transient heat losses from the core, and convective heat transport through it, is the same as the parabolic model in section 3, except that the heat losses are proportional to $(T_f - T_{\ell v})$ instead of $(T_f - T_e)$, and there is no axial conduction $(\beta = \lambda_f = 0)$. Thus, this equation becomes:

$$\frac{\partial T_f}{\partial t} + \alpha \frac{\partial T_f}{\partial x} + \gamma \, (T_f - T_{\ell v}) = 0 \qquad (4.5)$$

where α and y have definitions similar to those in section 3 (α is the same, y has an h_f instead of an $\bar{h}$):

$$\alpha \triangleq \frac{wC_w}{A_c M_f}$$

$$\gamma \triangleq \frac{h_f P}{A_c M_f} \qquad (4.6).$$

Thus, the pseudo two-dimensional mathematical model can be expressed as follows in terms of formation temperature, T_f, and lumped viton insulator temperature, $T_{\ell v}$:

$$\eta \frac{\partial T_{\ell v}}{\partial t} + T_{\ell v} = \delta + \gamma T_f, \; t>0, \; x \geq 0 \qquad (4.3)$$

$$\frac{\partial T_f}{\partial t} + \alpha \frac{\partial T_f}{\partial x} + \gamma \, (T_f - T_{\ell v}) = 0, \; t>0, \; x \geq 0 \qquad (4.6)$$

with boundary conditions

$$T_f \, (0,t) = T_i, \; t>0 \qquad (4.7)$$

$$\lim_{x\to\infty} \frac{\partial T_f}{\partial x}(x,t) = \lim_{x\to\infty} \frac{\partial T_{\ell v}}{\partial x}(x,t) = 0, \quad t>0 \tag{4.8}$$

and initial conditions

$$T_f(x,0) = T_{\ell v}(x,0) = T_e, \quad x \geq 0 \tag{4.9}.$$

The system of Eqs. 4.3 to 4.9 can be converted into non-dimensional form by defining nondimensional temperatures, time, and distance:

$$T_{Df} \triangleq \frac{T_f - T_e}{T_i - T_e}$$

$$T_{D\ell v} \triangleq \frac{T_{\ell v} - T_e}{T_i - T_e}$$

$$t_{DT} \triangleq \frac{1}{\eta} \cdot t \tag{4.10}.$$

$$x_{DT} \triangleq \frac{1}{\eta\alpha} \cdot x$$

For notational convenience, replace T_{Df} by u, and $T_{D\ell v}$ by v:

$$u \triangleq T_{Df}$$

$$v \triangleq T_{D\ell v} \, .$$

The initial boundary value problem (Eqs. 4.3 to 4.10) thus becomes:

$$\frac{\partial v}{\partial t_{DT}} + v = \zeta u, \; x_{DT} \geq 0, \; t_{DT} > 0 \tag{4.11}$$

$$\frac{\partial u}{\partial t_{DT}} + \frac{\partial u}{\partial x_{DT}} + \omega\,(u - v) = 0, \; x_{DT} \geq 0, \; t_{DT} > 0 \tag{4.12}$$

$$u\,(0, t_{DT}) = 1, \; t_{DT} > 0 \tag{4.13}$$

$$\frac{\partial u}{\partial x_{DT}}\,(\infty, t_{DT}) = \frac{\partial v}{\partial x_{DT}}\,(\infty, t_{DT}) = 0, \; t_{DT} > 0 \tag{4.14}$$

$$u\,(x_{DT}, 0) = v\,(x_{DT}, 0) = 0, \; x_{DT} > 0 \tag{4.15}$$

where
$$\omega \stackrel{\Delta}{=} \eta\gamma \tag{4.16}$$.

This problem is characterized entirely by the nondimensional parameters:

$$\zeta \stackrel{\Delta}{=} \frac{h_f}{h_e + h_f} \text{ , and}$$

$$\omega = \eta\gamma = \frac{h_f}{h_f + h_e} \cdot \frac{\rho_v C_v DP}{A_c M_f}$$

4.4 Analytic Solution to the Pseudo Two-Dimensional Mathematical Model

An analytic solution to the pseudo two-dimensional mathematical model is developed in Appendix E using the Laplace transform method. The result is in terms of a convolution integral, $I(x_{DT}, \xi)$:

$$T_{Df}(x_{DT}, t_{DT}) = \exp(-\omega x_{DT} - \xi) \cdot H(\xi) \cdot I(x_{DT}, \xi) \tag{4.17}$$

where

$$\xi \triangleq t_{DT} - x_{DT} \tag{4.18}$$

$$H(\xi) = \begin{cases} 0, & \xi < 0 \\ 1, & \xi \geq 0 \end{cases} \tag{4.19}$$

$$I(x_{DT}, \xi) \triangleq \int^{\xi} F_1(\lambda) \cdot F \quad (\xi - \lambda)\, d\lambda \tag{4.20}$$

$$\int_0^{\xi} \qquad \xi - \lambda) \cdot F_2(\lambda)\, d\lambda \tag{4.21}$$

$$F_1(\xi) = \frac{1}{\sqrt{\pi \xi}} + e^{\xi} \operatorname{erf}(\sqrt{\xi}) \tag{4.22}$$

$$F_2(\xi) = \frac{1}{\sqrt{\pi \xi}} \cdot \cosh\left(2\sqrt{\omega \zeta x_{DT} \xi}\right) \tag{4.23}$$

Eqs. 4.3 and 4.5 also describe the transient temperature behavior of certain limiting kinds of heat exchangers. Fig. 4.2 presents a schematic diagram for the lumped parameter heat transfer model of a direct transfer counterflow heat exchanger. R_1 and R_2 are the thermal resistances due to a film coefficient between the wall and fluids number 1, and 2, respectively. This heat exchanger model is directly analogous to the pseudo two-dimensional mathematical model being discussed in this section when the temperature of fluid number is constant. That is, when $(w_2C_2)/(w_1C_1) \to \infty$. Kays and London (1964, Ch. 3) have presented and referenced various

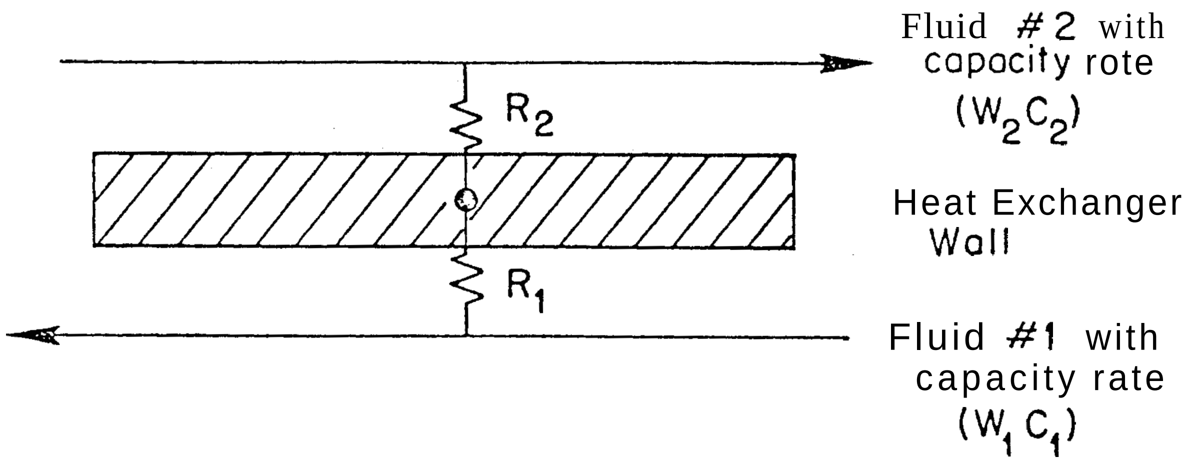

FIGURE 4.2. SCHEMATIC OF A LUMPED PARAMETER MODEL OF HEAT TRANSFER IN A DIRECT TRANSFER COUNTERFLOW HEAT EXCHANGER (MODIFIED FROM FIGURE 3.1, KAYS AND LONDON, 1964)

analytic, analog, and numerical solutions to simplified forms of this model. These solutions were not studied further, since they either incorporated specific assumptions or were presented for specific numerical values of the parameters which made them of little interest to the particular problem of heat transfer in the experiments of Arihara.

4.5 Behavior of the Analytic Solution for Constant Injection Temperature

4.5.1 Theoretical. Considerations: As $\xi \to 0$ from above, the solution approaches its value at the leading edge of a sharp temperature front, which is controlled by the Heaviside function, $H(\xi)$. This front moves with identically the same constant velocity as that of the wave equation in section 3:

$$\frac{x}{\bar{t}} = \frac{\eta\alpha}{\eta} \cdot \frac{x_{DT}}{t_{DT}} = \alpha = \frac{wC_w}{A_c M_f} \qquad (4.24)$$

since $x_{DT} = t_{DT}$ when $\xi = 0$. For ξ approaching zero from above, it can be shown that the integral expression approaches the value unity:

$$\lim_{\substack{\xi \to 0 \\ \xi > 0}} I(x_{DT}, \xi) = 1 \qquad (4.25)$$

Thus, the solution at the leading edge of the front is::

$$(x_{DT}, 0) = \exp\left(-\frac{h_f P}{wC} \cdot x\right) \qquad (4.26)$$

where $x_{DT} = t_{DT}$ when $\xi = 0$. This is similar to the equation for the temperature at the leading edge of the wave model solution, which contains an $\bar{h}$ term instead of an h_f term. Fig. 4.3 presents a schematic of the locii of the temperatures at the leading edge of the wave front for the wave and parabolic models.

For large ξ and small x_{DT}, the analytic solution should become a function of x_{DT} only, which should be the solution of the wave model for an equivalent $\bar{h}$. Attempts to demonstrate this analytically were unsuccessful. However, as will be seen in section 4.5.3 in the following, numerical calculations indicate that the analytic solution does show this behavior.

In order to carry out numerical evaluations of the analytic solution (Eqs. 4.17 to 4.23), it was necessary to rearrange the solution. First, the integral expressions in Eqs. 4.20 to 4.23 are singular at both end points. This is a problem from a numerical point of view. Fortunately it can be avoided by carrying out the numerical integration to within a small distance, ε, of the two singular end points, and performing an approximate analytic integration for the rest of the interval to the end points. The indefinite integrals do exist. The result, in terms of the integral, Eqs. 4.20, 4.22, and 4.23, is, for $\varepsilon \ll 1, \xi$:

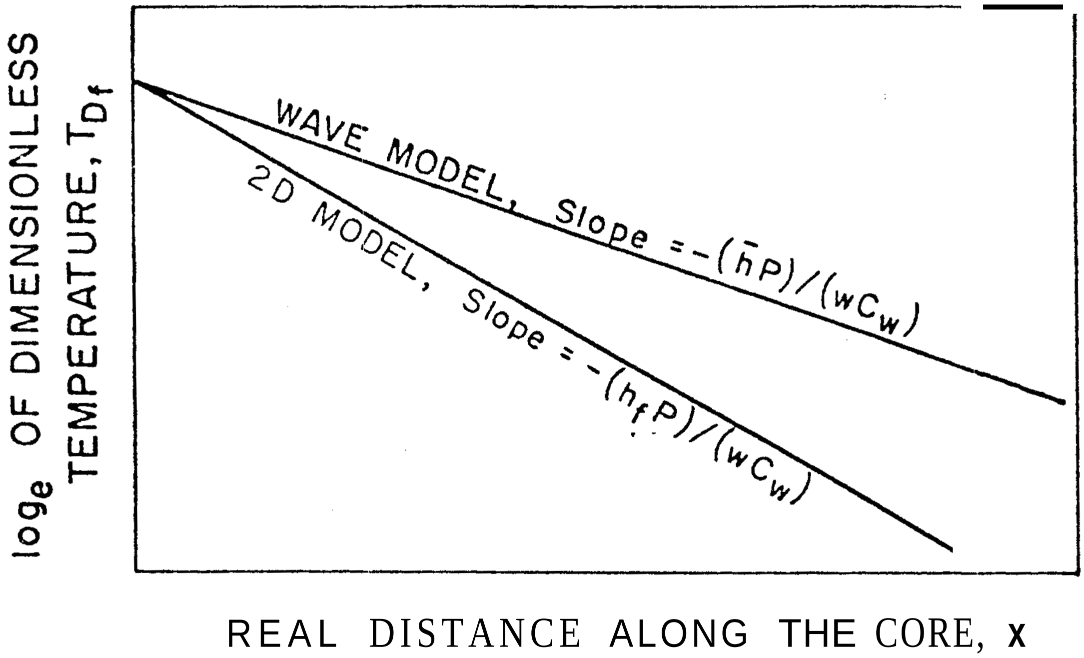

FIGURE 4.3. SCHEMATIC OF THE LOCII OF THE TEMPERATURES AT THE LEADING EDGE OF THE WAVE FRONT FOR THE WAVE AND PSEUDO TWO-DIMENSIONAL MODELS

$$I\ (x_{DT},\xi) \simeq \frac{\cosh\ (2\sqrt{\omega\zeta x_{DT}\xi})}{\pi\sqrt{\xi}} \cdot 2\ \sqrt{\varepsilon}$$

$$+ \int_{\varepsilon}^{\xi-\varepsilon} F_1\ (\lambda) \cdot F_2\ (\xi-\lambda)\ d\lambda$$

$$+ \frac{e^{\xi}\mathrm{erf}(\sqrt{\xi})}{\sqrt{\pi}} \cdot 2\ \sqrt{\varepsilon} \qquad (4.27)$$

As $\varepsilon \to 0$, the approximate relationship, Eq. 4.27, becomes an identity. This result is:

$$T_{Df}\ (x_{DT},\xi) = \exp\ (-\ x_{DT}-\xi) \cdot H\ (\xi) \Bigg[\sqrt{\varepsilon} \cdot \frac{2}{\sqrt{\pi}}$$

$$\cdot \left\{ \frac{\cosh\ (2\sqrt{\omega\zeta x_{DT}\xi})}{\sqrt{\pi\xi}} + e^{\xi}\ \mathrm{erf}\ (\sqrt{\xi}) \right\}$$

$$+ \frac{1}{\sqrt{\pi}} \int_{\varepsilon}^{\xi-\varepsilon} \left\{ \frac{1}{\pi\lambda} + e^{\lambda}\ \mathrm{erf}\ (\sqrt{\lambda}) \right\}$$

$$\cdot \frac{\cosh\ (2\sqrt{\omega\zeta x_{DT}\ (\xi-\lambda)})}{\sqrt{\xi-\lambda}}\ d\lambda \Bigg] \qquad (4.28)$$

where $\varepsilon<<1,\xi$.

There is one further numerical complication: the value of ξ is often greater than 100. Thus, numerical evaluation of terms like exp (ξ), or exp $(-\xi)$ may lead to serious round-off errors, if evaluation is possible. This problem can be avoided when evaluating products of exponentials by first summing the arguments of the exponentials. The result is:

$$T_f\,(x_{DT},\xi) = \exp\,(-\omega x_{DT}) \cdot H\,(\xi)$$

$$\left|\, \bar{\varepsilon} \cdot G\,(\xi) + \frac{1}{\;} \int_{\varepsilon}^{\xi-\varepsilon} F\,(\lambda,\xi)\; d\lambda \right| \qquad (4.29)$$

where:

$$G\,(\xi) = \frac{2}{\;} \left\{ \frac{e^{\sigma\sqrt{\xi}-\xi} + e^{-\sigma\sqrt{\xi}-\xi} + 2e^{-\xi}}{\;} + \mathrm{erf}\,(\sqrt{\xi}) \right\} \qquad (4.30)$$

$$\frac{e^{\sigma\sqrt{\xi-\lambda}-\xi} + e^{-\sigma\sqrt{\xi-\lambda}-\xi}}{2\sqrt{\pi\lambda(\xi-\lambda)}} + \left| \frac{e^{\sigma\sqrt{\xi-\lambda}-\xi+\lambda} + e^{-\sigma\sqrt{\xi-\lambda}-\xi+\lambda}}{2\sqrt{\xi-\lambda}} \right.$$

$$\cdot\; \mathrm{erf}\,(\sqrt{\lambda}) \qquad (4.31)$$

and $$\sigma = 2\sqrt{\omega\zeta x_{DT}}$$

The numerical evaluation of this expression is straightforward. This form was used in all calculations.

4.5.2 <u>Computational Considerations</u>: Prior to performing numerical integrations of Eqs. 4.29 and 4.30, the integrand, $F\,(\lambda;\xi)$, was examined for three different cases. These corresponded to:

(1) short times (15 minutes) near the leading edge of the front (very small ξ),

(2) short times (15 minutes) near the upstream end of the core [small ξ, but larger than in (1)], and

(3) long times (180 minutes) far away from the leading edge of the front (large ξ).

The calculations were carried out for:

$$t_{DT} = (0.3536)\ t,\ t \text{ in minutes}$$
$$x_{DT} = (9.25)\ x,\ X \text{ in feet}$$
$$\zeta = 0.99391$$
$$\omega = 0.56742$$

which correspond to a particular set of reasonable physical conditions. Graphs of the value of the integrand over the range of integration in each case are presented in Figs. 4.4, 4.5, and 4.6 for cases 1, 2, and 3 respectively.

An examination of these graphs indicates behavior which would be difficult to approximate accurately with polynomials, which are the basis of many numerical integration methods. Rather than try to develop a procedure for this particular problem, it was decided to use a numerical integration package available at the Stanford Center for Information Processing. This program is called DCADRE (Double Precision Integration using Cautious Adaptive Romberg Extrapolation), and is part of the IMSL programs library (IMSL, 1975).

Numerical experiments indicated that values of $\varepsilon = 1 \times 10^{-5}$ and RERR (specified desired relative accuracy) = 1×10^{-3} gave results with a maximum estimated error of 2% with an optimal number of function evaluations. As an indication of the severity of the numerical integration problem, more than 200 points were usually needed to achieve a maximum estimated *error* of 2%. Furthermore, the program usually gave messages indicating that it had encountered singularities or irregular

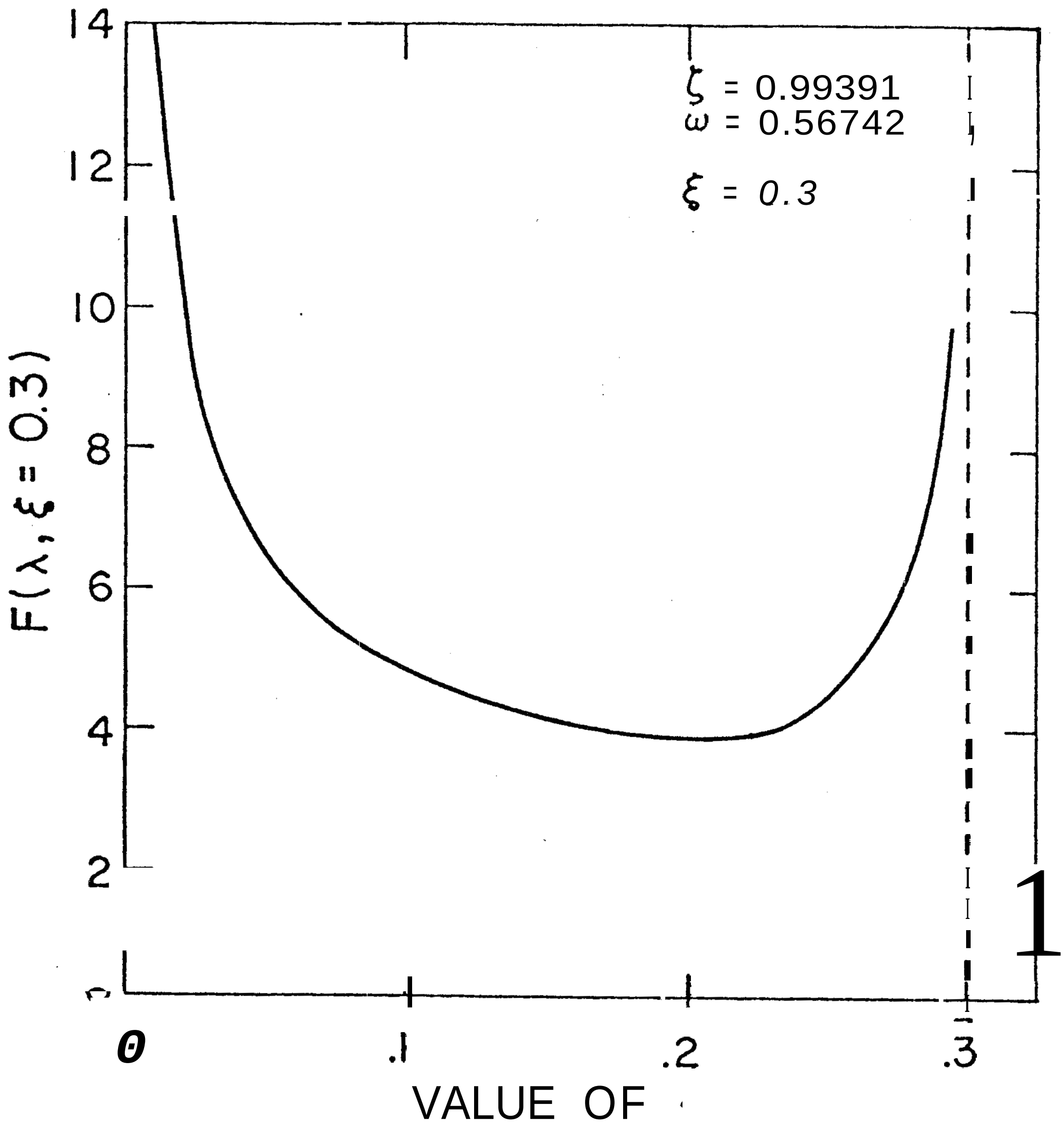

4.4 GRAPH OF THE INTEGRAND F (λ;ξ) AT SHORT TIMES, ANI) NEAR THE LEADING EDGE OF THE FRONT (ξ+0.3) F0? THE GIVEN PARAMETERS, VS. λ

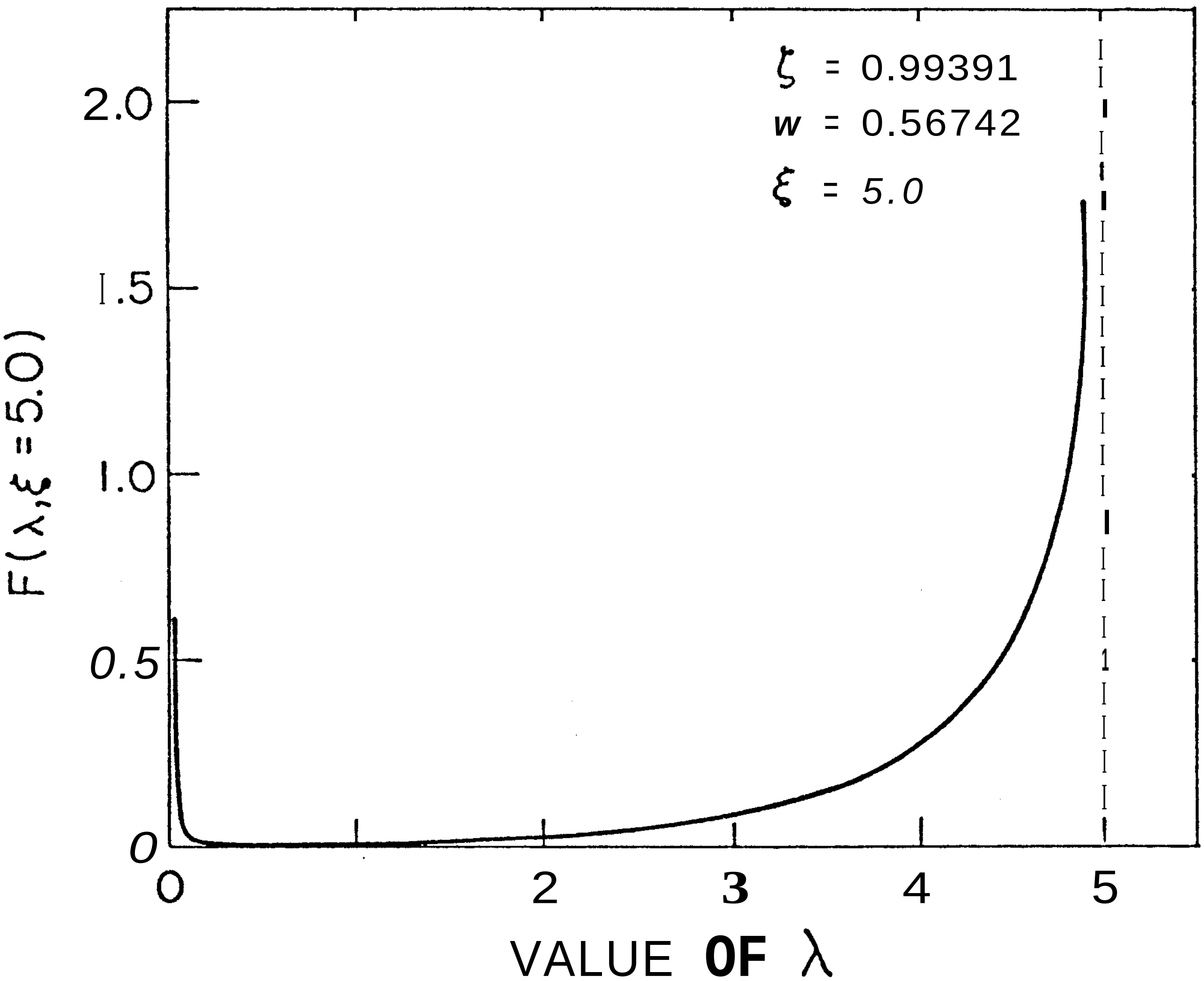

4.5 GRAPH OF THE INTEGRANT F (λ;ξ) AT SHORT TIMES NEAR THE UP-STREAM END OF THE CORE (SMALL ξ) VS. λ

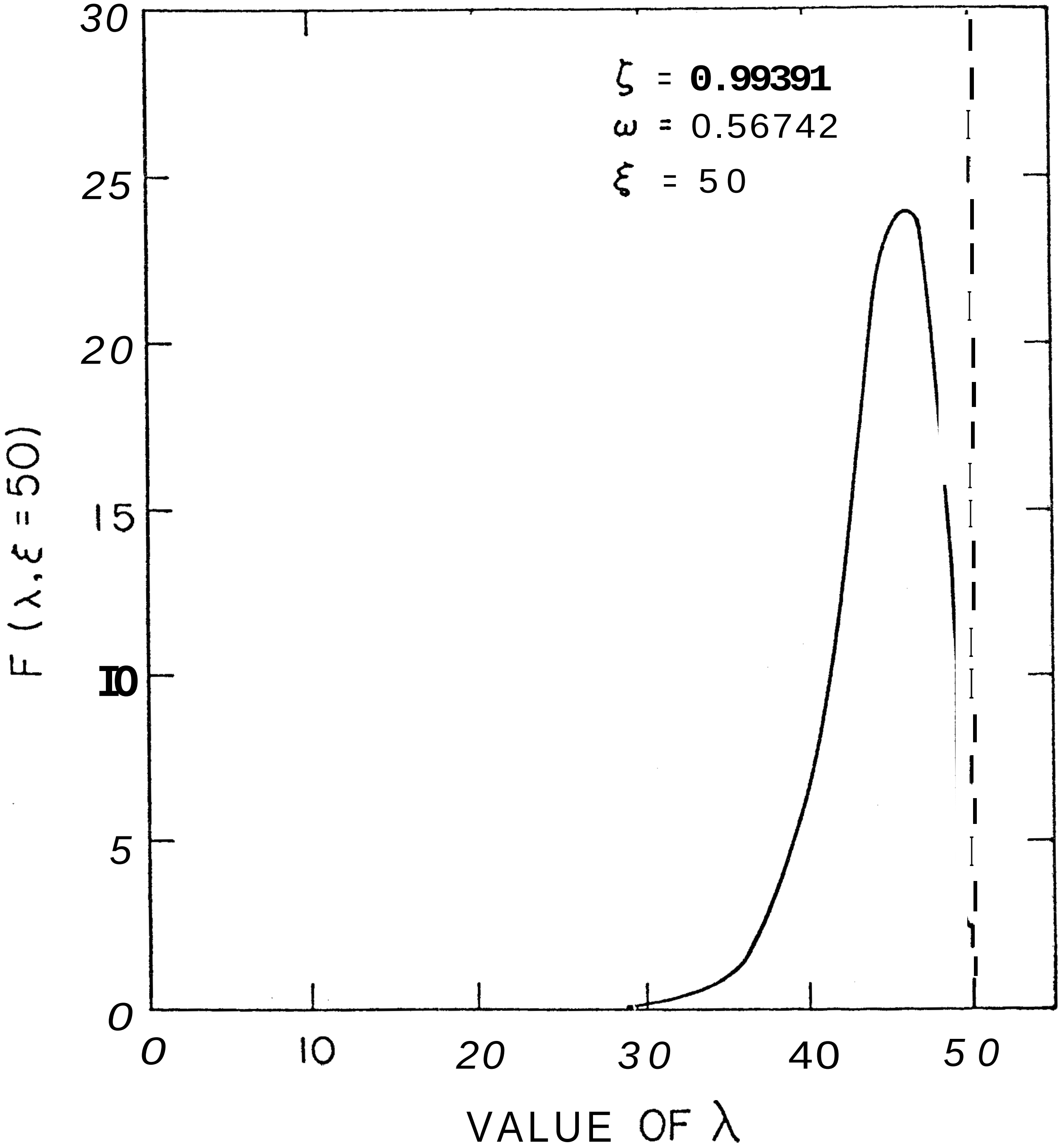

FIGURE 4.6. GRAPH OF THE INTEGRAND $F(\lambda;\xi)$ AT LONG TIMES FAR FROM THE FRONT (LARGE ξ), VS A

behavior. In both of these cases, the computed answer was accepted because the estimated error was small.

The numerical severity of the integration problem, in conjunction with the complexity of the integrand, $F(\lambda;\xi)$, required large amounts of computer time. A computer code executing in FORTRAN H on an IBM 370/168 could only evaluate 10 to 20 typical integral expressions, $I(x_{DT},\xi)$ per second to the desired accuracy. This was not serious for the evaluation of constant injection temperature profiles which required one integral evaluation per point. However, it did become a limiting factor for the case of variable injection temperature profiles (section 4.6) wherein effects of a sequence of constant temperature solutions had to be superposed.

4.5.3 <u>Results of the Computations for Constant Injection Temperature</u>: Fig. 4.7 presents calculated dimensionless temperature profiles for 15, 45, and 210 minutes for conditions corresponding to HWI-B-1 of Arihara. Profiles for h_f = 5, 10, 15, and 20 BTU/(hr-ft^2-^{o}F) are presented at each time, as is the wave equation solution, Eq. 3.20. The value of the external film coefficient, h_e, was chosen in each case so that the overall, steady-state heat transfer coefficient, $\bar{h}$, was 1.5 BTU/(hr-ft^2-^{o}F). It can be seen that the steady-state profile was approached only near the upstream end of the core at 45 minutes, while at 210 minutes, the entire core had reached the condition of steady heat losses.

Varying the value of h_f appeared to affect only the transient temperature profiles over the part of the core

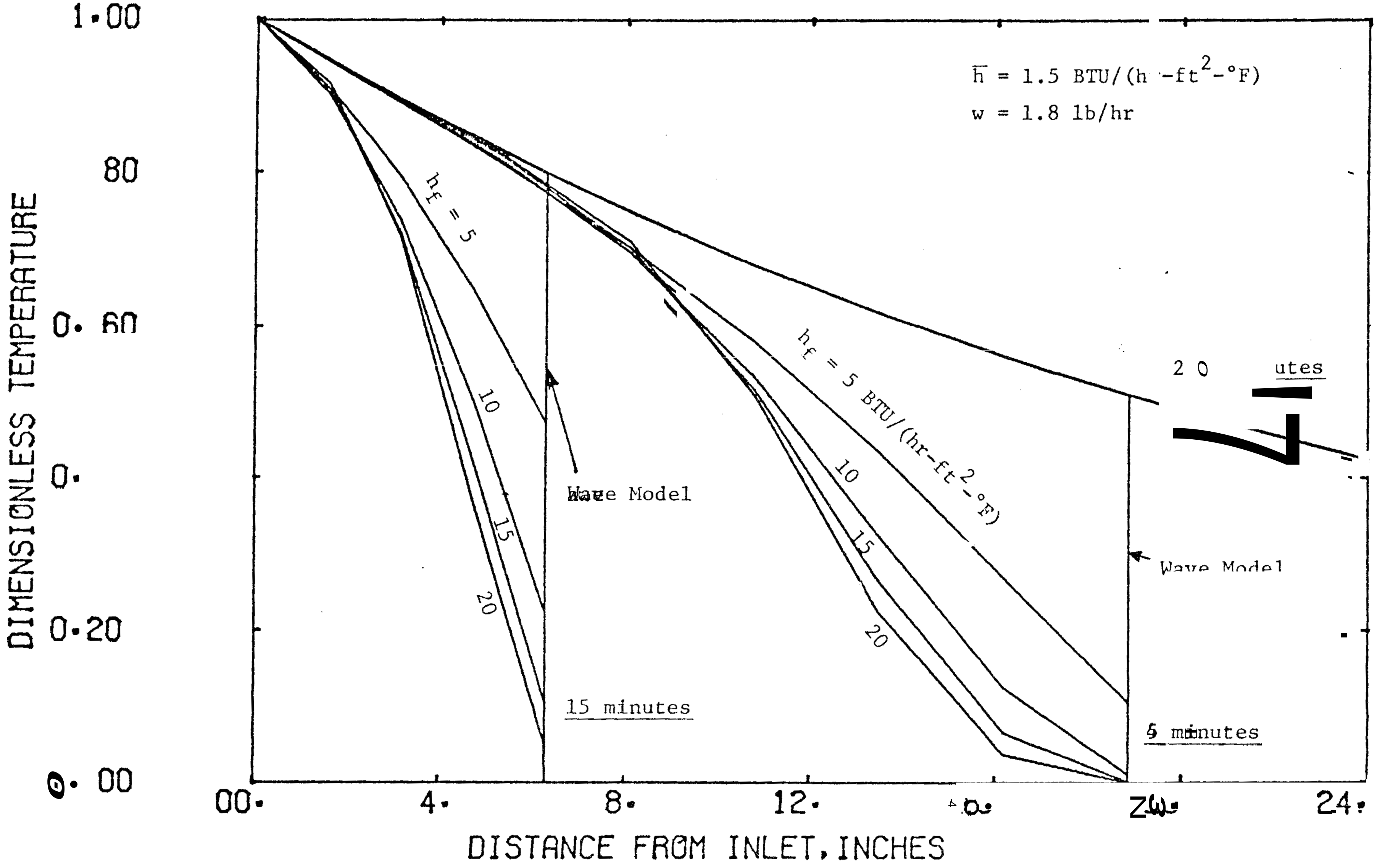

FIGURE 4.7. CALCULATED TEMPERATURES AT 15, 45, AND 210 MINUTES FOR CONSTANT INJECTION TEMPERATURE AND CONDITIONS COMPARABLE TO EXPERIMENT HWI-B-1 OF ARIHARA

immediately behind the heat wave front. This effect may also be seen in the variable injection temperature results. It becomes important when comparing calculated with experimental results.

Fig. 4.8 presents temperature profiles at 15 and 45 minutes computed from the wave, parabolic, and two-dimensional models for conditions comparable to experiment HWI-B-1 of Arihara. Both the parabolic and two-dimensional models yield lower temperatures than the wave model for the region immediately behind the wave front. However, the two-dimensional model does not approach the wave model behavior as rapidly as does the parabolic model. Thus, there is a region wherein temperatures are affected hy transient heat losses, but not by axial heat conduction. This conclusion is also valid for variable injection temperature, and a reasonable range of λ_f and h_f. It becomes important when trying to match calculated temperature profiles with the experimental results (Arihara) in section 4.6.

Fig. 4.9 presents calculated temperature profiles at 15, 45, and 90 minutes for both the wave and two-dimensional models, and for the conditions of Arihara's experiment HWI-B-1. The results are presented for $\bar{h}$ = 1.5 BTU/(hr-ft^2-$^\circ$F) and h_f = 5 BTU/(hr-ft^2-$^\circ$F), and various values of FAC. The parameter FAC is discussed in Appendix D. It modifies the thermal capacitance of the lumped parameter model, and has the effect of speeding (smaller FAC) or slowing (larger FAC) the transient heat losses. It can be seen from Fig. 4.9

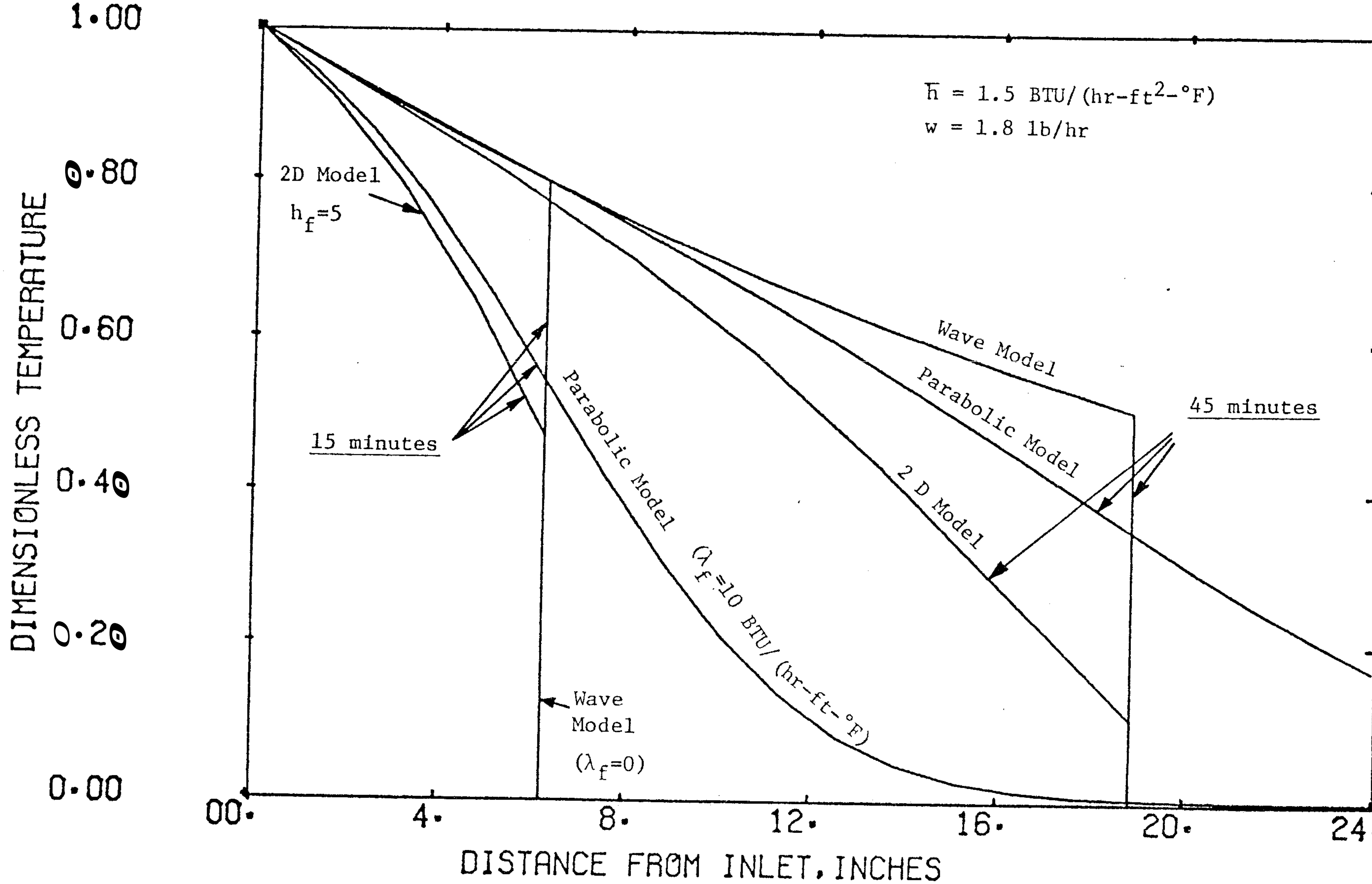

FIGURE 4.8. CALCULATED TEMPERATURES AT 15 AND 45 MINUTES FOR CONSTANT INJECTION TEMPERATURE AND CONDITIONS COMPARABLE TO EXPERIMENT HWI-B-1 OF ARIHARA

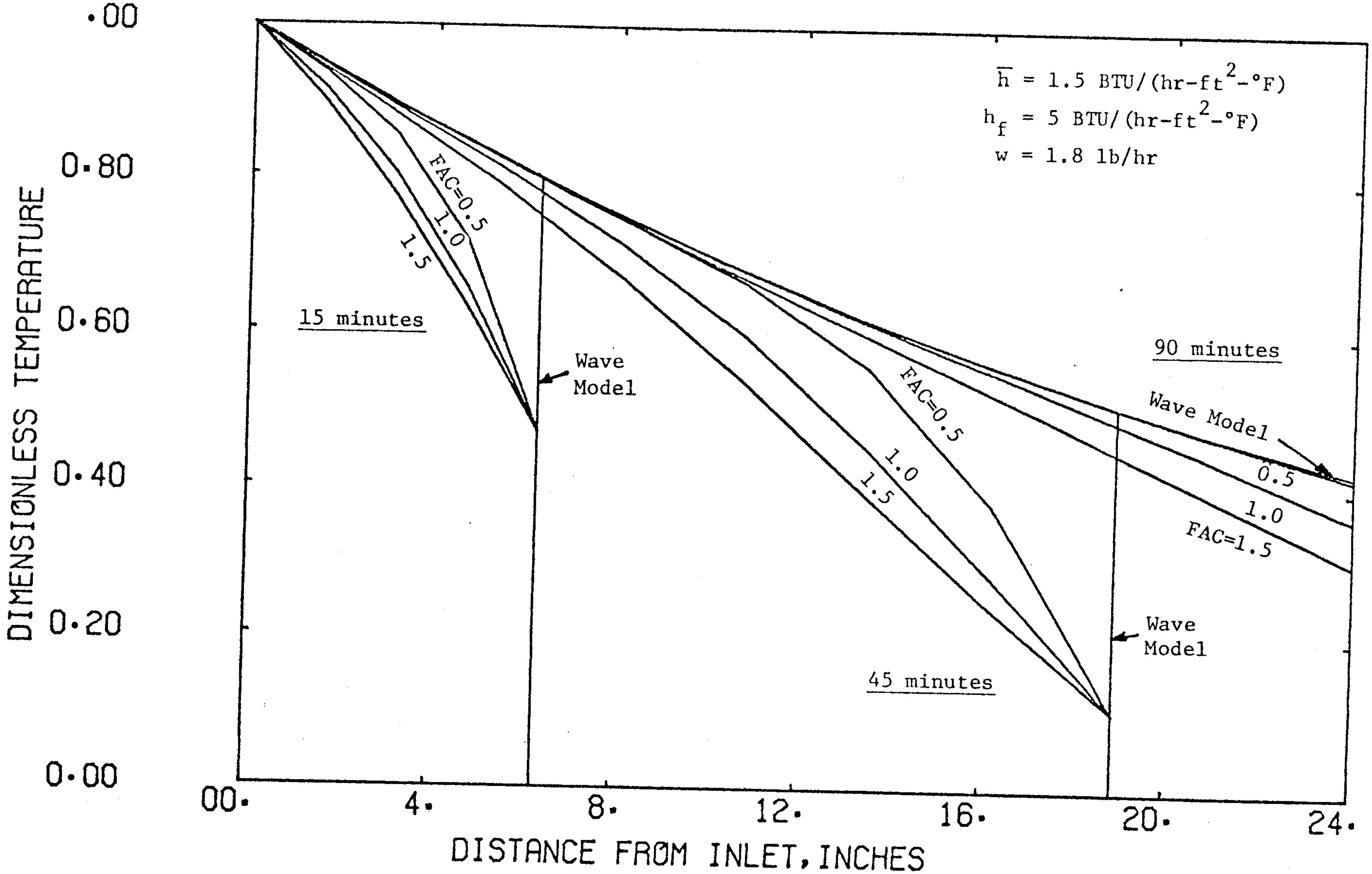

FIGURE 4.9. CALCULATED TEMPERATURES AT 15, 45, AND 90 MINUTES FOR CONSTANT INJECTION TEMPERATURE AND CONDITIONS COMPARABLE TO EXPERIMENT HWI-B-1 OF ARIHARA

that the value of FAC has an effect on the shape of the temperature profiles behind the wave front.

An examination of Figs. 4.7 to 4.9 and similar figures leads one to conclusions concerning the use of the two-dimensional model with the experimental results of Arihara. One conclusion is that the two-dimensional model would not be expected to be valid in the region near the sharp wave front. There is, however, a region behind the wave front where axial heat conduction is not important, but radial transient heat losses are. Calculated temperatures in this region are sensitive to the thermal capacitance of the lumped parameter model.

Finally, the heating efficiency of a hot-liquid-injection process described by the pseudo two-dimensional mathematical model must depend on the nature of the transient heat losses, as well as on time.

4.6 Behavior of the Pseudo Two-Dimensional Solution for Variable Injection Temperature

4.6.1 Computational Considerations: Prior to performing numerical calculations, it was necessary to solve the following problem. The simplified mathematical model discussed in Appendix D and section 4.3, and from which the analytic solution was developed, is based on linear transient heat losses through a slab. The physical system described in section 4.1 (Eq. 4.1 and Fig. 4.1) is radial. The mathematics were developed for a linear system for convenience. The resulting solution can he transformed to radial heat losses by modification of the thermal capacitance and the effective external thermal resistance, R_{el} (see Fig. D.3, Appendix D).

The effect of the radial geometry on the volume of the viton can be considered by using:

$$FAC = \frac{\text{Volume of Viton per Unit Length of Core for the Radial Geometry}}{\text{Volume of Viton per Unit Length of Core for the Linear Geometry}}$$

$$= \frac{\pi(r_{vo}^2 - r_o^2)}{DP} \tag{4.32}$$

$$= 1.125$$

for the dimensions under consideration. Unless indicated differently, it can be assumed that this value of FAC was used in all calculations which were made for comparison with the Arthara experimental results.

In order to consider both the radial geometry for heat losses and the effects of internal thermal resistance in the coreholder caused by finite conductivities, the following value of lumped, external thermal resistance was used:

$$R_{el} = \frac{(r_o/r_{so})}{(1/\bar{h}) - (1/h_f) - R_{int}} \tag{4.33}$$

where $\bar{h}$ is the overall steady state heat transfer coefficient defined by Eq. 3.1 and the other symbols are defined in the Nomenclature section, and are also discussed in section 4.1.

Variable injection temperature calculations were carried out using the superposition procedure described in Appendix B. The computational requirements of evaluating the integral solution, Eqs. 4.29 to 4.31, meant that restrictions had to be placed on both the number of superposition elements used and on the number of points in the core for which the superposition solution was generated. It was found satisfactory to use a value of DELTA which caused the construction of 10 superposition elements from the injection temperature history. While this restriction on the accuracy of the step function approximations caused occasional strange results, it did not affect overall behavior and interpretation.

No calculations were made with variable injection temperature history to simulate the long experimental times for which the temperatures become steady over the entire core. Such calculations were unnecessary, because the experiments approached constant injection temperature at long times, and the two-dimensional model approached the wave model at long times for constant injection temperature.

4.6.2 Comparison of the Pseudo Two-Dimensional Model with the Results of Experiment HWI-B-1 of Arihara: The wave and parabolic models were compared with the results of experiment HWI-B-1 of Arihara in section 3.6.3 (Figs. 3.16 and 3.17). It was seen that the comparison of calculated and experimental results was unsatisfactory at intermediate times (60 minutes in this case). Fig. 4.10 presents experimental and calculated temperatures for short (15 minutes) and

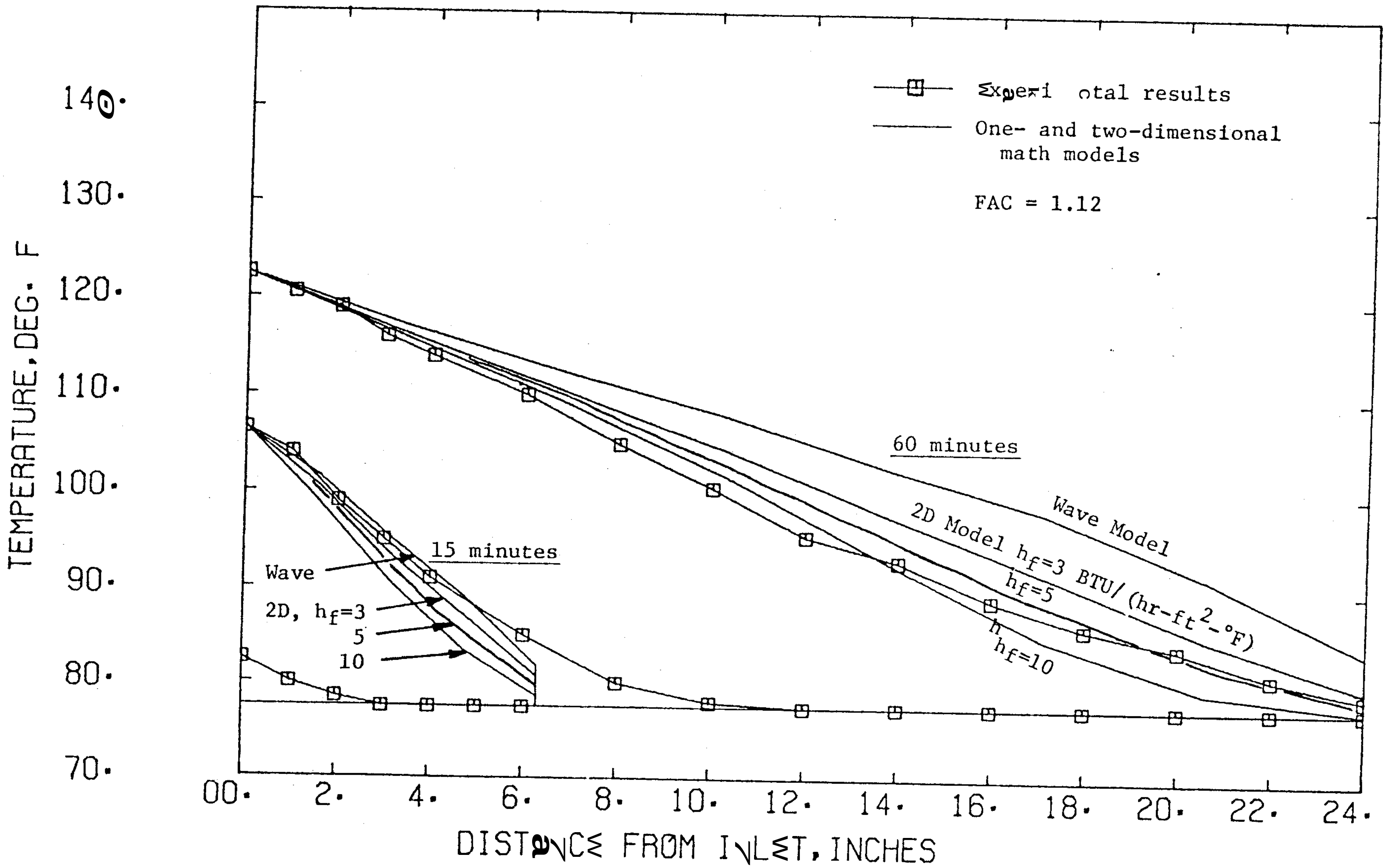

FIGURE 4.10. CALCULATED AND EXPERIMENTAL TEMPERATURES FOR EXPERIMENT HWI-B-1 OF ARIHARA, $\overline{h}$=1.0 BTU/(hr-ft^2-°F), h_f =3,5,10 BTU/(hr-ft^2-°F)

intermediate (60 minutes) times for the HWI-B-1 experiment. Calculations are presented for the wave equation with an accurate long-time heat loss coefficient, $\bar{h}$, and for the two-dimensional model for values of h_f = 3, 5, and 10 BTU/(hr-ft^2-^{o}F). It can be seen that a value of h_f = 5 BTU/(hr-ft^2-^{o}F) gives a satisfactory comparison of calculated and experimental temperatures.

4.6.3 <u>Comparison with the Results of the CWI-S Series of Experiments of Arihara</u>: The cold water injection experiments did not show end effects, as did some of the hot water injection experiments (section 3.6.1). For this reason, it was decided to compare the temperature behavior of the two-dimensional model to that of some of the cold water injection experiments. The series of experiments carried out on the synthetic consolidated core (CWI-S) was arbitrarily chosen. Physical and thermal parameters that were known with accuracy were used as fixed inputs for the calculations. These parameters included temperature history $[T_i(t)]$, system dimensions, average mass injection rate (w), bulk formation specific heat (M_f), and the overall steady heat loss coefficient ($\bar{h}$). The sensitivity of the calculations to parameters known with less accuracy was then tested. These parameters were the internal film coefficient, h_f, and the factor modifying the thermal capacitance of the viton, FAC. All two-dimensional model calculations were compared with parabolic calculations in order to determine if axial heat conduction was important.

There was only one part of the heat transfer calculations for which less than satisfactory parameters had to be used. It appeared incorrect to assume that heat transfer across the annulus occurred as if it were of uniform thickness and filled with nitrogen gas. This assumption was used by Arihara in his calculations of heat transfer through the coreholder system (Arihara, 1974, pp. 77-78, Tables 2 and 3). This assumption, in conjunction with estivates of the external film coefficient (from correlations), and the internal film coefficient (from matching two-dimensional calculations with experimental behavior), caused excessive calculated temperature drops across the entire coreholder. This difficulty can be resolved by hypothesizing the occurrence of some sort of short circuiting of heat transfer across the annulus. This may have been caused by sagging of the core in the steel shell, in conjunction with irregularities on the outside surface of the viton shell (Chen, 1976). The possibility of some water leakage into the annulus during these experiments (Arihara, 1976) is also consistent with this hypothesis.

Fig. 4.11 presents calculated and experimental profiles for experiment CWI-S-1 at 60 and 120 minutes. Calculations are presented for the two-dimensional model with values of FAC = 1.12, and h_f = 4 and 6 BTU/(hr-ft^2-^{o}F), as well as for the wave and parabolic models [λ_f = 4 BTU/(hr-ft-^{o}F)]. Both values of h_f provide a reasonable comparison with the experimental data, particularly if the effects of axial thermal conduction are qualitatively considered. Figs. 4.12 and 4.13

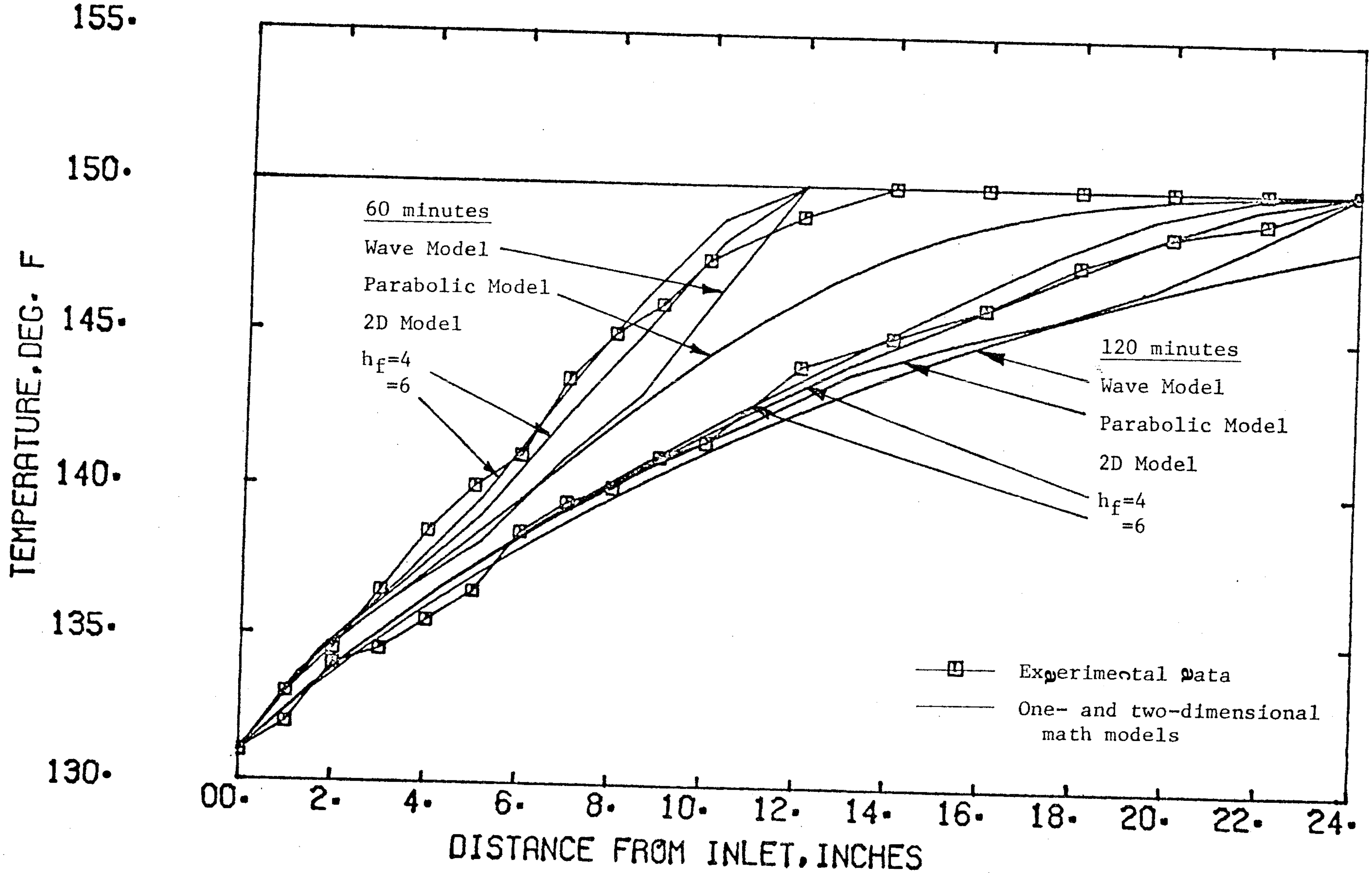

FIGURE 4.11. CALCULATED AND EXPERIMENTAL TEMPERATURES FOR EXPERIMENT CWI-S-1 OF ARIHARA, $\bar{h}$=1.81 BTU/(hr-ft^2-°F), h_f=4,6 BTU/(hr-ft^2-°F)

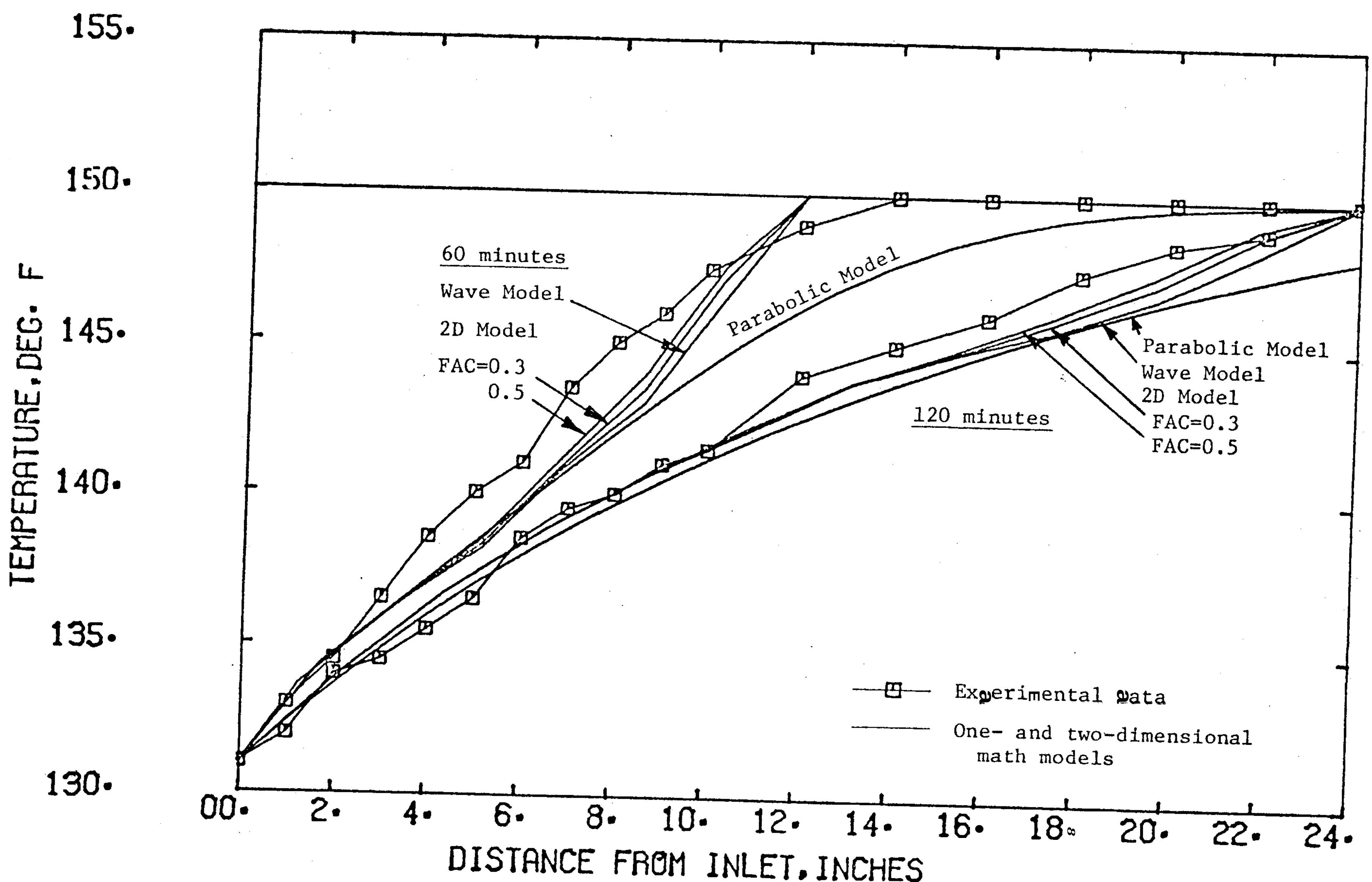

FIGURE 4.12. CALCULATED AND EXPERIMENTAL TEMPERATURES FOR EXPERIMENT CWI-S-1 OF ARIHARA,

$\overline{h}$=1 81 BTU/(hr-fc^2-°F), h_f=4 BTU/(hr-ft^2-°F), FAC=0.3, 0.5

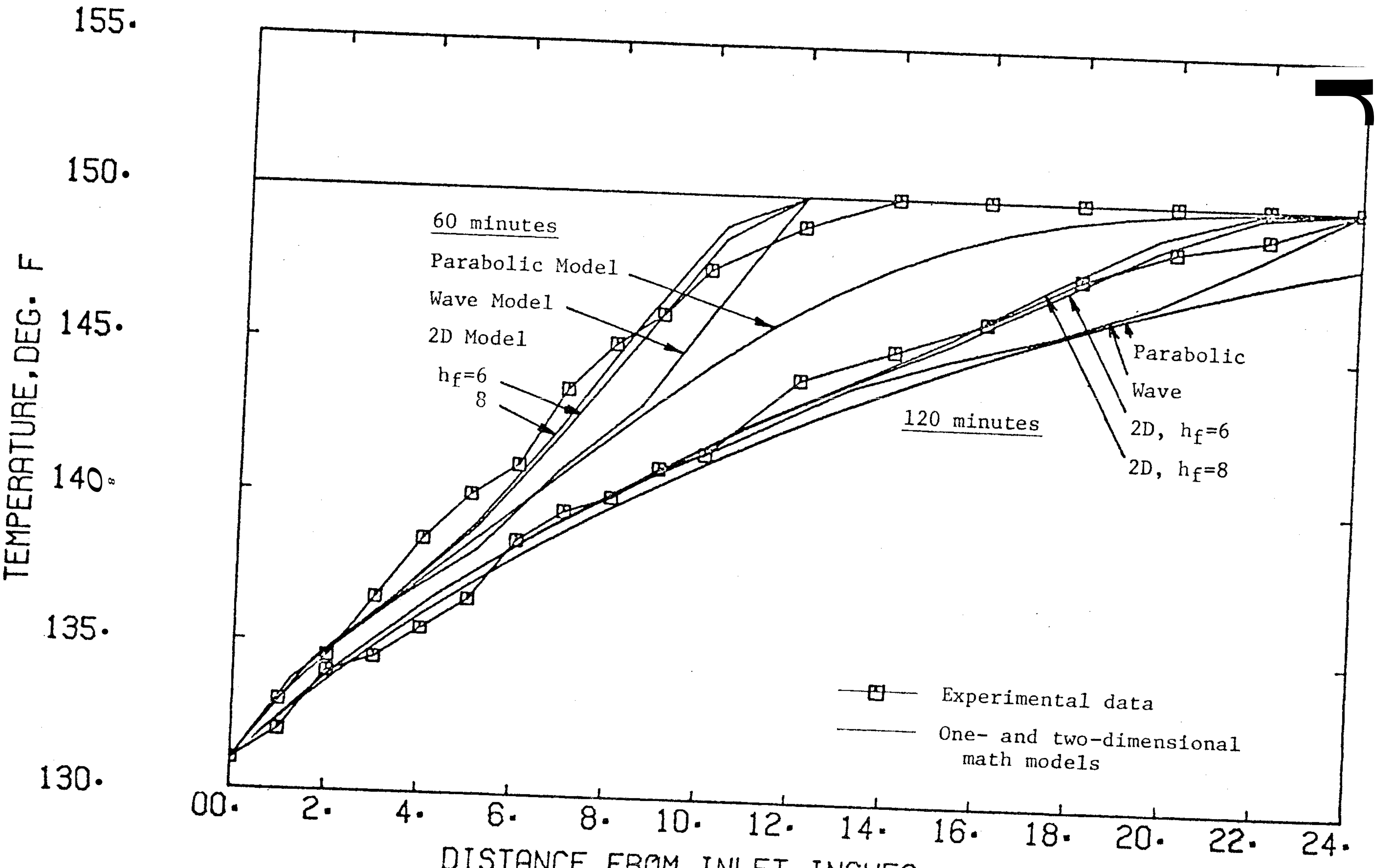

FIGURE 4.13. CALCULATED AND EXPERIMENTAL TEMPERATURES FOR EXPERIMENT CWI-S-1 OF ARIHARA, $\bar{h}$=1.81 BTU/(hr-ft^2-°F), h_f=6,8 BTU/(hr-ft^2-°F), FAC=0.7

present further calculations for the conditions of CWI-S-1, but with different values of h_f, and smaller values of FAC. It can be seen that these calculations do not compare well with the experimental data.

Fig. 4.14 presents calculated and experimental temperatures for the CWI-S-2 experiment of Arihara at 45 and 90 minutes. The two-dimensional model calculations are presented for FAC = 1.12, and h_f = 4 and 6 BTU/(hr-ft^2-^{o}F), while the parabolic model calculations are for λ_f = 6 BTU/(hr-ft-oF). It can be seen that if the effects of conduction are qualitatively considered, then both h_f = 4 and 6 BTU/(hr-ft^2-^{o}F) give reasonable comparisons with the experimental data. Other two-dimensional calculations were made for a range of h_f, and lower values of FAC. Fig. 4.14 presents the best comparison obtained between calculated and experimental results.

Fig. 4.15 presents calculated and experimental temperatures for the CWI-S-3 experiment of Arihara at 30 and 60 minutes. The two-dimensional calculations are presented for FAC ¤ 1.12, and h_f = 7 and 15 BTU/(hr-ft^2-^{o}F), while the parabolic calculations are for λ_f = 10 BTU/(hr-ft-^{o}F). It can be seen that if the effects of axial heat conduction are qualitatively considered, then a value part way between h_f = 7 and 15 BTU/(hr-ft^2-^{o}F) will give a good match between calculated and experimental temperature profiles. Other two-dimensional calculations were made for a range of h_f, and lower values of FAC. The results presented in Fig. 4.15 show the best comparison obtained between calculated and experimental results.

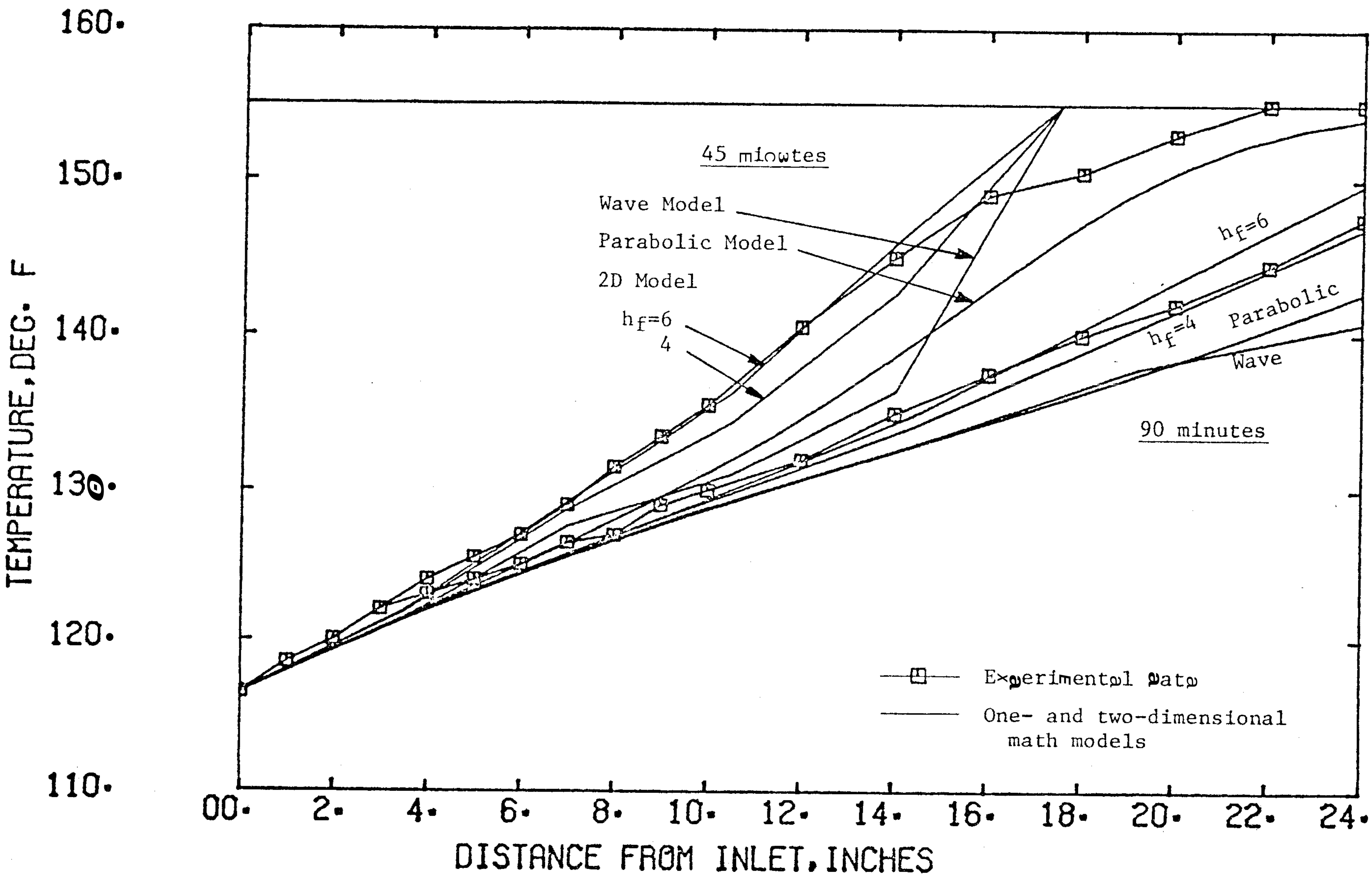

FIGURE 4.14. CALCULATED AND EXPERIMENTAL TEMPERATURE FOR EXPERIMENT CWI-S-2 OF ARIHARA, $h=1.68$ BTU/(hr-ft^2-°F), $h_f=4,6$ BTU/(hr- t^2-°F)

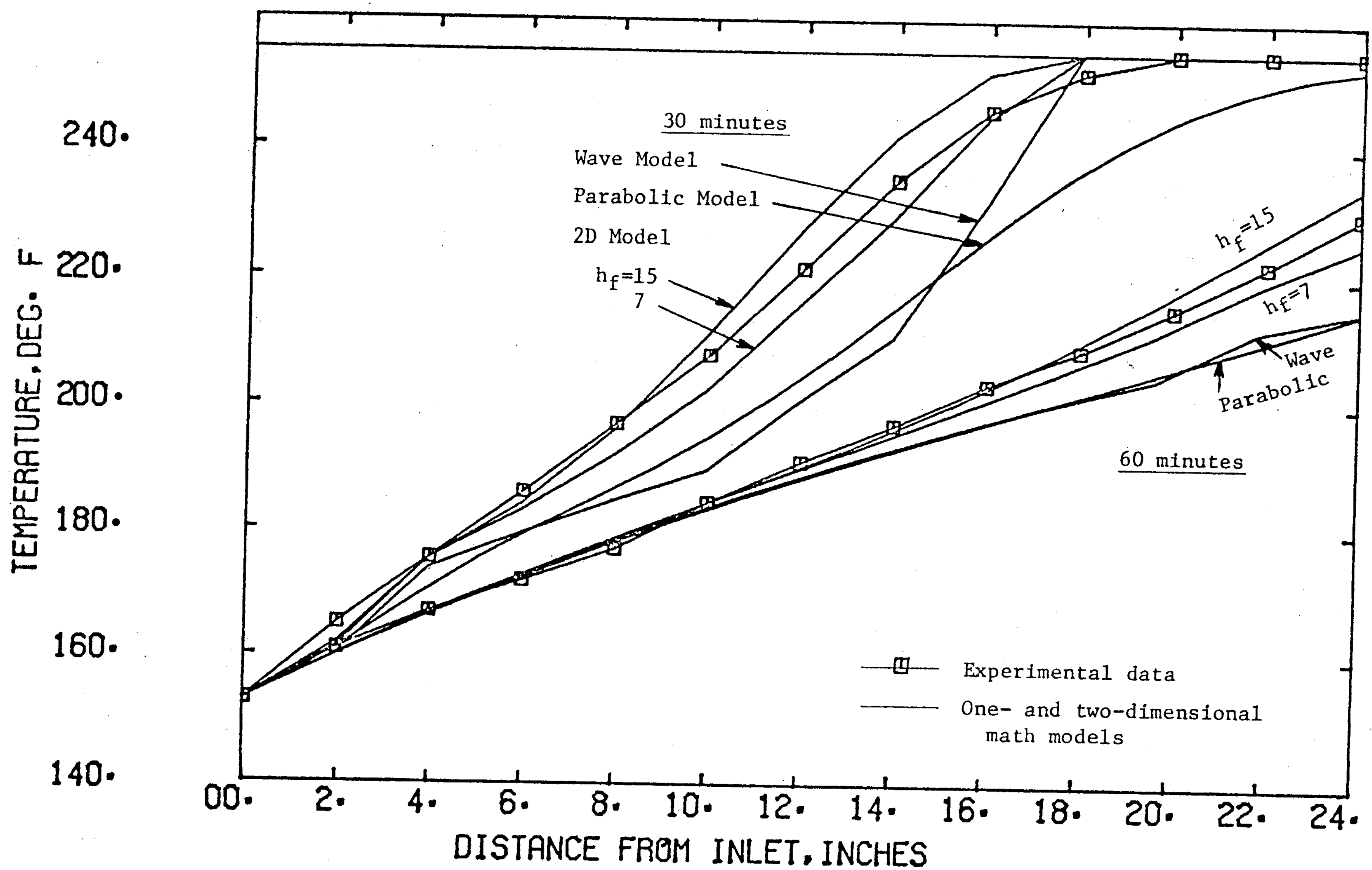

FIGURE 4.15. CALCULATED AND EXPERIMENTAL TEMPERATURES FOR EXPERIMENT CS-S-3 OF ARIHARA, $\bar{h}$=2.39 BTU/(hr-ft^2-°F), h_f=7, 15 BTU/(hr-ft^2-°F)

Fig. 4.16 presents calculated and experimental temperatures for the CWI-S-4 experiment of Arihara at 45 and 75 minutes. The two-dimensional calculations are presented for FAC = 1.12, and h_f = 8 and 12 BTU/(hr-ft2-$^{\circ}$F), while the parabolic calculations are for $\lambda_f \simeq$ 20 BTU/(hr-ft-$^{\circ}$F). While the comparison in this) figure is not satisfactory, it was the best one obtained. Other calculations using a range of h_f, and lower values of FAC were even less satisfactory. The calculated results indicated that values of FAC greater than 1.12 might give more satisfactory matches between the calculated and experimental results. The examination of the lumped parameter transient response in Appendix D suggested that lower values of FAC might give more realistic transient responses through the viton. However, there appears to be no physical basis for using values of FAC higher than 1.12, and hence this was not done.

4.7 Quantitative Estimation of Heat Transfer Parameters by Comparing the One- and Two-Dimensional Yodels to the Transient Temperature Profiles in the Nonisothermal Liquid Injection Experiments of Arihara

This section discusses attempts to obtain quantitative estimates of certain heat transfer parameters in Arihara's experiments. Since axial thermal conduction controlled early-time temperatures, and the core-viton coefficient controlled medium-time temperatures, it was thoupht that they could be estimated by comparing calculations to the experimental results.

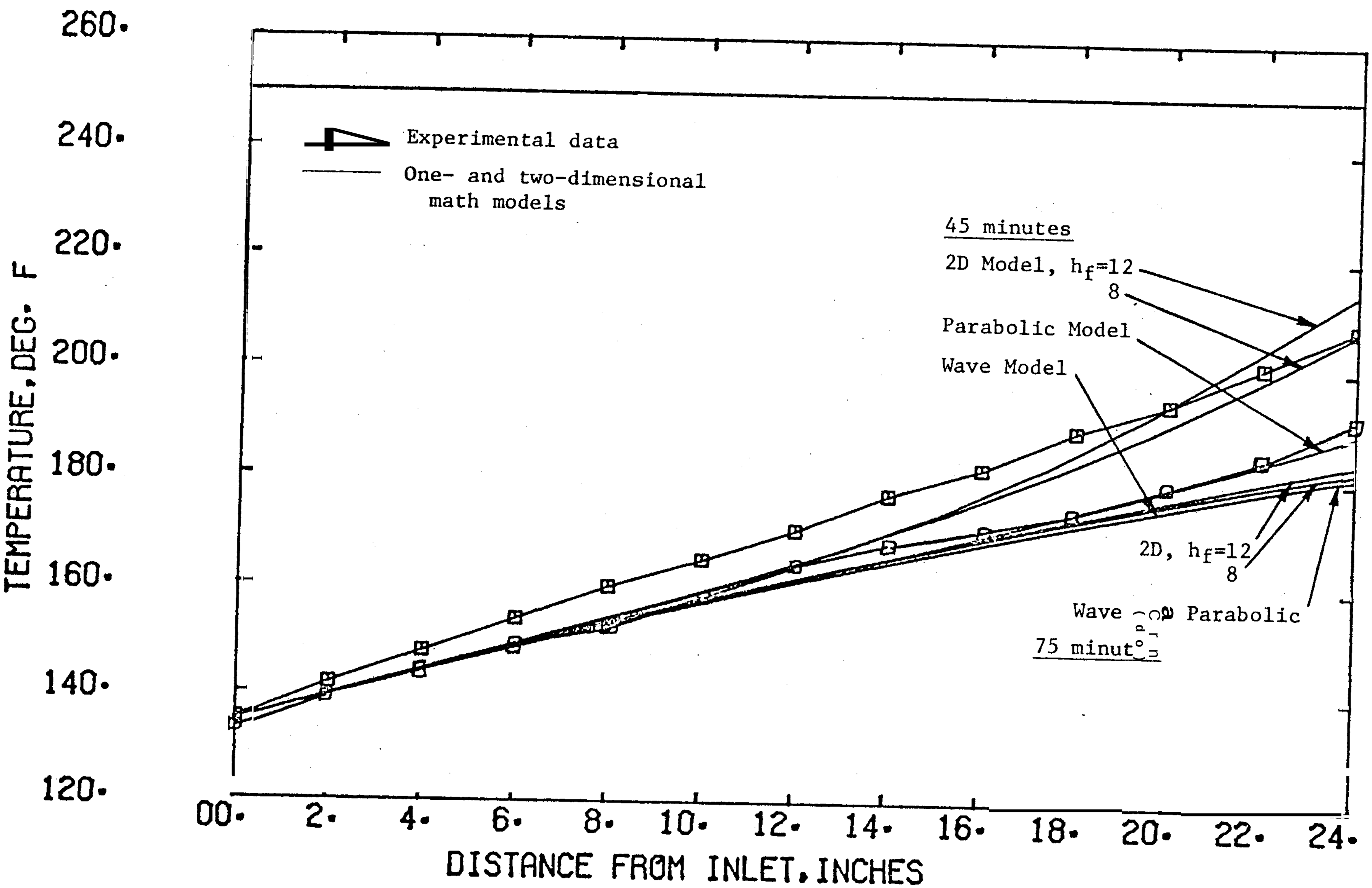

FIGURE 4.16. CALCULATED AND EXPERIMENTAL TEMPERATURES FOR EXPERIMENT CWI-S- [illegible] ARIHARA, $h=1.98$ BTU/(hr-ft^2-°F), $h_f=8,12$ BTU/(hr-ft^2-°F)

4.7.1 Axial Thermal Conductivity: In section 3.5, it was demonstrated that the early-time temperature behavior was partly controlled by axial heat conduction in the core. Section 3.6.3 concluded that intermediate-time transient behavior appeared to be controlled by an effective heat transfer coefficient higher than that at steady state, as well as by axial conduction near the wave front. Section 4 demonstrated that this result was caused by transient heat losses through the coreholder. It was hoped that axial heat conduction would dominate the early tine temperature profiles so that they would be insensitive to heat losses through the coreholder system. If this were the case, then there would be some hope of being able to determine effective axial thermal conductivities from the early time temperature data of Arihara.

Numerous calculations were carried out in order to determine the sensitivity of early time temperature profiles to both an effective heat loss coefficient, and axial thermal conductivity. These calculations were carried out for both constant and variable injection temperatures. The results showed that early time temperature profiles were sensitive to both the value of the effective overall heat loss coefficient, and the value of the axial thermal conductivity. In spite of this result, attempts were made to estimate axial thermal conductivities from the early time experimental data. These attempts were unsuccessful. While the interaction of axial heat conduction and transient heat losses appeared to play an important role, it could not be quantitatively described by any of the mathematical models for which solutions were available. In addition, some of the experiments had initial nonuniform temperature profiles. While the method of characteristics solution to the wave model could account for this, the solutions to the more complicated models could not.

4.7.2 The Film Coefficient between the Core and Viton: In sections 4.5 and 4.6, it was demonstrated that the intermediate-time temperature behavior of Arihara's data seemed to be dominated by transient heat losses through the coreholder. Furthermore, it was seen that the magnitude of the film coefficient, h_f, between the core and the viton sleeve seemed to play an important role in determining the shape of the intermediate-time temperature profiles. An attempt was made to find values of h_f which caused calculated temperature profiles to match the experimental temperature data of the CWI-S experiments of Arihara at intermediate- and long-times. The purpose was to deduce a relationship between h_f and the mass flowrate through the core. The results of these attempts are described in section 4.6. Fig. 4.17 summarizes these results in a graph of $\log_{10} h_f$ vs. $\log_{10} w''$. This figure presents results for the CWI-S series of experiments as well as for the HWI-B-1 experiment. While mass velocities were known with some accuracy, values of the film coefficient could only be estimated within the ranges shown. The range of h_f could not be bounded at one end for two of the experiments.

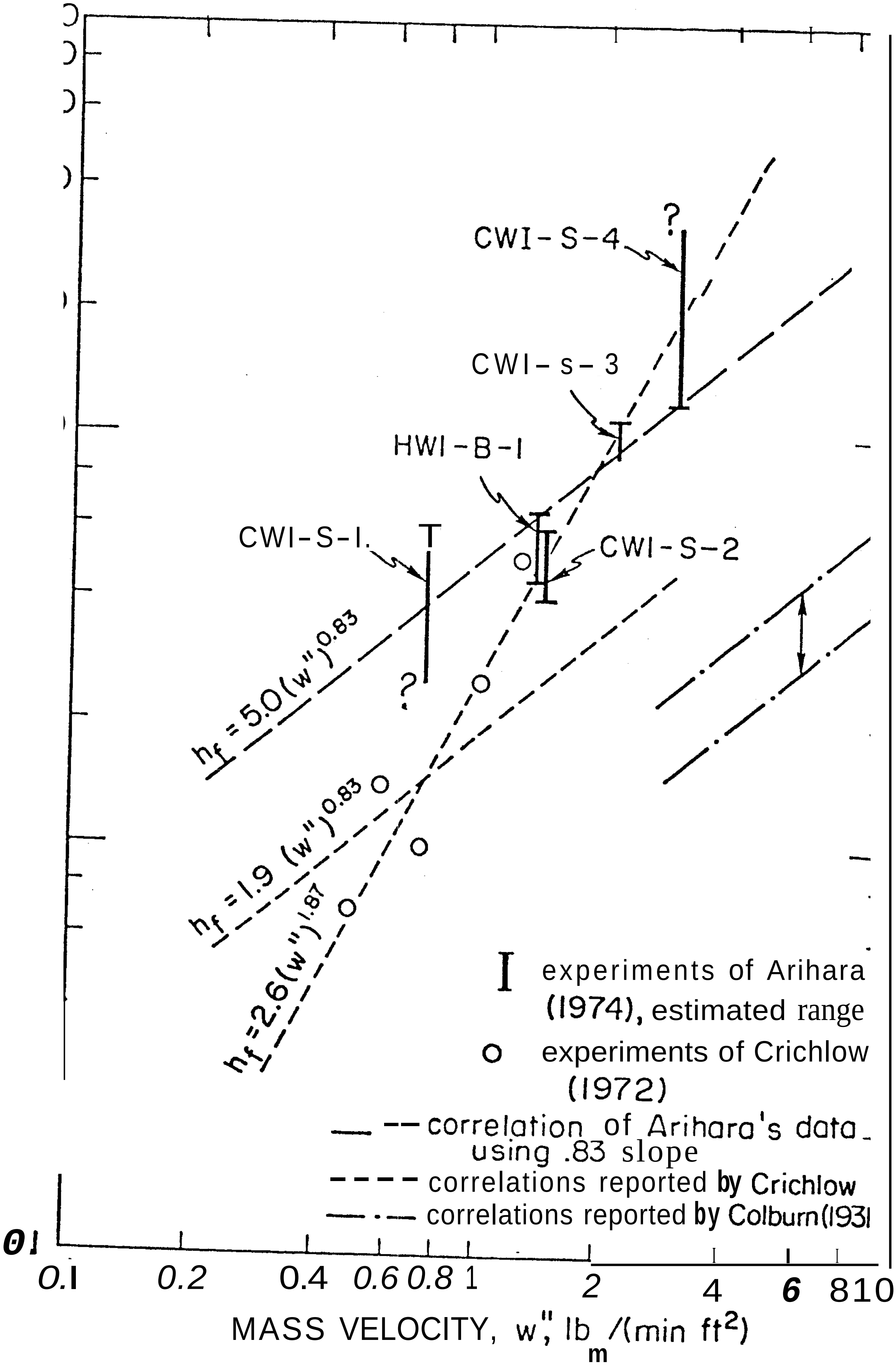

4.17 GRAPH OF THE FILM COEFFICIENT, h_f, VS. MASS VELOCITY, w''

Further calculations for these two experiments may be able to produce estimated upper or lower bounds on h_f.

Fig. 9.17 also presents information on correlations between the film coefficient, h_f, and the mass velocity, w'', which are available in the published literature. The relationship reported by Colburn (1931; discussed by Jakob, 1957, p. 553) is shown as an envelope of straight lines indicating the range of his correlations for different particle sizes. These results indicated that the film coefficient was,proportional to the mass velocity raised to the 0.83 power:

$$h_f \propto (w'')^{0.83} \qquad (4.34)$$

The constant of proportionality in this expression was found to depend on the ratio of tube diameter to equivalent particle diameter, as well as on the specific heat and viscosity of the fluid (Jakob, 1957, p. 556). Colburn's data was based on experiments carried out in two tubes (1-1/4 and 3 in, internal diameter) packed with particles of uniform size. These experiments were carried out under conditions different from those of Arihara. The mass velocity rates of Colburn were in the range of 12 to 390 lb/(min-ft2), as compared to the range of Arihara of 0.5 to 3.5 lb/(min-ft2). In addition, the particle sizes used in Colburn's experiments were much larger than those in Arihara's experiments. The smallest particles that Colburn used were 1/8 in. granules. The effective particle sizes in Arihara's experiments were orders of magnitude smaller. Thus, while the relationship between h_f and w" determined by Colburn may be correct for the conditions of Arihara's experiments, it is also possible that it is incorrect.

Fig. 4.17 also presents five data points reported by Crichlow (1972). These are based on matching the results of finite difference calculations with his experimental results. Crichlow did not report bounds on these results. His mass velocities were within the range reported by Arihara, although some of them were lower than those used in the CWI-S experiments of Arihara, Fig. 4.17 shows an interesting relationship between the results of Crichlow and Arihara. For one thing, the limited information available suggests that the h_f vs. w" relation for the Berea Sandstone (experiment HWI-B-1) may be the same as for the synthetic consolidated sandstone (CWI-S experiments). Furthermore, the original relationship between h_f and w" that was deduced by Crichlow:

$$h_f = 2.6 \, (w'')^{1.87} \tag{4.35}$$

seems to be consistent with the experimental data of Arihara. This was unexpected, because Crichlow used an unconsolidated sandstone with an effective pore size much larger than the two porous media of Arihara. It may be that below a certain particle size the constant of proportionality between h_f and $(w'')^{1.87}$ becomes independent of particle size. This suggestion is consistent with the agreement between the HWI-B-1 and CWI-S-2 experiments, which were carried out using different porous media. Fig. 4.17 also shows Crichlow's least squares correlation of his data using the 0.83 slope of Colburn. This figure also shows a straight line of 0.83 slope which approximately passes within the ranges of h_f deduced from Arihara's experiments.

We thus see that there is not enough information to deduce a relationship between the film coefficient and mass velocities in the experiments of Arihara with any satisfactory level of confidence. Crichlow indicates that for the same mass velocity, w", the overall magnitude of h_f decreases as particle size increases. While this is consistent with the observation from Fig. 4.17 that the correlating lines of slope 0.83 move upwards as particle size decreases, it is not entirely consistent with the results of Colburn as discussed by Jakob (1957, Figs. 42-15 and 42-16).

Calculations could have been carried out for more of Arihara's experiments in order to try to obtain more information about the relationship between h_f and w". Arihara's experiments were not designed with such a determination of h_f in mind, and hence it is not likely that better bounds on h_f could be determined from them. Hence such calculations were not made. It would be better to design a set of experiments to obtain an h_f vs. w" relationship using the theoretical and numerical results of this study. Such experiments could use both the proposed steady state method (section 3.4.1, Appendix C), as well as the results of section 4.

5. DYNAMIC DISPLACEMENT EXPERIMENTS FOR THE DETERMINATION OF ABSOLUTE PERMEABILITY UNDER NONISOTHERMAL FLOWING CONDITIONS

5.1 Introduction

Temperature effects on the absolute permeability of porous media are currently determined using a single experimental method: that of steady-state isothermal flow determinations at various temperature levels (Cassé, 1975). Because these experiments require constant temperature throughout the flowing system, it is usually necessary to wait for the core and its environment to reach the same temperature. Thus, the determination of absolute permeability at various temperature levels can be a tedious and time-consuming endeavor.

This situation is analogous to that of the experimental determination of isothermal two-phase relative permeability characteristics. Early experimental techniques were based on steady-state methods which required much time and care (Amyx, Bass, and Whiting, (1960), p. 184; Bear, (1972), 9.3.7), and which could only produce one data point from one experiment. Dynamic displacement methods based on the theory of Buckley and Leverett (1942) were later developed by Welge (1952), Johnson, Bossler, and Naumann (1959), and Jones (Ramey, 1971). These methods are based on the analysis of changing system properties during a transient-type of experiment rather than on single measurements made on a series of steady-state experiments. As a result, a single dynamic displacement experiment can produce information about relative permeabilities over a broad range of volumetric fluid saturations.

Two-phase dynamic displacement methods are based on an integration of Darcy's law over the length of the core, and on an understanding of the fluid saturation behavior in the core during the injection of a displacing fluid. There is a direct analog to this extraction of relative permeability functions available in nonisothermal, single-phase fluid injection experiments. Suppose we inject hot liquid at constant mass rate into a core which is at some base temperature T_e. Suppose further that the core has heat losses to the sides such that temperature profiles will advance down it in some known manner as shown in Fig. 5.1. If the liquid viscosity and density, and the absolute permeability of the medium are known functions of temperature, the pressure drop across the core should change as the temperature profiles change. This pressure drop can he calculated at any time by integrating Darcy's law over the length of the core. As a result, the pressure drop history, $\Delta p(t)$, can be evaluated. However, we often do not know the relation between the absolute permeability of the core and its temperature, $k(T)$, while at the same time we do have a measured pressure drop history, $\Delta p(t)$, for the experiment. Thus, it would seem that we still have the same amount of information as before, and in principle

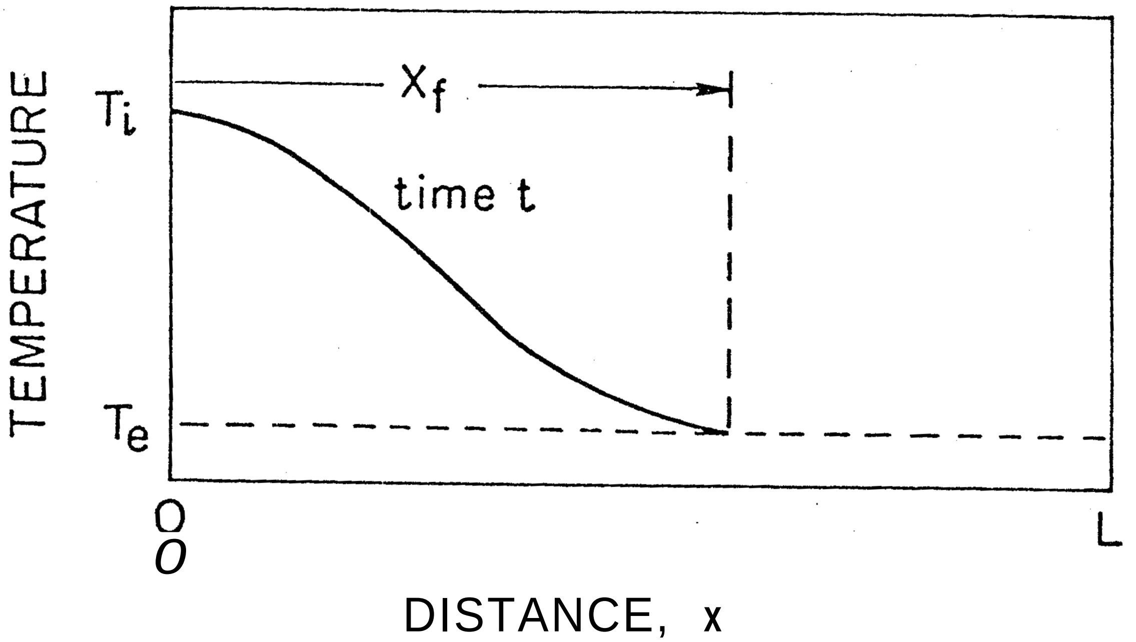

FIGURE 5.1. SCHEMATIC DIAGRAM OF TEMPERATURES IN A COLD CORE DURING THE INJECTION OF A HOT FLUID

should be able to determine the unknown function, $k(T)$, from the experimental data. This problem of "inverting" the $k(T)$ function from the experimental data is formulated in terms of an integral equation below.

5.2 Formulation of the Problem in Terms of an Integral Equation

Assume that Darcy's law is valued for single-phase non-isothermal flow, and that the absolute permeability is a single-valued function of temperature. Then we have:

$$\begin{matrix}\text{Volumetric} \\ \text{Flowrate}\end{matrix} = \frac{w(t)}{\rho(T)} = -\frac{k(T)A_c}{\mu(T)} \cdot \frac{\partial p(x,t)}{\partial x} = -\Lambda(T)\, A_c \frac{\partial p(x,t)}{\partial x} \tag{5.1}$$

where: T = temperature, a function of space and time, $T(x,t)$

w = mass flowrate, a function of time, $w(t)$

p = fluid density, a function of temperature, $\rho(T)$

A = fluid mobility, absolute permeability/viscosity, a function of temperature, $\lambda(T)$

A_c = cross-sectional area to flow

$\frac{\partial p}{\partial x}$ = local pressure gradient, a function of distance, x, and time, t.

Rearranging:

$$\frac{1}{w(t)} \cdot \frac{\partial p}{\partial x}(x,t) = -\frac{1}{A_c \Lambda(T) \rho(T)} \tag{5.2}$$

Integrating along the core:

$$\frac{\Delta p(t)}{w(t)} = \frac{1}{w(t)}\int_{x=0}^{L} \frac{\partial p}{\partial x}(x,t)\, dx = \frac{-1}{A_c}\int_{x=0}^{L} \frac{1}{\Lambda(T)\rho(T)}\, dx \qquad (5.3).$$

Let $x_f(t)$ **be** a measure of the distance the front edge of the temperature profile has moved, as shown in Fig. 5.1. After breakthrough, define $x_f(t)$ a L, such that

$$x_f(t) \triangleq \begin{cases} x_f(t), \text{ when } T(L,\cdot` \quad ^m \\ \end{cases} \qquad (5.4).$$

Of the three apparent independent variables in Eq. 5.3, T, x, and **t**; only two are truly independent. Choose temperature, T, and time, **t**, as the independent variables, and recast the right-hand side of Eq. 5.3 in terms of these in the region $0 \le x \le x_f$.

$$-\frac{\Delta p(t)}{w(t)/A_c} = \int_{T=t_i(t)}^{T_f} \frac{1}{\Lambda(T)\rho(T)} \cdot \left(\frac{dx}{dt}\right) dT + \int_{x=x_f(t)}^{L} \frac{1}{\Lambda(T_e)\rho(T_e)} \qquad (5.5)$$

where :

$$\begin{cases} T_e, \text{ for } x_f < L \\ T(L,t), \text{ for } x_f = L \end{cases}$$

Evaluating the second integral explicitly, rearranging, and reversing the limits on the integral, we obtain:

$$\frac{\Delta p(t)}{w(t)/A_c} + \frac{[L-x_f(t)]}{\Lambda(T_e)\rho(T_e)} = \int_{T=T_f)t)}^{T_i(t)} \frac{1}{\Lambda(T)\rho(T)\frac{dT}{dx}(T,t)} dT \qquad (5.6)$$

This is an equation of the form:

$$F(t) = \int_{T_f(t)}^{T_i(t)} G(T) \cdot H(T,t)\, d \qquad (5.7)$$

where
$$F(t) \triangleq \frac{\Delta p(t)}{w(t)/A_c} + \frac{[1-x_f(t)]}{\Lambda(T_e)\rho(T_e)}$$

$$G(t) \triangleq 1/[\Lambda(T)\rho(T)]$$

$$H(T,t) \triangleq 1/\frac{dT}{dx}(T,t)$$

Eq. 5.7 is a Linear Integral Equation of the First Kind, which may be singular at the point $T_f(t) = T_e$, if $\frac{dT}{dx}(x_f,t) = 0$ (Courant and Hilbert (1953), Ch. III; Squires (1970)). If the injection temperature, T_i, is constant, the equation is a Fredholm Equation (i.e., it has fixed limits of integration) so long as $x_f<L$.

If the temperature behavior in the system is known, and in addition the pressure drop history is measured, then both the function F(t) and the Kernel H(T,t), are known, and hence we can in principle solve Eq. 5.6 for the function G(T). If F(t) and H(T,t) were both simple analytic functions, then it might be possible to determine G(T) for the Fredholm problem in analytic form using classical methods for solving integral equations. However, since F(t) is composed of measured experimental data, and H(T,t) is seldom simple, we must either resort to numerical methods for inverting G(T) from the experimental data, or else attempt to find the solution to a simplified problem. These two alternative approaches are discussed in the following.

5.3 Numerical Solution of the Integral Equation

The application of finite differencing techniques to Eq. 5.7 converts the problem into that of solving a linear algebraic system of equations (Squires, 1970). Unfortunately this system is commonly overdetermined as well as ill-conditioned, and the task of obtaining a meaningful answer is not always easy. This difficulty arises because the expression (5.7) represents a mathematically ill-posed problem (Heath, 1974). While various methods are available for solving such overdetermined and ill-conditioned systems of equations, this approach has not been pursued further.

Recognition of the fact that this problem is ill posed allows us to obtain insight into the nature of any solution which we can find to the dynamic displacement experiment. In effect this tells us that small errors in the experimental data can cause large errors in the resulting answers.

5.4 Graphical Solution to a Simplified Problem

If certain simplifying assumptions can be made about the nature of energy movement in the physical system, then a particularly elegant and simple graphical solution to the inversion problem can be obtained. These simplifying assumptions are:

(1) constant flowrate throughout the core

(2) constant injection temperature

(3) zero axial thermal conductivity and infinite radial thermal conductivity in the core

(4) heat losses from the side of the core can be represented simply by a temperature difference times an overall heat transfer coefficient

(5) both the core and fluid have constant thermal properties

The solution to this simplified problem is presented as Eq. 3.20. The resulting transient temperature profile is that of a constant velocity, exponentially-decaying sharp front moving through the core, leaving constant temperatures behind (shown schematically in Fig. 3.3). The sharp front moves with a constant velocity:

$$\frac{dx_{\perp}}{dt} = \frac{wC_w}{A_c M_f} \tag{5.8}$$

where: C_w = specific heat of the fluid per unit mass

M_f = bulk volumetric specific heat of the core-water system

The result of a sharp front is a direct consequence of the assumption of zero axial thermal conductivity. This is directly analogous to the sharp saturation front which results in Fuckley-Leverett frontal advance calculations when the capillary pressure is assumed to be zero.

This simplified temperature model can be applied to the integral form of Darcy's law, Eq. 5.3:

$$\frac{\Delta p(t)}{w(t)} = \frac{1}{w(t)} \int_{x=0}^{L} \frac{\partial p(x,t)}{\partial x}\, dx = \frac{-1}{A_c} \int_{x=0}^{L} \frac{1}{\Lambda(T)\rho(T)}\, dx \qquad (5.3)$$

Differentiating both sides with respect to time, t, and using Leibniz's rule for differentiating under an integral:

$$\frac{d}{dt}\left\{\frac{\Delta p(t)}{w(t)}\right\} = -\frac{1}{A_c}\left[\frac{1}{\Lambda(T_f)\rho(T_f)} \cdot \frac{dx_f}{dt} + \int_0^{x_f(t)} \frac{d}{dt}\left\{\frac{1}{\Lambda(T)\rho(T)}\right\} dx + \frac{1}{\Lambda(T_e)\rho(T_e)} \frac{d}{dt}\{L - x_f(t)\}\right]$$

$$= -\frac{1}{A_c} \cdot \frac{dx_f}{dt} \cdot \left|\frac{1}{\Lambda(T_f)\rho(T_f)} - \frac{1}{\Lambda(T_e)\rho(T_e)}\right|$$

$$= -\frac{wC_w}{A_c^2 M_f} \cdot \left[\frac{1}{\Lambda(T_f)\rho(T_f)} - \frac{1}{\Lambda(T_e)\rho(T_e)}\right] \qquad (5.9)$$

Thus, a graph of the experimental data in the form $(\Delta p(t)/w)$ versus time should give a curve whose slope for fixed system properties is a function of the front temperature only. This is indicated in Fig. 5.2. Fence, if we know the temperature of the front, T_f, as a function of time, then it is possible to invert the mobility, and consequently the absolute permeability of the core, as a function of temperature.

It is clear that a sharp temperature front in the core is physically unrealistic, and that hence the zero axial thermal conductivity assumption of this simplified temperature model is not entirely reasonable. This effect of axial thermal conductivity on temperature profiles in cores is discussed in section 3.

The effect of applying this simple graphical method to experimental results which include axial thermal conductivity and other nonideal effects is not known, but can be easily determined from numerical experiments.

This simple graphical method is analogous to the graphical methods for inverting relative permeability curves of Johnson, et al. (1959), and Jones (Ramey, 1971). Furthermore, although the relative permeability inversion methods are based on frontal advance theory with no capillary pressure, they are successfully applied to real systems which are affected by capillary pressure.

5.5 Summary

This section has discussed the novel idea of designing a nonisotherrnal dynamic displacement experiment for the determination of absolute permeability under nonisothermal flowing

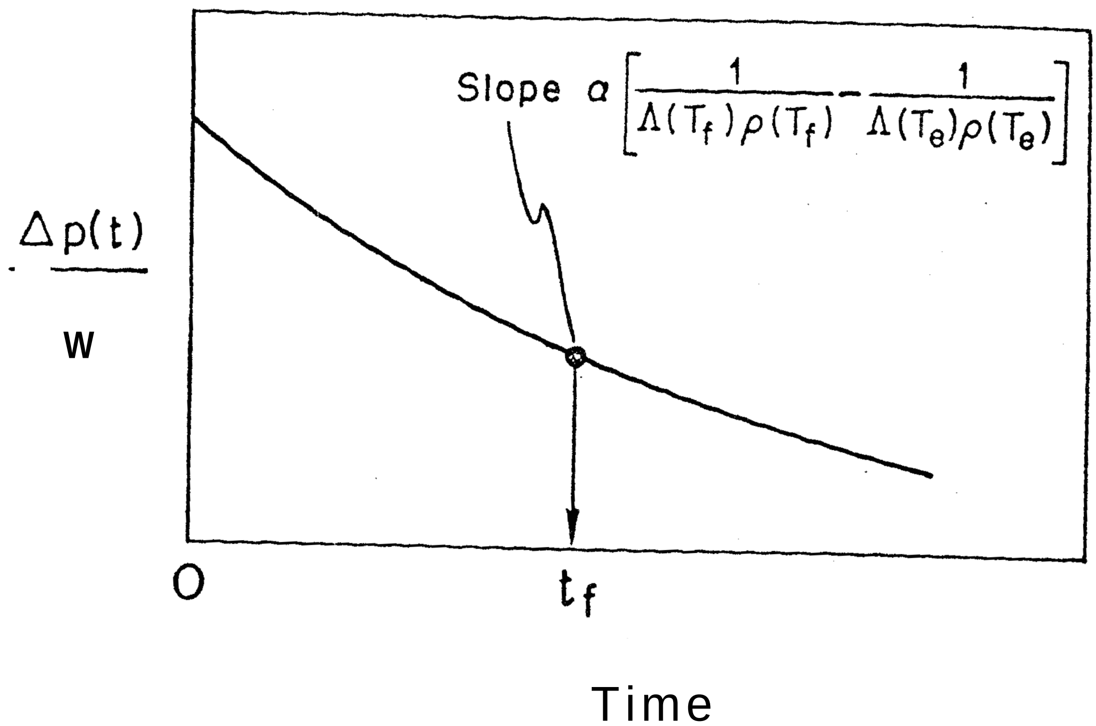

FIGURE 5.2. SCHEMATIC OF THE GRAPHICAL SOLUTION TO THE SIMPLIFIED PROBLEM OF INVERTING A NONISOTHERMAL DYNAMIC DISPLACEMENT EXPERIMENT

conditions. It was observed that such an experiment could significantly reduce the tedium involved in determining the variation of absolute permeability of porous media with temperature. However, an integral formulation of the problem led to the conclusion that it was ill-posed. Thus, small errors in the experimental, or input, data can cause large errors in the solution to the problem.

Two methods for obtaining useful information from the experimental data of a nonisothermal dynamic displacement experiment were discussed. The first requires measured pressure drops as well as measured temperature profiles, both as a function of time. The input data are processed by using a particular kind of numerical technique. While the ill-posed nature of the problem may cause specific numerical results to be of questionable validity, methods are available for attempting to obtain reasonable answers from such data. The second method for analyzing nonisothermal dynamic displacement data requires that the thermal behavior of the core approximate an idealized mathematical model. If this requirement is met, then a simple and elegant graphical solution technique can be used.

The idea of a nonisothermal dynamic displacement experiment does not seem to have been proposed before. While such experiments would not be easy to interpret, both of the techniques discussed in this section hold some promise of being useful in interpreting the results of nonisothermal single-phase experiments.

CONCLUSIONS

This study has developed a series of mathematical models of heat transfer during nonisothermal liquid flow in fine-grained porous media. The models describe heat transfer in cylindrical laboratory cores mounted in Hassler-type core-holders. The results of the analysis of these models may be summarized in the following conclusions:

(1) Both the nature of heat losses to the environment, as well as heat convection due to liquid flow, play important roles in heat transfer in laboratory experiments.

(2) The mathematical models were verified by comparing them to published experimental data. No one model could match the experimental data over the full range of time. However, each model incorporated heat transfer mechanisms which were important during some time period.

(3) Long-time temperatures were controlled by the interaction of steady heat losses to the environment, and convective heat transport due to liquid flow. An axial thermal conduction mechanism was important during early times. Finally, intermediate-time temperatures were strongly affected by transient heat losses through the coreholder.

(4) It was determined that the transient heat losses through the coreholder system were controlled by a film coefficient between the core and coreholder. The magnitude of this film coefficient was found to depend on the mass velocity

of liquid flow through the core. The nature of this dependence can be determined by performing a suitably designed experiment. While the execution of this experiment was outside the scope of this study, a description of it is presented for future consideration.

(5) No fundamental differences were observed in the heat transfer behavior of the hot and cold liquid injection experiments of Arihara. However, some of the hot water injection experiments did show an end effect which was caused by heat conduction through the brass endcap and the steel shell of the coreholder system.

(6) It was theoretically confirmed that the heating or cooling efficiencies of hot or cold liquid injection experiments in the laboratory should depend on mass flowrate through the core. The variation with flowrate of both the axial thermal conduction mechanism, as well as the core-coreholder film coefficient, plays an important role in the nature of the heating efficiency dependence on mass injection rate. It is. unlikely that these effects will be important in field operations. Hence, heating and cooling efficiencies in field projects should not depend on mass injection rate.

(7) The new idea of a dynamic displacement single-phase nonisothermal Liquid injection experiment has been discussed. Such an experiment would be convenient to perform, and could determine the variation with temperature of the absolute permeability of a porous medium. Furthermore, this determination would be accomplished under nonisothermal flowing conditions.

NOMENCLATURE

As far as possible, the nomenclature has been made consistent with standard Society of Petroleum Engineers nomenclature.

English

A = area

A_c = cross-sectional area of core to fluid flow (macroscopic)

$A_{[illegible]}$ = cross-sectional area of the steel shell to heat conduction

B_i = Biot dimensionless number

c = a constant with specified definition

C = specific heat on a mass basis

D = thickness of the viton insulator

e_w = specific energy of the liquid on a unit mass basis

e_f''' = specific energy of the formation on a unit volume basis

E_h = efficiency of heating

E_c = convective heat transfer coefficient, (energy)/(time-area-temperature difference)

$\bar{h}$ = overall steady state heat loss coefficient from the core

h_e = film coefficient between the steel shell of the coreholder and the external airbath environment

$h_{e\ell}$ = effective lumped external film coefficient to account for the temperature drop across the coreholder

h_f = internal film coefficient between the formation and the viton sleeve in the coreholder system

I = convolution integral in the pseudo two-dimensional analytic solution

k = absolute permeability

M_f = specific heat of the formation (liquid-matrix continuum) on a unit volume basis

P = perimeter of the core

p = pressure

Δp = pressure drop across the core

$\dot{Q}$ = heat transfer rate, (energy/time)

Q' = heat transfer rate per unit length of core, (energy/time)/(length)

Q'' = heat transfer rate per unit exposed surface area of core, (energy/time)/(area)

r = distance in the radial direction

r_o = radius of the core

r_{si} = inside radius of the steel shell

r_{so} = outside radius of the steel shell

r_{vo} = outside radius of the viton sleeve

R = thermal resistance for steady heat transfer per unit time per unit exposed surface area of core

R_A = thermal resistance due to heat conduction across the annulus

R_e = thermal resistance due to a film coefficient at the external surface of the steel shell

$R_{e\ell}$ = $R_e + R_{ss} + R_A + R_v$: thermal resistance due to conduction across the coreholder and a film coefficient at the external surface of the steel shell

R_{int} = $R_v + R_A + R_{ss}$: thermal resistance due to conduction across the coreholder system

R_{ss} = thermal resistance due to conduction across the steel shell

R_v = thermal resistance due to conduction across the viton sleeve

s = Laplace transform variable

t = time

T = temperature

T_b = base or datum temperature for specifying energy content

T_e = temperature of' the airbath external to the core system

T_i = injection temperature at the upstream end of the core

T_f = temperature of the formation, used when distinguishing it from the viton temperature

$T_{9,v}$ = lumped temperature of the viton

u,v = dimensionless temperatures

w = macroscopic mass flowrate through the core, (mass/time)

w'' = mass velocity (macroscopic mass flowrate through the core on a unit cross-sectional area to flow basis), (mass)/(time-area)

x = distance in the axial direction

Greek Symbols

ϕ = porosity

λ = thermal conductivity, (energy)/(time-area-temperature gradient)

A = liquid mobility, defined as permeability/viscosity

ρ = density, (mass/volume)

κ = thermal diffusivity, $\triangleq \lambda/(\rho C)$, (length2/time)

α, β, γ, 6, η, ω, ζ, ξ = parameters in various differential equations

SUBSCRIPTS

English

b = base or datum level

c = macroscopic cross-section to fluid flow

D = dimensionless value

DP = dimensionless value for the parabolic model

DT = dimensionless value for the pseudo two-dimensional model

DW = dimensionless value for the wave model

e = value on the exterior

$e\ell$ = lumped value on the exterior

f = formation, or core-rock matrix continuum

i = injection

ℓv = lumped value of the viton insulator

ma = rock matrix, sand grains

o = outside dimension of the core

P = parabolic model

si = inside of steel shell

so = outside of steel shell

ss = stainless steel shell

v = viton insulator

w = water or liquid

W = wave model

MATHEMATICAL NOTATION

$\triangleq$ = is defined by

Laplace Transform Notation:

$L\{a\}$ = Laplace transform of (a)

$L^{-1}\{a\}$ = inverse Laplace transform of (a)

$(\bar{\ })$ = Laplace transform of the variable of interest, e.g.:

$$L\{x\} = \bar{x},\ L^{-1}\{\bar{x}\} = x$$

s = Laplace transform variable

$f(s)$ = function in Laplace space

$F(s)$ = function in real space

note: $f(s)$ □ $L\{F(t)\}$; $F(t) = L^{-1}\{f(s)\}$

$H(x)$ = Heaviside function, 0 when $x<0$, 1 when $x \geq 0$

$\mathrm{erf}(x)$ = error function,

$$\sqrt{\pi} \quad \int_{u=o}^{u=x} \qquad du$$

$\cosh(x)$ □ hyperbolic cosine function = $\dfrac{e^{x} + e^{-x}}{2}$

<u>SUPERSCRIPTS</u>

$(\ )'$ = quantity based on a unit length

$(\ )''$ = quantity based on a unit area

$(\ )'''$ = quantity based on a unit volume

$(\ )^{(i)}$ = quantity at the ith time level

REFERENCES

Acrivos, A.: "Method of Characteristics Technique," Ind. Engr. Chem. (1956), 48, 1, p. 703.

Adivarahan, P., Kunii, D., and Smith, J.M.: "Heat Transfer in Porous Rocks through which Single-phase Fluids are Flowing," Soc. Pet. Engr. J. (September 1962), p. 290.

Amyx, J.W., Bass, D.M., and Whiting, R.L., Petroleum Reservoir Engineering, McGraw-Hill, New York, N.Y., 1960.

Antimirov, M.: "The Question of Integral Volume of Thermal Loss during Thermal Injection into Strata," Ya. Neft. i Gaz, 8 (11) (1965), p. 45.

Arihara, N.: A Study of Nonisothermal Single and Two-Phase Flow through Consolidated Sandstones, SGP-TR-2, NSF Grant No. GI-34925, Stanford University, November 1974.

Arihara, Norio: Personal Communication, April 1976.

Baker, P.E.: "Heat Wave Propagation and Losses in Thermal Oil Recovery Processes," Proc., 7th World Petroleum Congress, Mexico City (1968).

Bear, J.: Dynamics of Fluids in Porous Media, Elsevier, 1972.

Bodvarsson, G.: "On the Temperature of Water Flowing through Fractures," Journal of Geophysical Research, Vol. 74, No. 8 (April 15, 1969), p. 1987.

Bodvarsson, G.: "Thermal Problems of Siting of Reinjection Wells," Geothermics, Vol. 1, No. 2 (June 1972), p. 63.

Bodvarsson, G.: "Geothermal Resource Energetics," Geothermics, Vol. 3, No. 3 (September 1974), p. 83.

Brigham, W.E.: "Mixing Equations in Short Laboratory Cores," Soc. Pet. Engr. J. (February 1974), p. 91.

Buckley, S.E., and Leverett, M.D.: "Mechanism of Fluid Displacement in Sands," Trans AIME, 146 (1942), p. 107.

Carslaw, H.S., and Jaeger, J.C., Conduction of Heat in Solids, Oxford University Press, 2nd Edition, 1959.

Cassé, F.J. : "The Effect of Temperature and Confining Pressure on Fluid Flow Properties of Consolidated Rocks," Ph.D. Thesis, Stanford University, November 19'74.

Chappelear, J.E. , and Volek, C.W.: "The Injection of a Hot Liquid into Porous Medium," Soc. Pet. Engr. J. (March 1969), p. 100.

Chen, H.K. : Personal Communication, April 1976.

Churchill, R.V. : Operational Mathematics, McGraw-Hill, 2nd Edition (1958).

Colburn, A.P. : "Heat Transfer and Pressure Drop.in Empty, Baffled, and Packed Tubes," Ind. Enp. Chem., ~~23~~ (1931), p. 910.

Courant, R., and Friedrichs, K.O. : Supersonic Flow ~~and Shock~~ Waves, Interscience Publishers, New York, 1948.

Courant, R. , and Hilbert, D. : Methods of Mathematical ~~Physics~~, Interscience Publishers, 1953, Vol. I.

Craig, F.F., Jr.: The Reservoir Engineering Aspects of Water-flooding, Society of Petroleum Engineers Monograph, Vol. 3, 1971.

Crichlow, H.B.: "Heat Transfer in Hot Fluid Injection in Porous Media," Ph.D. Thesis, Stanford University, May 1972.

Dupont Publication: The Engineering Properties of Viton (A-65053,4/69), E.I. duPont Nemours & Co. (Inc.), Elastomer Chemicals Department, Wilmington, Delaware 19898.

Ersoy, Demir: "Temperature Distributions and Heating Efficiency of Oil Recovery by Hot Water Injection," Ph.D. Thesis, Stanford University, August 1969.

Fayers, F.J. : "Some Theoretical Results Concerning the Displacement of a Viscous Oil by a Hot Fluid in a Porous Medium," J. Fluid Mech., 13 (1962), Pt. 1, p. 65.

Geertsma, J., Croess, G.A., and Schwarz, N.: "Theory of Dimensionally Scaled Models of Petroleum Reservoirs," Trans. AIME (1956) 207, p. 118.

Green, D. W.: "Heat Transfer with a Flowing Fluid through Porous Media," Ph.D. Dissertation, University of Oklahoma, 1962.

Gringarten, A.C. , Witherspoon, P.A., and Ohnishi, Yuzo: "Theory of Heat Extraction from Fractured Hot Dry Rock," J. of Geophysical Research, Vol. 80, No. 8 (March 10, 1975), p. 1120.

Gringarten, A.C., and Sauty, J.P.: "Recovery of Heat Energy from Aquifers," presented at the Second United Nations Symposium on the Development and Use of Geothermal Resources, May 19-29, 1975, San Francisco, California.

Heath, Michael, T.: "The Numerical Solution of Ill-Conditioned Systems of Linear Equations," Oak Ridge National Laboratory Report No. 4597, UC-32-Mathematics and Computers (July 1974).

IMSL: International Mathematical E Statistical Libraries, Inc., September 1975, Sixth Floor, GNB Building, 7500 Bellaire Blvd., Houston, Texas 77036.

Jaeger, J.C., and Martha Clarke: "Numerical Results for Some Problems on Conduction of Heat in Slabs with Various Surface Conditions," Phil. Mag. (7) 38 (1947), p. 504.

Jakob, M.: Heat Transfer, John Wiley and Sons, Inc., 1957, Vol. 11.

Jenkins, R., and Aronofsky, J.S.: "An Analysis of Heat Transfer Processes in Porous Media--New Concepts in Reservoir Heat Engineering," Producers Monthly (1955) 19, p. 37.

Johnson, E.F., Bossler, D.P., and Naumann, V.O.: "Calculation of Relative Permeability from Displacement Experiments," Trans. AIME, 216 (19591, p. 370.

Kays, W.M., and London, A.L.: Compact Heat Exchangers, McGraw-Hill, New York, N.Y., 1964.

Keenan, J.H., and Keyes, F.G.: Thermodynamic Properties of Steam, John Wiley and Sons, Inc., New York, N.Y., 1936.

Keenan, J.H., Keyes, F.G., Hill, P.G., and Moore, J.G.: Steam Tables: Thermodynamic Properties of Water including Vapor, Liquid, and Solid Phases (English Units), John Wiley and Sons, Inc., New York, N.Y., 1969.

Kreith, F.: Principles of Heat Transfer, Intext, 3rd Ed., 1973.

Lauwerier, H.A.: "The Transport of Heat in an Oil Layer Caused by Injection of Hot Fluid," Applied Scientific Res., Sec. A.5 (1955), p. 145.

Malofeev, G.E.: "Experimental Study of Formation Heating when Injecting Hot Water," Neft i Gaz, Vol. 1, No. 12 (19581, p. 77.

Malofeev, G.E.: "Simulation of the Formation-Heating Process during the Injection of Hot Fluid into a Well," Neft i Gaz, Vol. 3, No. 7 (1960), p. 59.

Marx, J.W., and Langenheim, R.H.: "Reservoir Heating by Hot Fluid Injection," Trans. AIME, 216 (1959), p. 312.

Nathenson, M.: Physical Factors Determining the Fraction of Stored Energy Recoverable from Hydrothermal Convection Systems and Conduction Dominated Areas, U.S. Geological Survey, Open-File Report 75-525 (October 1975).

Penberthy, W.L., and Ramey, H.J., Jr.: "Design and Operation of Laboratory Combustion Tubes," Soc. Pet. Engr. J. (June 19661, p. 183.

Prats, M.: "The Heat Efficiency of Thermal Recovery Processes," J. Pet. Tech. (March 1969), p. 323.

Ramey, H.J., Jr.: "Reservoir Heating by Hot Fluid Injection, Discussion," Trans. AIME, 216 (19591, p. 364.

Ramey, H.J., Jr.: "Hot to Calculate Heat Transmission in Hot Fluid Injection," Petr. Engr. (November 1964), p. 110.

Ramey, H.J., Jr.: "A Current Review of Oil Recovery by Steam Injection," Proceedings of the Seventh World Petroleum Congress, Mexico City, 1968.

Ramey, H.J., Jr.: Petroleum Engineering Course Number 280, "Modern Fluid Injection," Stanford University, Spring Quarter, 1971.

Roberts, G.E., and H. Kaufman: Table of Laplace Transforms, W.B. Saunders Co., 1966.

Rubinstein, L.I.: "The Total Heat Losses in Injection of a Hot Fluid into a Stratum," Neft i Gaz, 2, No. 9 (1959), p. 41.

Somerton, Wilbur H.: "Some Thermal Characteristics of Porous Rocks," Trans. AIME, 213 (1958), p. 375.

Spillette, A.G.: "Heat Transfer during Hot Fluid Injection into an Oil Reservoir," J. Canadian Pet. Tech. (Oct.-Dec. 1965), p. 213.

Squires, W.: Integration for Engineers and Scientists, American Elsevier, 1'370.

Thomas, G.: "Heat Transfer during Hot Fluid Injection into an Oil Reservoir, Discussion," J. Canadian Pet. Tech. (Oct.-Dec. 1965), p. 26.

Welge, H. J.: "A Simplified Method for Computing Oil Recovery by Gas or Water Drive," Trans. AIYE, 195 (19521, p. 91.

Weinstein, H.G., Wheeler, J.A. , and Woods, E.G.: "Numerical Model for Steam Stimulation," SPE Paper No. 4759, presented at the Improved Oil Recovery Symposium of the Society of Petroleum Engineers, Tulsa, Oklahoma, April 22-24, 1974.

Willhite, G.P. , Dranoff, J.S. , and Smith, J.M.: "Heat Transfer Perpendicular to Fluid Flow in Porous Rocks," Soc. Pet. Engr. J. (September 1963), p. 185.

Willman, B.T., Valleroy, V.V., Runberg, G.W., Cornelius, A.J., and Powers, L.W.: "Laboratory Studies of Oil Recovery by Steam Injection," J. Pet. Tech. (July 1961), p. 681.

APPENDIX A

DISCUSSION OF THE ASSUMPTIONS INVOLVED IN THE ONE-DIMEMSIONAL MODEL

The various idealizations required to obtain the one-dimensional mathematical models presented in section 3 are discussed below in the order in which they were presented.

(1) The assumption of a uniform radial temperature distribution at any axial distance and time is not strictly correct. Temperature differentials between the core axis and circumference of as much as 25% of the total temperature drop in the system have been reported by Penberthy and Ramey (1966) for combustion tube experiments. Ersoy (1969) reported a maximum temperature differential of 15% for his hot water injection experiments. However, Chappelear and Volek (1969) concluded on the basis of both experimental and numerical experiments that while the Lauwerier theory is not adequate for describing the details of temperature profiles accurately, it does tend to give a good approximation for the average temperatures in the reservoir.

(2) The phenomenon of an effective axial thermal conductivity of a porous medium in the direction of fluid flow is well known, and has been studied, for example, by Adivarahan, et al. (1962), arid Green (1962). The assumption that

axial heat conduction in the coreholder is negligible is reasonable. Table A.1 presents the dimensions and thermal properties of the various components of the core/coreholder system which is depicted in detail in Fig. 4.1. An examination of this table suggests that while the steel shell may conduct as much heat as the core in an axial direction, this effect is substantially reduced by the insulating effect of the viton and annulus.

(3) The assumption of simple convective heat losses. from the side of the core is justified for steady-state flow by experimental observations. However, this assumption ignores thermal capacitance effects in the coreholder system during transient heat flow. An examination of the thermal diffusivities of the components of the coreholder system (Table A.1) suggests that the viton layer has the largest effect on the propagation of heat transients.

The effect of this viton layer along on the passage of transients through the coreholder can be examined by considering the following heat transfer problem:

$$\frac{\partial^2 T}{\partial x^2} = \frac{1}{\kappa}\frac{\partial T}{\partial t}, \quad 0<x<D \tag{A.1}$$

$$T(x,0) = 0, \quad 0<x<D \tag{A.2}$$

$$-\lambda_v \frac{\partial T}{\partial x} + h_f (T_i - T) = 0, \quad x = 0, \quad t>0 \tag{A.3}$$

$$\lambda_v \frac{\partial T}{\partial x} + h_e T = 0, \quad x = D, \quad t>0 \tag{A.4}$$

Table A.1 Dimensions and Heat Transfer Parameters for Various Components of the Core and Coreholder System

Component	Outside Diameter Inches	Thickness Inches	Thermal Conductivity BTU/(hr-ft^2-^oF	Thermal Diffusivity ft^2/hr	Film Coefficient BTU/(hr-ft^2-^oF)
Steel Shell	3.5	0.438	10[1]	0.15[1]	Steel Shell/ External Environment
Annulus			0 0[illegible]6[1,2]	0 045[1,2]	h_e=0.7 to 3.6[6]
Viton	2.5	0.25	0 [illegible]3[3]	0 003[3]	Core/Viton,
Core	2.0	-	Radial: ~[illegible][4] Axial: ~10[5]	Radial: ~ 025[4] Axial: ~ 25[5]	$h_f = \begin{cases} 10 \text{ to } 35^{(6)} \\ 1 \text{ to } 6^{(7)} \end{cases}$

References: (1) Kreith (1973), Tables A-1, -2, and -3
(2) Arihara (1974), pp. 70-80.
(3) Dupont Publication (1969).
(4) Crichlow (1972), p. 82; Willhite, Dranoff, and Smith (1963).
(5) Adivarahan, Kunii, and Smith (1962).
(6) Arihara (1974), Tables 2 and 3.
(7) Crichlow (1972), Fig. 39.

This corresponds to the physical problem of the linear conduction of an input step function temperature, T_i, through a viton slab of thickness D, thermal diffusivity, κ, thermal conductivity, λ_v, and with simple convective heat transfer at the boundaries X = 0 and D with coefficients h_f and h_e, respectively (Carslaw and Jaeger (1959), p. 118). The solution to this initial boundary value problem has been evaluated by Jaeger and Clarke (1947) for the case of h_f effectively infinite, or $T(0,t) = T_i$. An examination of this solution using the parameters and dimensions of the viton in the coreholder system can be made. Such an examination indicates that the effect of the step function at X = 0 will only begin to be felt at x = D after a time of approximately one minute, while steady heat conduction will be approached after about ten minutes.

Thus, if temperature changes in the core are rapid with respect to a time scale of ten minutes, then it would be expected that thermal capacitance effects in the coreholder system will affect the temperature profiles in the core.

(4) The rock and fluid thermal properties of interest involve the specific heats of both the liquid and saturated formation, In the ranges of pressure and temperature of interest (as high as 500 psia, 70°F to 400°F), the specific heat of water can be approximated by:

$$C_w = 0.9975 + (8.67\times10^{-7})\cdot(T-100)^2 \tag{A.5}$$

where T is in ^{o}F, and C_w is in BTU/(lb-^{o}F) (data from Keenan and Keyes (1936), Fig. 5, p. 79; and Keenan, et al. (1969), Fig. 2, p. 120). To 200^{o}F, the specific heat of water can be considered to have a value of 1.00 BTU/(lb-^{o}F). The formation thermal properties of interest are the formation volumetric specific heat, M_f, and the ratio of formation volumetric specific heat to liquid mass specific heat, $de_{f'''}/de_w$. These properties can be estimated using known properties of water (see references above) and dry porous media (Somerton, 1958).

Fig. A.1 presents M_f, BTU/(ft^3-^{o}F), vs. temperature for various values of porosity, while Fig. A.2 presents $de_{f'''}/de_w$, ft^3/lb, vs. temperature, ^{o}F, for the same porosities. Because both M_f and de_f'''/de_w vary slowly with temperature, it would be expected that they can be considered as constant over limited ranges of temperature.

(5) The assumption that density is independent of temperature is not strictly correct. The error that this assumption involves can be estimated by applying a one-dimensional mass balance to the core system. This gives:

$$0 = \frac{\partial w}{\partial x} + A_c \frac{\partial}{\partial t} (\phi\rho) \qquad (A.6)$$

where: w = local mass flow rate

x = axial distance

A_c = cross-sectional area of core to flow

ϕ = porosity

ρ = local fluid density

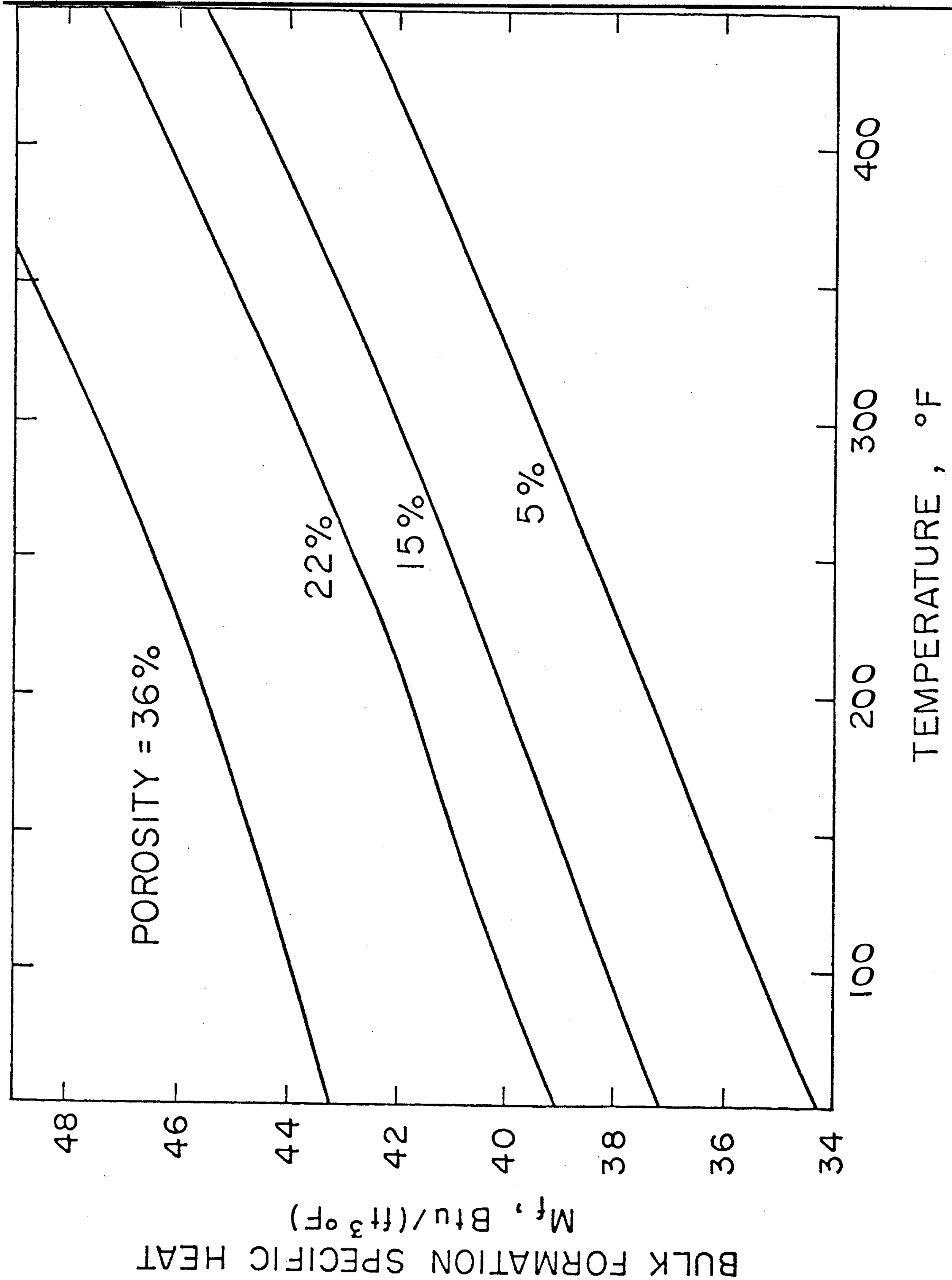

FIGURE A.1. VOLUMETRIC SPECIFIC HEAT OF THE FORMATION, M_f, BTU/(lb_m-°F), VS TEMPERATURE, °F, FOR VARIOUS POROSITIES

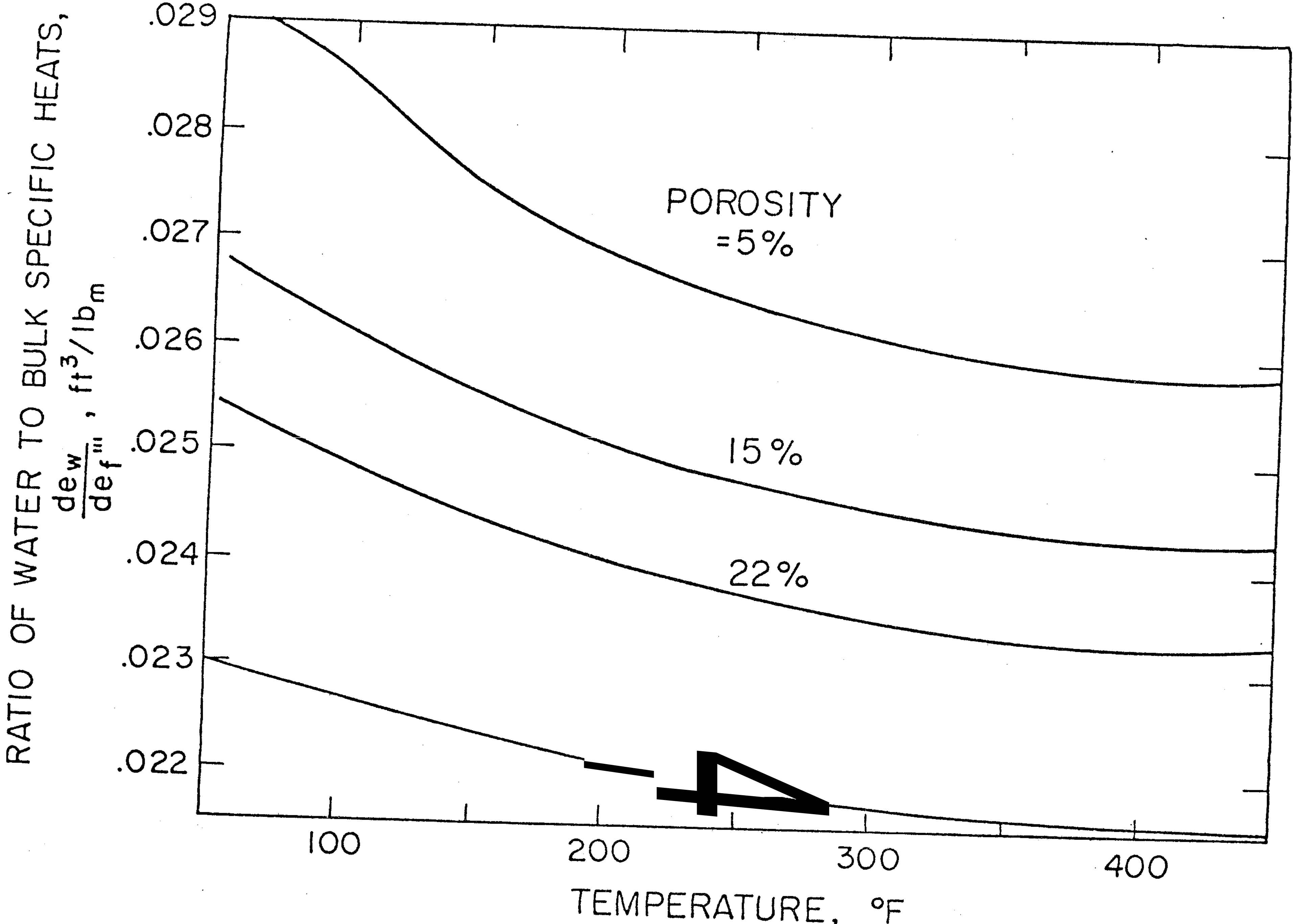

FIGURE A.2. RATIO OF WATER TO BULK FORMATION SPECIFIC HEATS, de_w/de_f''', ft^3/lb_m, VS TEMPERATURE, °F, FOR VARIOUS POROSITIES

Therefore:

$$\frac{\partial w}{\partial x} = - A_c \frac{\partial}{\partial t} (\phi\rho)$$

$$= - A_c \frac{\partial(\phi\rho)}{\partial T} \cdot \frac{\partial T}{\partial t} \qquad \text{(A.7)}$$

Estimating $\partial w/\partial x$ during the hot water injection experiment HWI-S-4 of Arihara (1974, p. 53):

$$\left(\frac{\partial T}{\partial t}\right)_{x=4\ \text{in.},\, t=30\ \text{min}} \simeq \frac{116-78}{30} = 1.26\ \frac{F^{o}}{\text{min}}$$

Assuming ϕ = constant: $\frac{\partial(\phi\rho)}{\partial T} = \phi \frac{\partial\rho}{\partial T}$

Since the thermal expansion coefficient, β, is given by:

$$\beta = \frac{1}{v}\left(\frac{\partial v}{\partial T}\right)_P = - \frac{1}{\rho}\left(\frac{\partial\rho}{\partial T}\right)_P = \frac{1}{B_w}\frac{\Delta B_w}{\Delta T} \qquad \text{(A.8)}$$

where B_w is the formation volume factor of the water (Amyx, Bass, and Whiting (1960), pp. 455-456); we have:

$$\left(\frac{\partial\rho}{\partial T}\right)_P = - \frac{\rho}{B_w}\frac{\Delta B_w}{\Delta T} \cdot$$

At $100^{o}F$, this has the approximate numerical value:

$$\left(\frac{\partial\rho}{\partial T}\right)_P \simeq - \frac{(60\ \text{lb}/\text{ft}^3)}{(1.0\text{ft}^3/\text{ft}^3)} \cdot \frac{(1.02-1.00)}{(70F^{o})}$$

$$\simeq 0.017\ \text{lb}/\text{ft}^3\text{-}^{o}F$$

where $\Delta B_w/\Delta T$ is taken from curve A, Fig. 6-3, of Amyx, Sass, and Whiting (1960).

Thus:

$$\frac{\partial w}{\partial x} \simeq -\left(\frac{\pi}{1.44}\right)\left(0.3\ \frac{ft^3}{ft^3}\right)\left(0.017\ \frac{lb}{ft}\right)(1.26\ min)$$

$$= 1.40 \times 10^{-4}\ \frac{lb}{min\ ft}$$

This is negligible relative to a mass injection rate of 1.6 $\frac{lb}{hr} = 2.7 \times 10^{-2}\ \frac{lb}{min}$.

(6) The assumption of one-dimensional fluid flow is reasonable for the experimental conditions of Arihara. If the Lauwerier assumption were strictly correct, and fluid was injected into and withdrawn from the core uniformly, there would be no tendency for vertical density contrasts to cause gravity override or convection currents in the core. However, radial temperature distributions in the core are not uniform, and there may be a tendency for convection currents to arise. The magnitude of this tendency may be examined by considering a system wherein there may be a flow, W_x, in the horizontal direction driven by an externally imposed pressure drop, and a local flow, W_z, in the vertical direction driven by buoyancy forces. The Darcy rate equations relate local pressure and density gradients:

$$W_x = -\frac{k}{\mu}\left(\frac{\partial p}{\partial x}\right) \qquad (A.9)$$

$$W_z = -\frac{k}{\mu}\left(\frac{\partial p}{\partial z} - \rho\frac{g}{g_c}\right) \qquad (A.10)$$

where: k = the local Darcy permeability

μ = the local viscosity

ρ = the local density

g = the local acceleration due to gravity

g_c = the gravitational constant in appropriate units

The tendency for the flow to be two-dimensional, that is to have a vertical component, may be expressed as the ratio of vertical to horizontal driving forces, R:

$$R = \left(\frac{\partial p}{\partial z} - \rho\frac{g}{gc}\right)/\frac{\partial p}{\partial x} \qquad (A.11)$$

Suppose that the fluid has a local density, ρ_o, and temperature, T_o, and that **it** has a constant coefficient of thermal expansion, β:

$$\rho = \rho_o\ (1-\beta(T-T_o)$$

$(\partial p/\partial z)$ can then be expressed:

$$\frac{\partial p}{\partial z} = \frac{\partial}{\partial z}\left(\frac{mg/g_c}{A}\cdot\frac{\Delta z}{\Delta z}\right) = \frac{\partial}{\partial z}\left(\rho\frac{g}{gc}\Delta z\right)$$

$$= \frac{g}{g_c}\left\{\rho\ \frac{\partial\Delta z}{\partial z} + \Delta z\ \frac{\partial}{\partial z}\left[\rho_o\ (1-\beta(T-T_o))\right]\right\}$$

$$= \frac{g}{g_c} \{\rho_o - \rho_o \beta (T-T_o) - \Delta z \, \rho_o \, \beta \frac{\partial T}{\partial z}\}$$

Then, R can be expressed locally as:

$$R_o = \frac{g}{g_c} \left\{ \rho_o - \rho_o \beta (T_o - T_o) - \Delta z \, \rho_o \, \beta \frac{\partial T}{\partial z} - \rho_o \right\} / \frac{\partial p}{\partial x}$$

$$= - \frac{g}{gc} \rho_o \, \beta \, \Delta z \frac{\partial T}{\partial z} / \frac{\partial p}{\partial x} \simeq - \frac{\rho_o \beta \Delta T}{(\Delta p / \Delta x)} \cdot \frac{g}{g_c}$$

Estimating R_o for the HWI-S-4 experiment of Arihara (1974):

$$(-\rho_o \beta) = \left(\frac{\partial \rho}{\partial T}\right)_P \simeq 0.017 \text{ lbm/ft}^3\text{-}^oF,$$ from section 5

in the preceding;

$$\frac{\Delta p}{\Delta x} \simeq \frac{60}{2} \frac{\text{psia}}{\text{ft}} = 30 \frac{\text{lb}_f}{\text{in}^2 \text{ ft}} \frac{144 \text{ in}^2}{\text{ft}^2} = 30 \times 144 \frac{\text{lb}_f}{\text{ft}^3}$$

$$R_o = \frac{0.017 (\text{lb/ft}^3\text{-}^oF)(\Delta T, {}^oF)}{(30 \times 144 \text{ lb}_f)} \cdot \left(\frac{g}{g_c} \frac{\text{ft/sec}^2}{\frac{\text{lb}}{\text{lb}_f} \frac{\text{ft}}{\text{sec}^2}}\right)$$

$$\simeq (4.0 \times 10^{-6}) \, \Delta T$$

This is negligible for any reasonable AT.

(7) The assumption of local thermal equilibrium is equivalent to assuming that the (hA) product between the liquid and sand grains is infinite. This is known to he a reasonable assumption for fine grained porous media (Jenkins and Aronofsky (1955); Rear (1972), pp. 646-647).

APPENDIX B

COMPUTATIONAL PROCEDURES USED TO CALCULATE TEMPERATURE PROFILES FOR TIME-DEPENDENT INJECTION TEMPERATURE

Two procedures were used. The method of characteristics solution (Eqs. 3.15 and 3.18) required the tracking of particles along their characteristics (integrating dx/dt), while at the same time following their temperature decav (solving the dT/dt equation for the particle). The two equations involved are weakly coupled and weakly nonlinear, and hence their numerical solution was straightforward.

The constant coefficient analytic solutions were developed for the case of constant injection temperature. Solutions for time-dependent injection temperature can be generated by using superposition. This can be done either by using Duhamel's theorem, or with an explicit superposition algorithm. Because many cases of interest involved experimental injection temperature data as a function of time that might not be amenable to a compact and accurate analytic expression, an explicit superposition algorithm was developed.

The experimental injection temperature history was reported by Arihara as a set of discrete points. Intermediate values were obtained using both linear interpolation and cubic spline interpolation. The latter representation gave a smooth description of the history for values between the discrete points, if the injection temperature did not change rapidly, as was often the case. However, if the discrete points changed rapidly, the cubic splines gave oscillating and unrealistic intermediate values. In this case, linear interpolation between the data points was used. This resulted, however, in some calculated profiles manifesting discontinuous behavior in the temperature gradients. These discontinuities are a consequence of the calculational procedure and the discrete nature of the input data rather than inherent in the mathematical models.

<u>Method of Characteristics Computational Procedure</u>

The problem was that of simultaneously integrating Eqs. 3.15 and 3.18:

$$\frac{dx}{dt} = c_1 \frac{\partial e_w}{\partial e_f'''} \tag{B-1}$$

$$\frac{dT}{dt} = -\frac{c_2}{M_f}(T-Te) \tag{B-2}$$

where: $c_1 \stackrel{A}{=} w/A_c$, and may be a function of time

$\partial e_f'''$ may be a function of temperature

$c_2 \stackrel{A}{=} (\bar{h}P)/A_c$ may be a function of distance, x,

M_f may be a function of temperature

The two equations were integrated successively to track characteristic particles injected at regular time intervals at temperatures corresponding to those times. Eq. B-1 was integrated first using the Euler, or two-level, explicit scheme. Eq. B-2 was next integrated, using the most recent information from Eq. B-1, with an implicit two-level scheme written about $T^{(n+1/2)}$, midway between the two time levels $T^{(n)}$ and $T^{(n+1)}$. The central difference approximation to the derivative was used, and a value of $T^{(n+1)}$ in the nonlinear term was estimated by assuming exponential temperature decay from the previous two time levels. The estimated value at $T^{(n+1)}$ was thus $(T^{(n)}/T^{(n-1)}) \cdot T^{(n)}$

In addition to allowing thermal properties to change with temperature, and injection temperature a function of time, this procedure could also handle. an arbitrary initial temperature distribution in the core, and a heat loss coefficient a function of distance. These additional capabilities were not used extensively.

Extensive numerical experiments using different time step sizes and reasonable functional dependencies in Eqs. B-1 and B-2 gave an empirical demonstration of the convergence and stability of the computational scheme.

Algorithm for Generating Time-Dependent Injection Temperature Solutions by Superposition of Constant Injection Temperature Solutions

Let the variation of injection temperature with time, $T_i(t)$, be a continuous function which may be monotonic to some time, and constant thereafter. Let this function be approximated in some fashion by a series of step functions, u_j, operating at times t_j, as shown in Fig. B-1. If $T_D(x_D,t_D)$ is the solution to the particular problem of interest for constant injection temperature, then the solution to the problem of changing injection temperature, $T_i(t)$, is given by:

$$T(x_D,t_D) = \sum_{j=1}^{KOUNT} u_j \, T_D \, (x_D,t_D-t_{Dj}) \qquad \text{(B-3).}$$

The superposition solution increases in accuracy as the step function approximating functions more closely represent the $T_i(t)$ function.

This section describes an algorithm for approximating the continuous monotonic or constant function, $T_i(t)$, by a series of step functions, u_j, j = 1, 2, ..., KOUNT, where KOUNT is the number of step functions used up to some real time, t, or dimensionless time, t_D. The step functions, u_j, operate at real times, t_j, and dimensionless times, t_{Dj}. In the procedure described in this section, the value of the injection temperature is taken relative to the datum of initial and external temperature, T_e. Thus, if injection temperature is initially the external temperature, then $T_i(0) = 0$.

The logic of the superposition algorithm is presented in the flowchart diagrams, Figs. B-2 and B-3, and is described below. The basic procedure (Fig. B-3) is to advance the testing

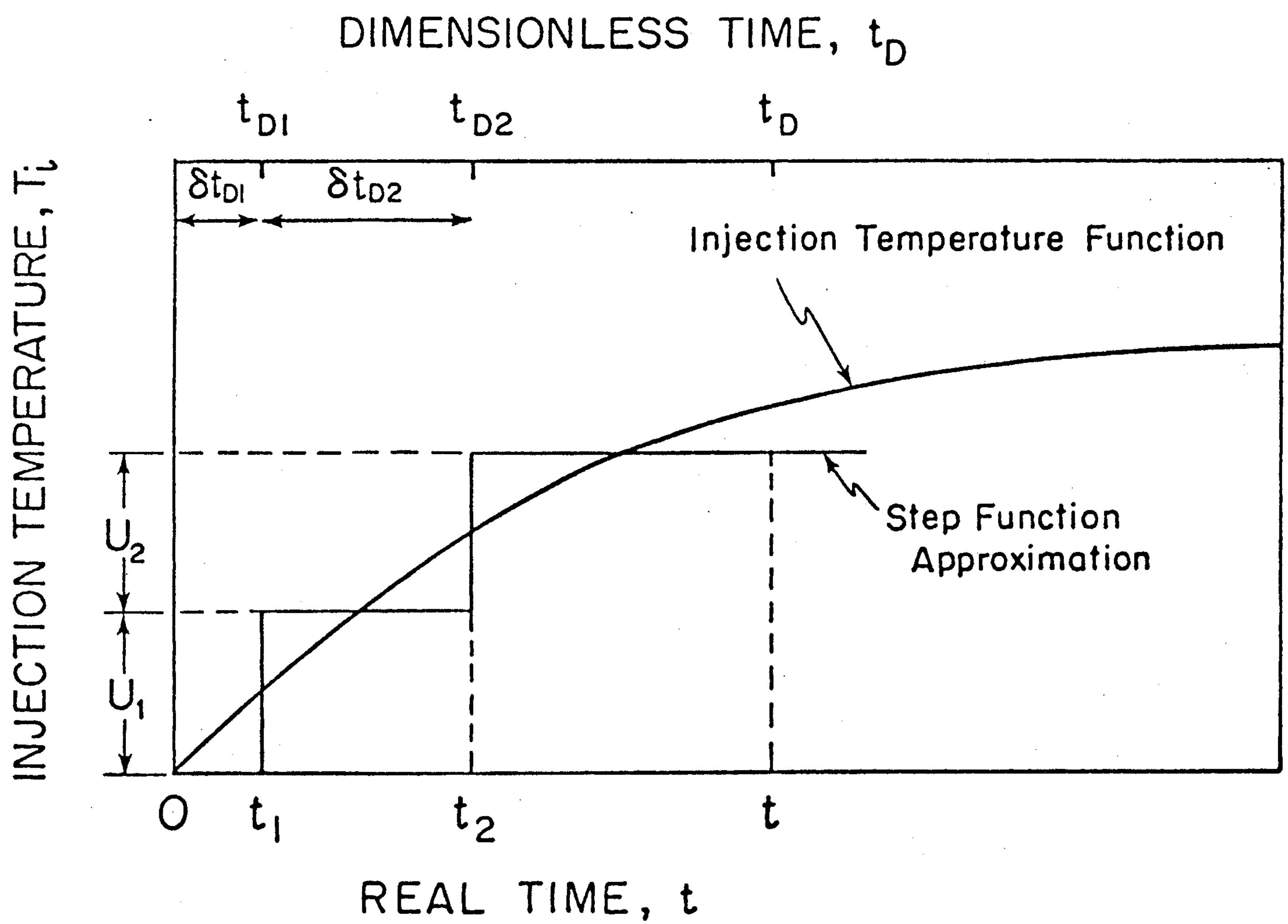

FIGURE B.1. DIAGRAM OF THE STEP FUNCTION APPROXIMATION TO THE INJECTION TEMPERATURE FUNCTION.

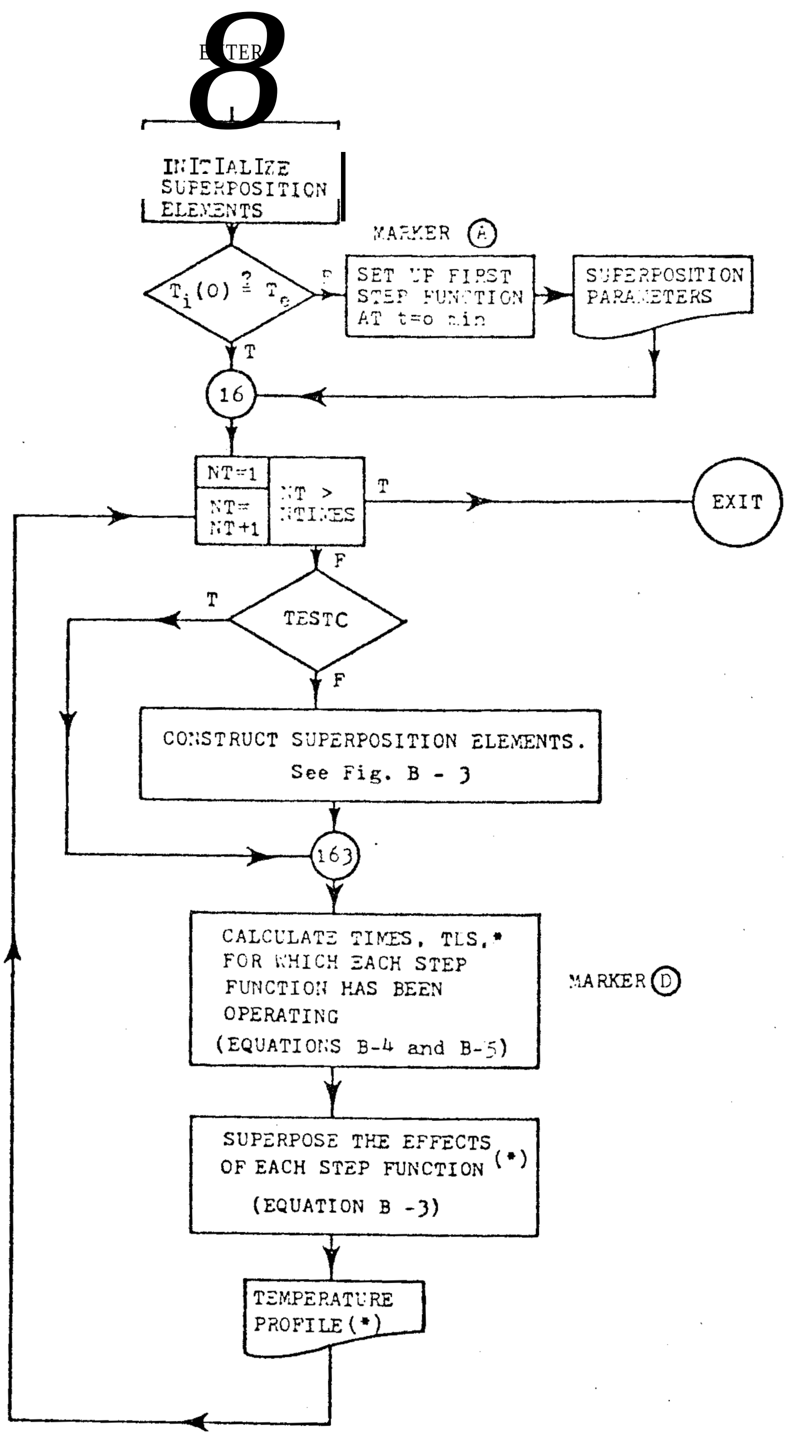

B. 2 FLOW DIAGRAM OF ALGORITHM FOR CALCULATING TEMPERATURE PROFILES FOR TIME-DEPENDENT INJECTION TEMPERATURE BY SUPERPOSITION (ELEMENTS WHICH ARE SUPERSCRIPT STARRED MUST BE EXECUTED FOR EACH CASE OF INTEREST DURING A SINGLE RUN)

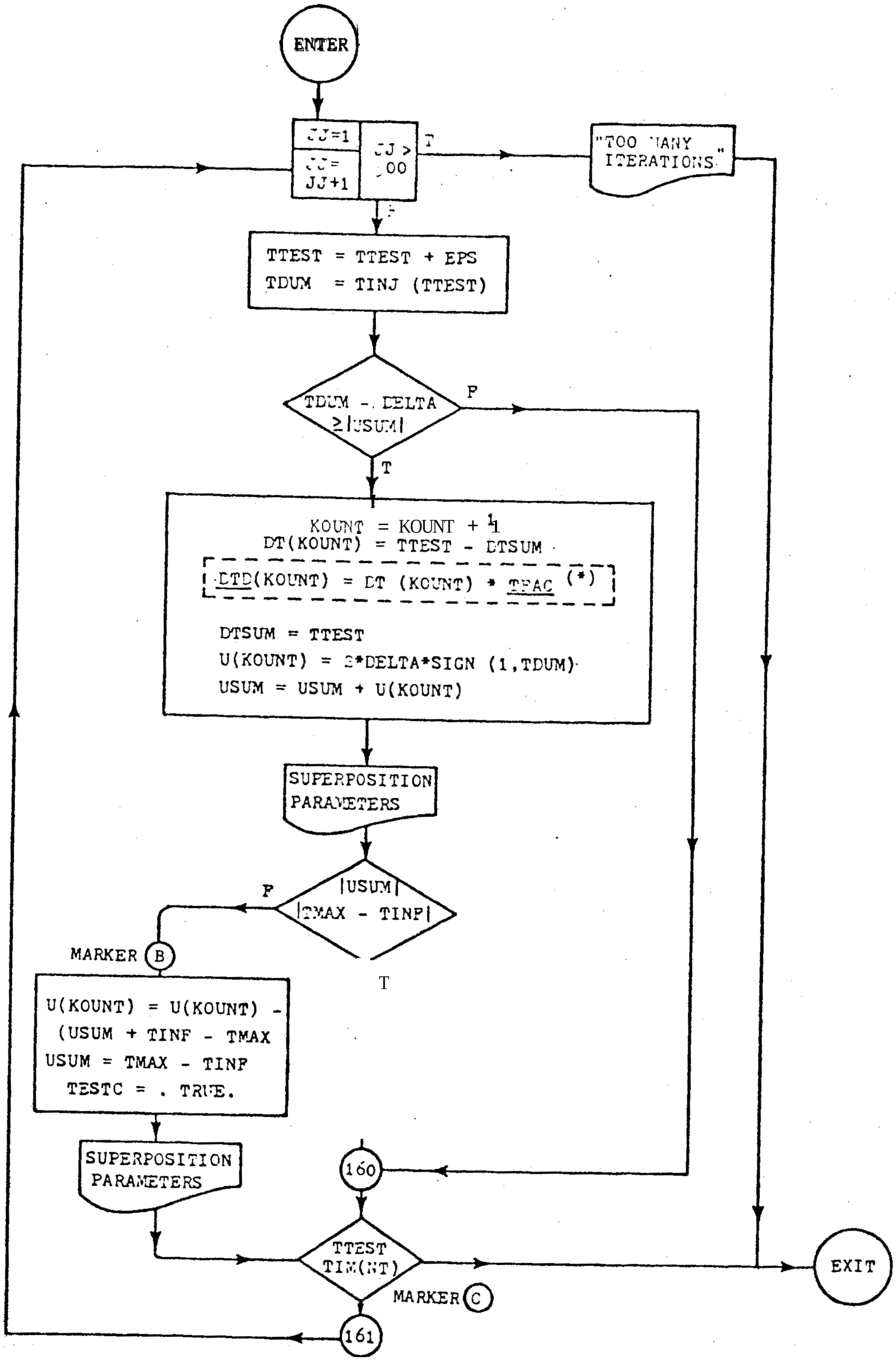

B. 3 FLOW DIAGRAM OF ALGORITHM FOR CONSTRUCTING THE STEP FUNCTION APPROXIMATION TO THE INJECTION TEMPERATURE HISTORY (*: DASHED BOX INDICATES STEPS WHICH MUST BE DONE FOR EACH CASE OF INTEREST DURING A SINGLE RUN) time, TTEST, in increments, TEPS, until the absolute value of T_i(TTEST) exceeds the current absolute value of the sun, USUM, of the currently operating step functions by an amount greater than or equal to the parameter DELTA. When this occurs, KOUNT is incremented by 1, and a step function of strength (2*DELTA) operating at the current time, TTEST, is added to the step function approximation.

The algorithm must account for variations in this procedure at time zero if the initial injection temperature is different from initial core temperature, T_e, and at longer times, if the injection temperature becomes constant. In the former case, the first step function, u_1, is set equal to T_i (0), which is nonzero, and operates at a time $t_1 = t_{d1} = 0$ (see Marker A, Fig. B-2). In the latter case of injection temperature becoming constant, the final step function must be set such that the summation of all step functions, USUM, is equal to the constant injection temperature (see Marker B, Fig. B-3).

When it is time, NTIME(J) (see Marker C, Fig. B-3), to evaluate the summation of the effects of each step function, the dimensionless time, t_{DSj}, for which each step function has been operating is calculated from the differences, δt_{Dj}, between t_{Di} and $t_{D,j-1}$.

$$t_{DS1} = t_D - \delta t_{D1} \tag{B-4}$$

$$t_{DSj} = t_{DS,j-1} - \delta t_{Dj} \tag{B-5}$$

(Marker D, Fig. B-2)

The parameters in this algorithm are the time increment, TEPS, and the nominal step function strength, DELTA. Numerical experiments using an analytic approximation to $T_i(t)$ typical of the experiments of Arihara were performed. Fig. B-4 presents the form of the step function approximation to $T_i(t) = 53.0 - 48.0 * \exp(-0.0387*t)$, where t is in minutes, for values of DELTA = 2 and 5. It can be seen that while both approximations look reasonable at early times when $T_i(t)$ is changing rapidly, they become less satisfactory at longer times when $T_i(t)$ is changing more slowly. As a result of numerical experimentation using different values of DELTA and TEPS, it was concluded that values of DELTA = 0.5 and TEPS = 0.25 were needed in order to assure negligible discretization error in temperature profiles such as these. Fig. B.5 compares the temperature profile which results when using a value of DELTA = 5 (and TEPS = 1), to the accurate base case using DELTA = 0.5 (and TEPS = 0.25). Runs using DELTA = 1 and 2 were much closer to the base case, but tended to have occasional localized anomalous behavior near the injection end of the core.

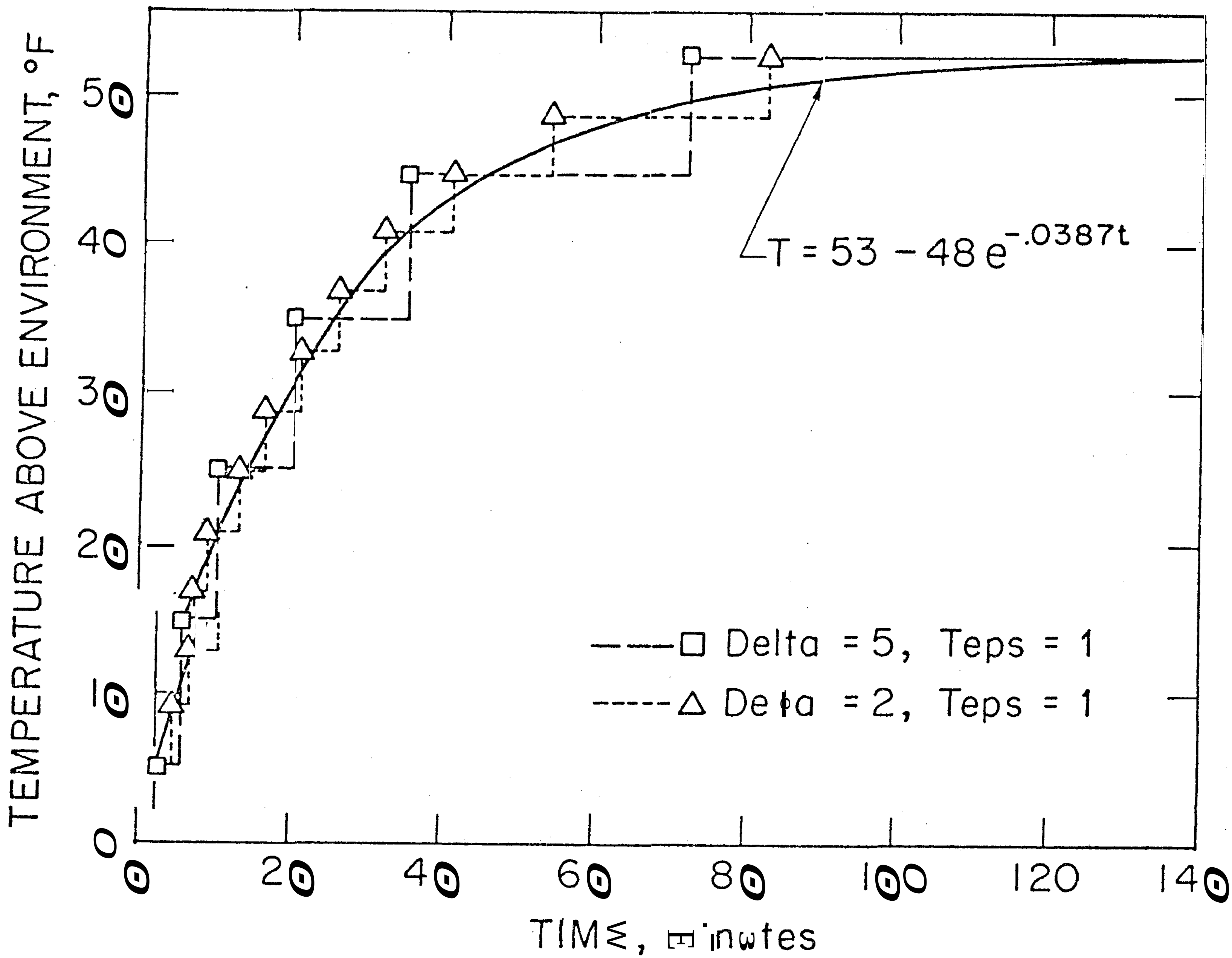

FIGURE B.4 VARIOUS STEP FUNCTION APPROXIMATIONS TO THE GIVEN ANALYTIC INJECTION TEMPERATURE HISTORY

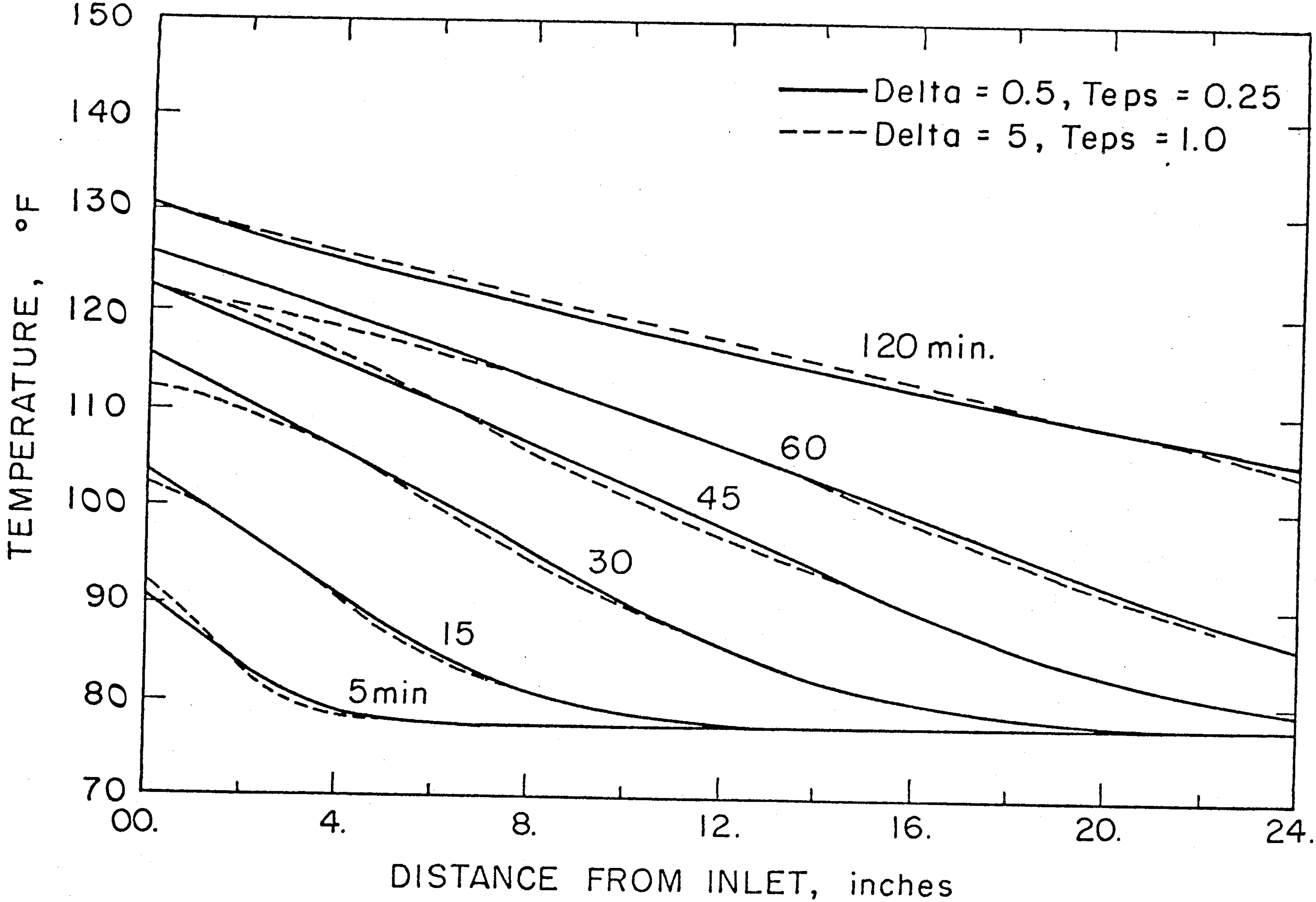

FIGURE B.5. CALCULATED TEMPERATURE PROFILES FOR THE CONDITIONS OF EXPERIMENT HWI-B-1 OF ARIHARA

APPENDIX C

ANALYSIS AND EVALUATION OF PROPOSED STEADY STATE EXPERIMENT FOR MEASURING FILM COEFFICIENTS BETWEEN THE CORE AND COREHOLDER

If the core-coreholder film coefficient depends on the mass velocity, w , by a power relation of the form $h_f =$ $a(w)^m$, then the relationship between $\bar{h}$ and w is:

$$\bar{h} = 1/\{R_{int} + r_o/(r_{so}h_e) + (w'')^{-m}/a\} \qquad (C.1)$$

If R_{int} and $r_o/(r_{so}h_e)$ are known exactly, then a graph of $\log\{1/\bar{h} - R_{int} - r_o/(r_{so}h_e)\}$ versus $\log(w'')$ will give a straight line with slope (-m) and intercept (1/a) at $w'' = 1$. The parameter h_e in the ordinate will depend on experimental conditions external to the core. It must either be measured experimentally, or else it must be estimated using available correlations. Such estimates may be inaccurate, and may consequently jeopardize the validity of the internal film coefficient correlation obtained. As a result of this observation, a series of simulated numerical experiments were carried out in order to examine the sensitivity of the straight-line graphical method to errors in estimating h_e. Values of $\bar{h}$ were calculated as a function of w'' for the given parameters a, m, h_e, and R_{int}. Then the value of $\log\{1/\bar{h} - r_o/(r_{so}$

$(h_e+\varepsilon)) - R_{int}\}$ was graphed versus log (w'') for various values of the external film coefficient error, ε.

These numerical experiments were run for three cases shown in Table C.1. These cases correspond to the range of physical and experimental parameters reported by Crichlow (1972) and Arihara (1974). The resulting graphs of the ordinate grouping versus w" on log-log paper are presented in Figs. C.1 to C.3. Examination of these figures indicates that the desired straight line requires an accurate value for h_e. Thus, a parametric graphical study using various estimated values of h_e could be made. The best straight line would give reasonably accurate values for h_e as well as for (a) and (m).

Figs. C.1 to C.3 indicate that the straight line becomes more sensitive to an accurate value of h_e as h_f becomes larger than h_e. This is indicated mathematically by the fact that when there is an error ε in the value of h_e, the expression in the ordinate is really:

$$\{1/h - (r_o/(r_{so}(h_e+\varepsilon)) + R_{int})\} \qquad (C.2)$$

$$= 1/h_f + r_o/(r_{so}h_e) + R_{int} - \{r_o/(r_{so}(h_e+\varepsilon)) + R_{int}\} \qquad (C.3)$$

$\simeq 1/h_f$ (correct value in the ordinate in the absence of an error, ε, in h_e)

$+ (r_o/rso)(\varepsilon/h_e^{\,2})$, if $\varepsilon \ll h_e$ (error in the ordinate caused by an error, ε, in the estimated value of h_e) (C.4)

$= A + B$

Table C.l Physical and Experimental Parameters for the Simulated Experiments

Range of w" : 0.3-3.0 lb/min-ft2				
Case	h_e, BTU/hr-ft^2-$^\circ$F	Range of h_f, BTU/(hr-ft^2-$^\circ$F)	a	m
I	1	5-18	34.38	1.5
II	1	0.5-18	3.438	1.5
III	5	0.5-18	3.438	1.5

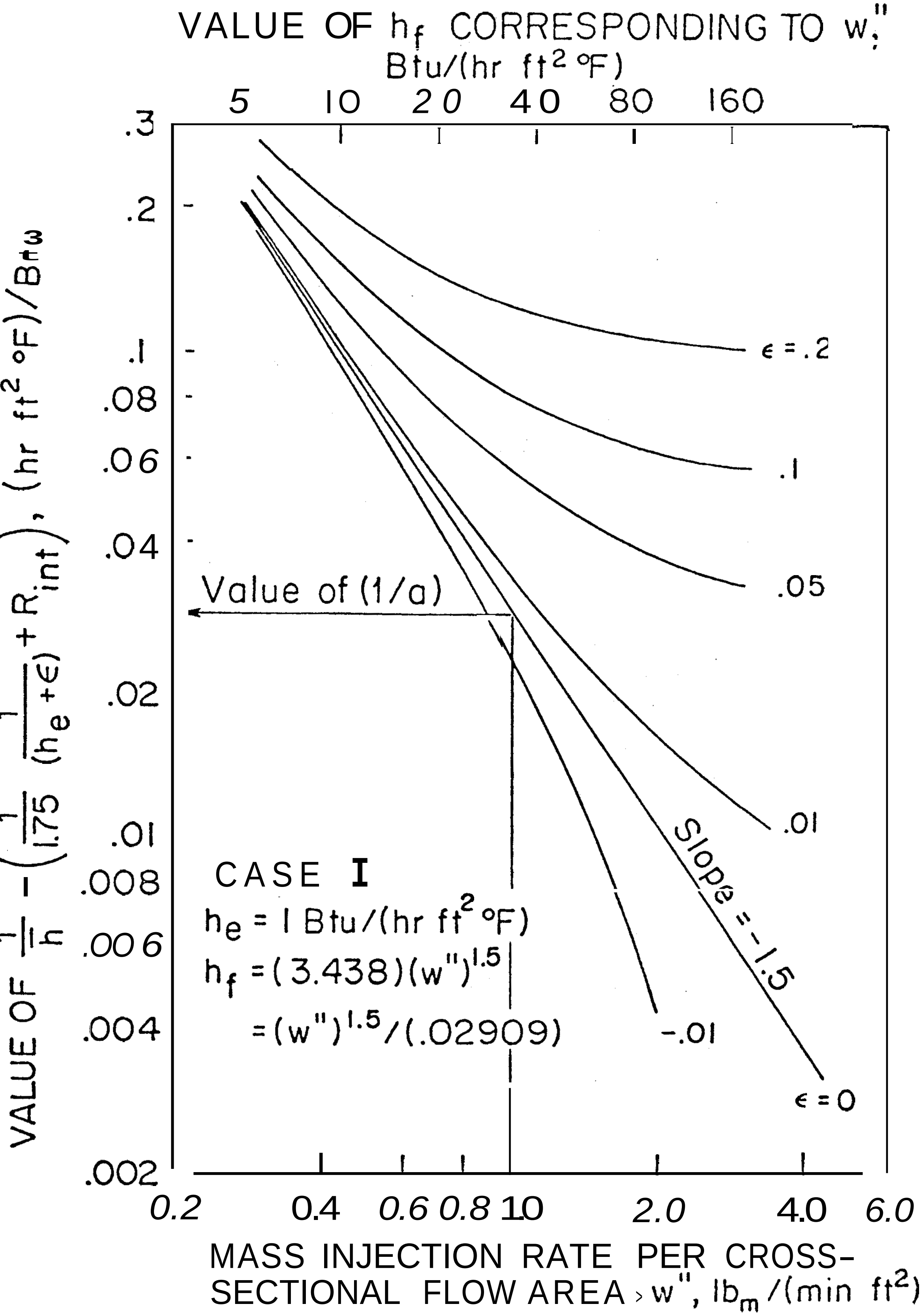

FIGURE C.1. GRAPH OF THE ORDINATE GROUPING IN THE STEADY STATE EXPERIMENT GRAPHICAL METHOD VS MASS VELOCITY, w'', FOR CASE I AND A RANGE OF ε VALUES

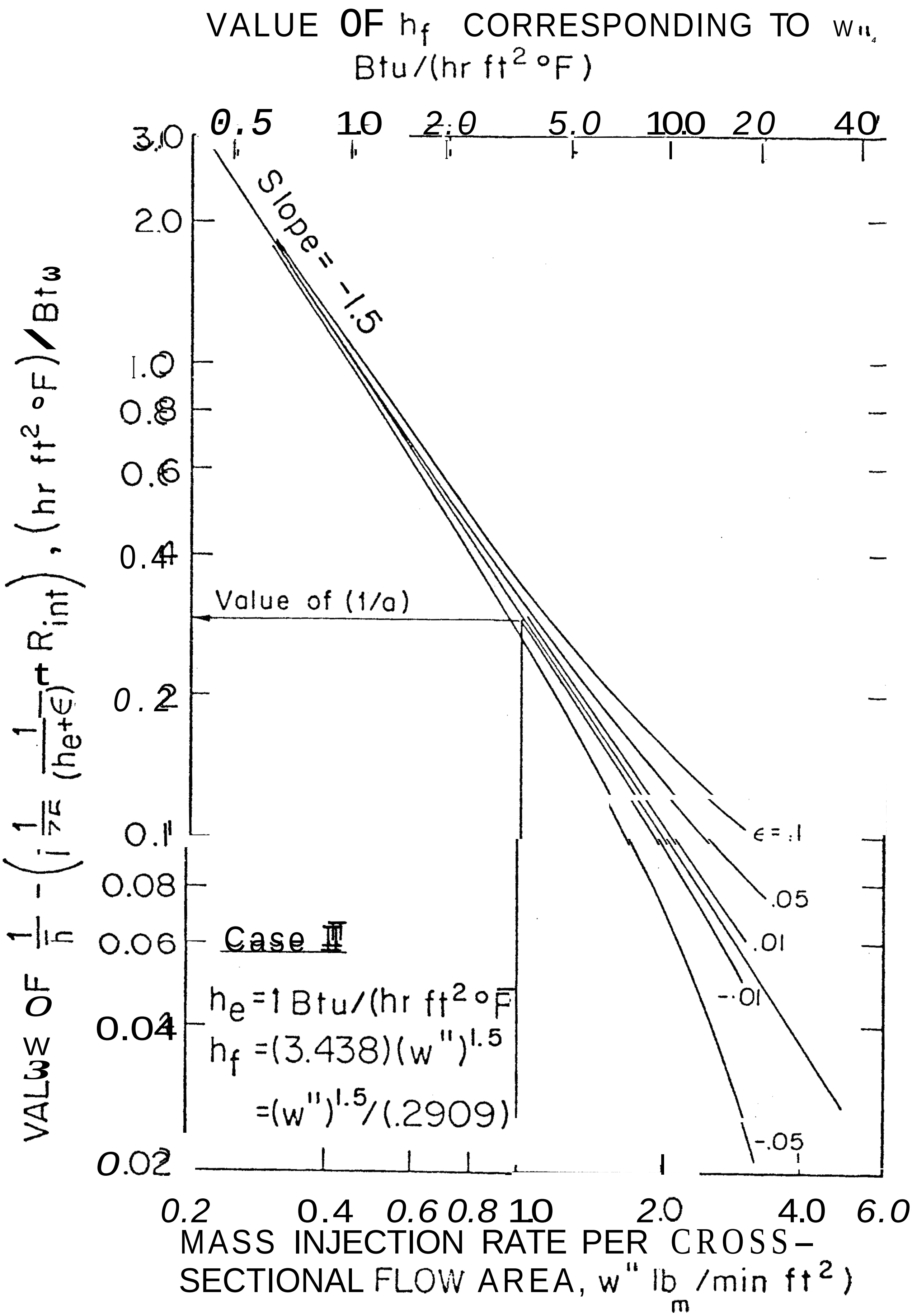

C.2 GRAPH OF THE ORDINATE GROUPING IN THE STEADY STATE EXPERIMENT GRAPHICAL METHOD VS. MASS VELOCITY, w", FOR CASE II AND A RANGE OF ε VALUES

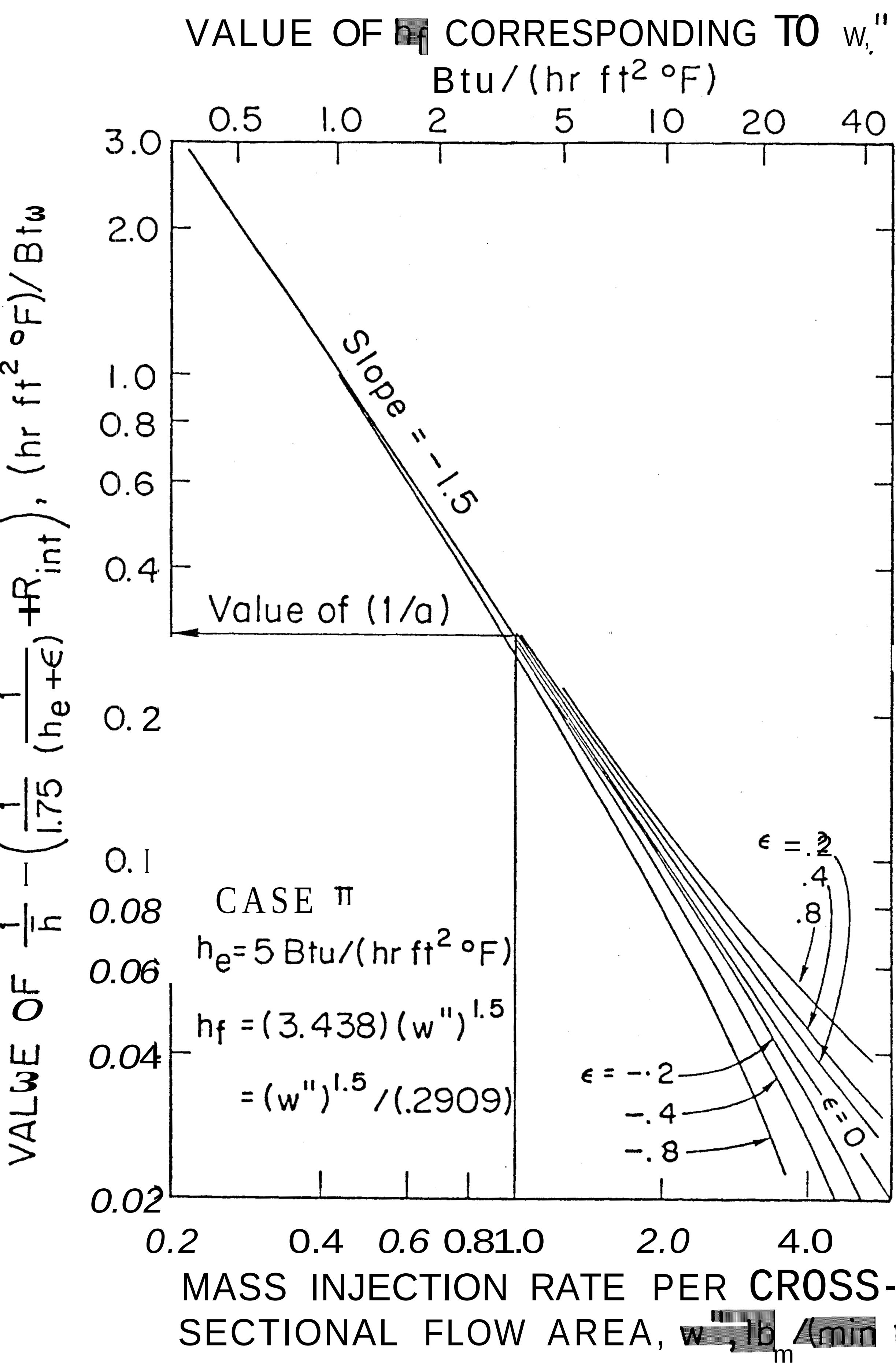

C.3 GRAPH OF THE ORDINATE GROUPING IN THE STEADY STATE EXPERIMENT GRAPHICAL ^ THOD VS. MASS VELOCITY, w", FOR CASE III AND A RANGE OF ε VALUES

The ratio of B to A is:

$$(r_o/r_{so})(\varepsilon/h_e^{\,2})/(1/h_f) = (h_f/h_e^{\,2})\ \{(r_o/r_{so})\ \varepsilon\} \qquad \text{(C-5)}$$

which goes to zero as ε goes to zero. The error caused by a nonzero value of ε will lead to a graph that is not a straight line. For fixed r_o/r_{so}, and ε, the sensitivity of this graphical method to errors in h_e is directly proportional to $(h_f/h_e^{\,2})$. Thus, in designing an experiment, one would try to obtain values of h_f that are larger than $(h_e^{\,2})$.

All of the above discussion assumes that the errors in estimating h_e dominate the results, and, furthermore, that the relation $h_f = a(w'')^m$ is valid.

APPENDIX D

A COYPARISON OF THE LUMPED PARAMETER MODEL WITH THE FULLY ANALYTIC SOLUTION

Fully Analytic Solution

We are interested in the propagation of transients through a coreholder considered to be of uniform thermal diffusivity. If the thickness of the coreholder is small compared to the core radius, then radial heat flow in the coreholder can be approximated as linear. Thus, we wish to examine the behavior of normalized transients for:

$$\frac{\partial^2 v}{\partial x^2} = \frac{1}{\kappa}\frac{\partial v}{\partial t}, \quad 0 \leq x \leq D, \quad t>0 \tag{D.1}$$

where: v = normalized temperature

$\kappa \triangleq \lambda_v/\rho_v C_v$ = viton thermal diffusivity

λ_v = viton thermal conductivity

ρ_v = viton density

C_v = viton specific heat

The boundary conditions of interest correspond to the physical situation of film coefficients h_f and h_e at $X = 0$ and D, respectively, with a normalized step function temperature at $x = 0$, $v\,(x=0) = v_1$, and normalized initial temperature of zero at $X = D$:

$$- \lambda_v \frac{\partial v}{\partial x} + h_f (v-v_1) = 0, \; x = 0; \; t>0 \tag{D.2}$$

$$\lambda_v \frac{\partial v}{\partial x} + h_e v = 0, \; x = D, \; t>0 \tag{D.3}$$

The initial condition is:

$$v(x,0) = 0, \; 0<x<D$$

The solution to this initial boundary value may be obtained with the aid of Carslaw and Jaeger (1959, pp. 118, 126) as:

$$v(x,t) = u(x) + w(x,t) \tag{D.4}$$

u (x) is the solution to

$$\frac{d^2u}{dx^2} = 0, \; 0<x<D$$

$$- \lambda_v \frac{du}{dx} + h_f (u-v_1) = 0, \; x=0$$

$$\lambda_v \frac{du}{dx} + h_e u = 0, \; x=L \tag{D.5}$$

and is $$u(x) = Ax + B$$

where: $A = -h_f h_e v_1/\alpha$

$B = h_f v_1 (\lambda_v + Dh_e)/\alpha$

$\alpha = \lambda h_e + h_f (\lambda_v + Dh_e)$

w (x,t) is the solution to:

$$\frac{1}{\kappa_v}\frac{\partial w}{\partial t} = \frac{\partial^2 w}{\partial x^2}, \quad 0<x<D, \ t>0$$

$$-\lambda_v \frac{\partial w}{\partial x} + h_f w = 0, \quad x=0, \ t>0$$

$$\lambda_v \frac{\partial w}{\partial x} + h_e w = 0, \quad x=D$$

$$w(x,0) = -u(x) = - Ax+B, \quad 0<x<D$$

and is

$$w(x,t) = -\sum_{n=1}^{\infty} C_n E_n \left\{ \lambda_v \beta_n \cos(\beta_n x) + h_f \sin(\beta_n x) \right\} e^{-\kappa \beta_n^2 t} \tag{D.8}$$

where:

$$C_n = \frac{2(\lambda_v^2 \beta_n^2 + h_e^2)}{(\lambda_v^2 \beta_n^2 + h_f^2)\left[D(\lambda_v^2 \beta_n^2 + h_e^2) + \lambda_v h_e\right] + \lambda_v h_f (\lambda_v^2 \beta_n^2 + h_e^2)}$$

$$E_n = \cos(\beta_n D) \cdot \left\{\frac{\lambda_v A - h_f(AD+B)}{\beta_n}\right\} + \sin(\beta_n D) \cdot$$

$$\left\{\lambda_v(AD+B) + \frac{h_f A}{\beta_n^2}\right\} + \frac{1}{\beta_n} \cdot \{h_f B - \lambda_v A\}$$

and β_n are non-negative roots to

$$\tan(\beta D) = \frac{\beta}{(\beta^2 - F)} \cdot G$$

where $F \triangleq h_f h_e / \lambda_v^2$, and $G \triangleq (h_f + h_e)/\lambda_v$ (D.9)

The behavior of this analytic solution at various times for physical parameters similar to those of the viton in the coreholder is shown in Figs. D.1 and D.2.

Lumped-Parameter Solution

For heat transfer purposes, consider the coreholder to be simply a viton sleeve whose thickness is substantially less than its radius. The simplified single lumped-parameter model follows directly if the internal thermal resistance in the viton is small compared to the thermal resistances of the two film coefficients h_e and h_f. In such a case, the temperature of the viton can be considered to be at the lumped temperature, $T_{\ell v}$. A schematic of the simplified physical system and its corresponding thermal circuit network (Kreith (1973), section 4-2) is shown in Fig. D.3. The application of an energy balance to this system gives:

$$\frac{\rho_v C_v D}{h_f+h_e} \frac{\partial T_{\ell v}}{\partial t} + T_{\ell v} = \frac{h_f T_f + h_e T_e}{h_f+h_e} \quad (D.10)$$

where the symbols are defined in the Nomenclature section. Although the formation temperature, T_f, varies with time, it is considered to be constant in this discussion. This equation is of the following form:

$$\eta \frac{\partial T_{\ell v}}{\partial t} + T_{\ell v} = \beta \quad (D.11)$$

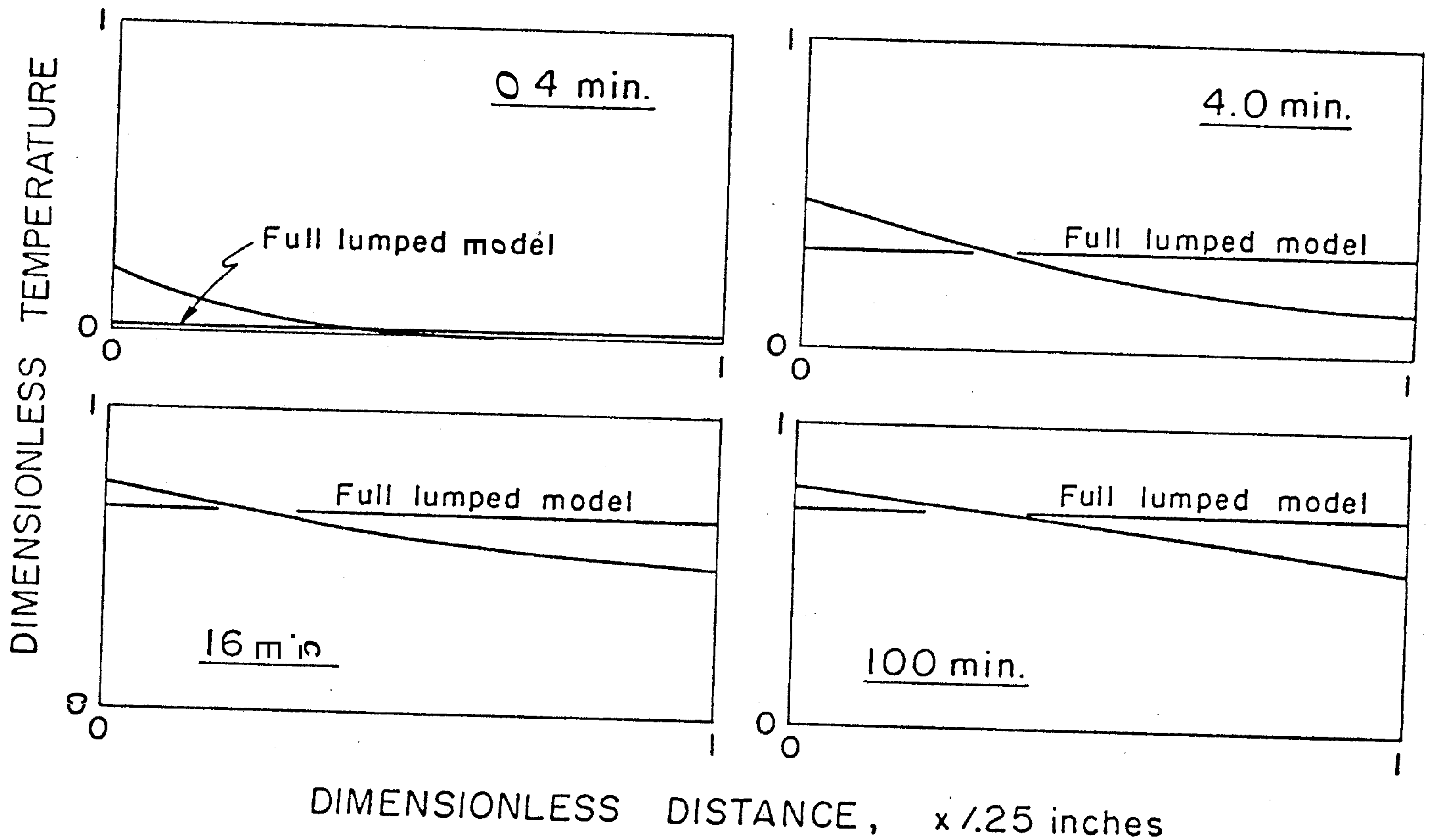

FIGURE D.1. CALCULATED TEMPERATURES AT VARIOUS TIMES ACROSS A SLAB IN RESPONSE TO A UNIT STEP FUNCTION INCREASE IN TEMPERATURE AT $x = 0$. (FILM COEFFICIENT, h_f, AT $x = 0$, IS 5 BTU/(hr-ft^2-°F). FILM COEFFICIENT, h_e, AT $x=0.25$ IN., IS 2 BTU/(hr-ft^2-°F). $\kappa = 0.0024$ ft^2/hr. $\lambda = 0.087$ BTU/(hr-ft-°F).

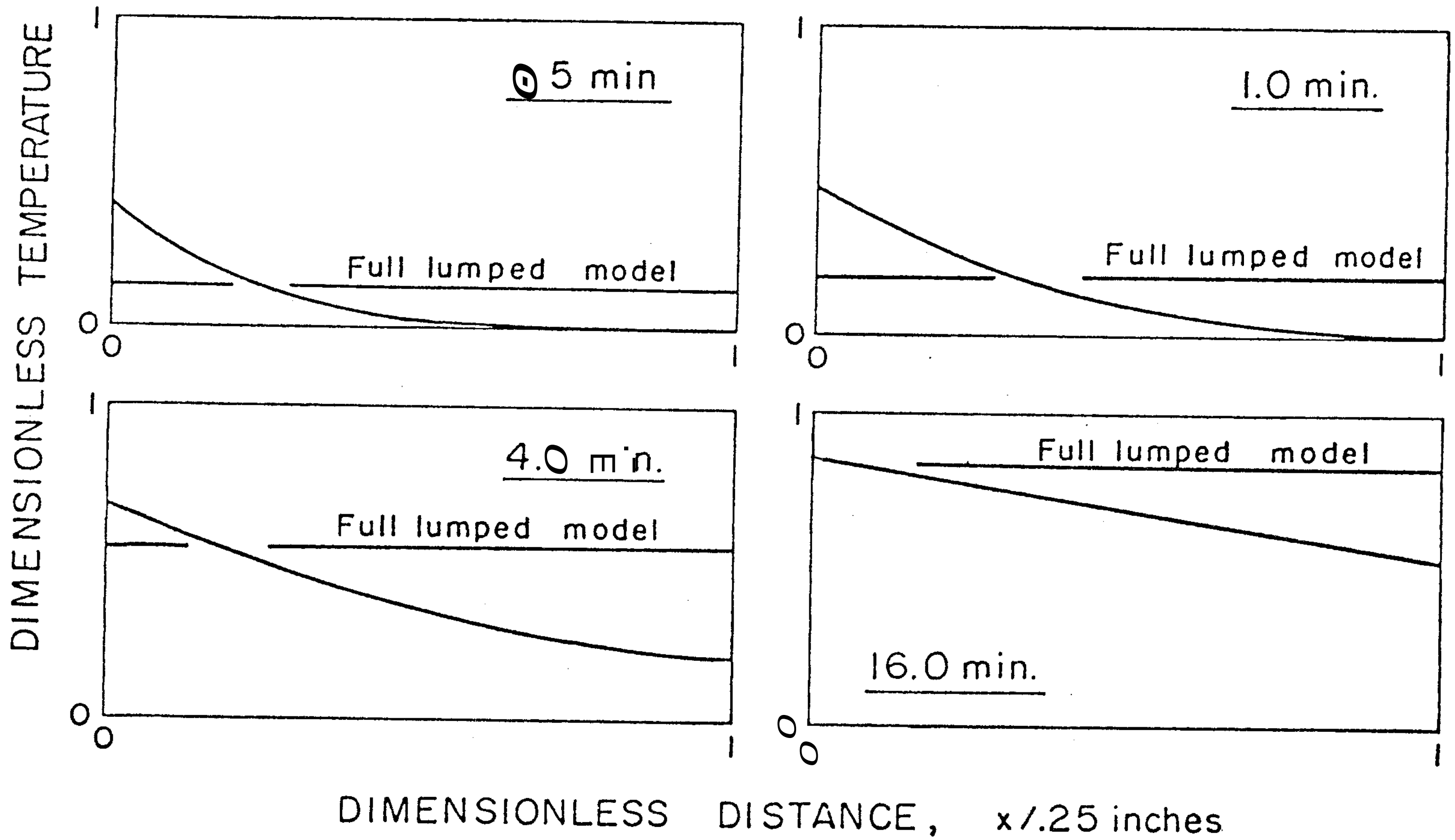

FIGURE 2 CALCULATED TEMPERATURES AT VARIOUS TIMES ACROSS A SLAB IN RESPONSE TO A UNIT STEP FUNCTION INCREASE IN TEMPERATURE AT $x = 0$ (FILM COEFFICIENT, h_f, AT $x = 0$ IS 10 BTU/(hr-ft^2-°F). FILM COEFFICIENT h_e, AT $x = 0.25$ IN. IS 2 BTU/(hr-ft^2-°F). $\kappa = 0.0024$ ft^2/hr. $\lambda = 0.087$ BTU/(hr-ft-°F)).

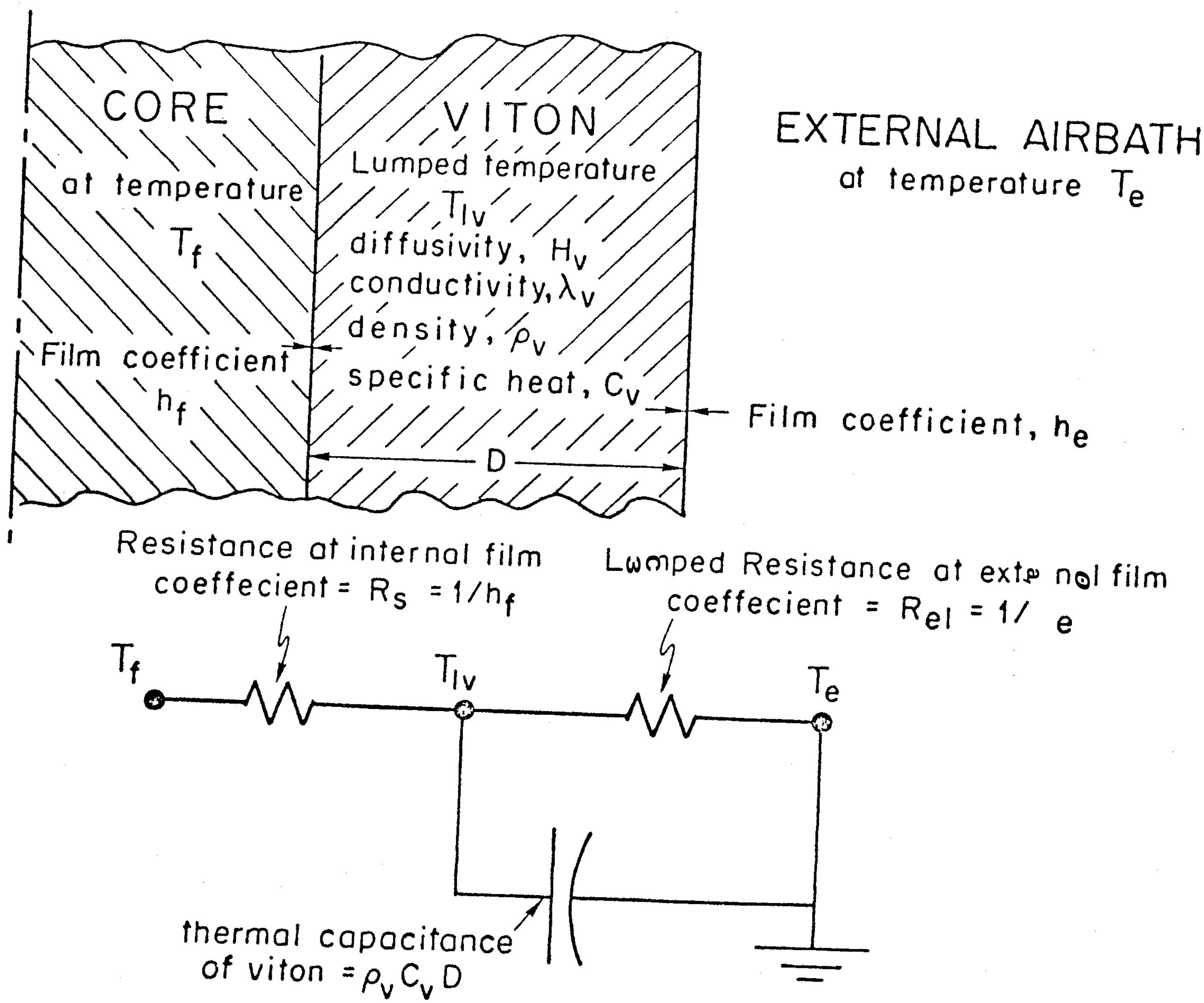

FIGURE D.3 SCHEMATIC OF THE SIMPLIFIED LINEAR MODEL OF HEAT LOSSES THROUGH THE COREHOLDER, AND ITS THERMAL CIRCUIT REPRESENTATION where $$\eta \triangleq \frac{\rho_v C_v D}{h_f+h_e}$$ (D.12)

$$\beta \triangleq \frac{h_f T_f + h_e T_e}{\quad}$$

For nondimensional lumped temperature and time:

$$v_\ell \triangleq \frac{T_{\ell v}-T_e}{T_f-T}$$ (D.13)

$$t_{DT} \triangleq t,$$

the problem becomes

$$\frac{dv_\ell}{\quad} + v = \zeta \quad t \geq 0$$

$$v\ (t_{DT}=0) = 1$$

where $$\zeta \triangleq \frac{h_f}{h_f+h_e}$$ (D.14)

This has the solution

$$\quad = \zeta\ (1 - e^{-t_{DT}})$$ (D.12)

A Comparison of the Lumped-Parameter Solution to the Fully-Analytic Solution at $X = 0$

Assuming that there is a film coefficient, h_f, between core and coreholder, heat losses from the core to the coreholder will be directly proportional to the temperature difference across this contact. We are interested in the behavior of the core temperature, which is partly controlled by heat losses at the core-coreholder boundary. Thus, in order to compare heat losses computed from the lumped-parameter model with those computed from the continuum model, it is necessary to compare the lumped' temperature response with the temperature response of the continuum at $X = 0$.

Figs, D.1 and D.2 also show calculated temperatures for the lumped model (Eq. D.12) for the same physical parameters used with the fully analytic calculations. It is apparent from these figures that the comparison of results from the two models is not good. Although both models begin with the same initial normalized temperature of zero, they do not approach the same steady-state value. This is a serious difference, because it means that a more complex model which incorporates this lumped model of transients through the coreholder will not give correct steady-state heat losses if true physical parameters are used. This discrepancy can be eliminated by forcing the lumped parameter solution (Eq. D.12) to have the correct asymptotic behavior. Thus, the condition of equivalent steady-state heat losses for the full analytic and forced lumped models is:

$$\left[1 - v(0,\infty)\right] \cdot h_f = \left[1 - v_\ell(\infty)\right] \cdot h_{f\ell} \qquad \text{(D.13)}$$

where $h_{f\ell}$ is the film coefficient at $X = 0$ in the lumped model. This leads to the following condition of equivalent steady-state temperatures, $v(0, t_{DT} \to \infty) = v_\ell(t_{DT} \to \infty)$. First, specify the constraints:

$$h_{f\ell} = h_f$$

$$\frac{h_{f\ell}}{h_{f\ell} + h_{e\ell}} = v(0, t_{DT} \to \infty) = \frac{1}{\left\{\frac{\lambda_v h_e}{h_f(\lambda_v + Dh_e)} + 1\right\}} \triangleq \gamma \qquad \text{(D.14)}$$

where: $h_{f\ell}$ and $h_{e\ell}$ are the modified parameters used in the forced lumped model. Solving for $h_{e\ell}$ gives

$$h_{e\ell} = \frac{\lambda_v h_e}{\lambda_v + Dh_e} \qquad \text{(D.15)}$$

Thus a forced lumped solution using correct values of h_f and $(\rho_v C_v D)$, and an effective modified value for the external film coefficient of $h_{e\ell} = \lambda_v h_e/(\lambda_v + Dh_e)$ to force the steady state match will be described by:

$$v_\ell = \gamma \cdot \left[1 - \exp\left(- \frac{t\, h_f}{(\rho_v C_v D)\gamma}\right)\right] \qquad \text{(D.16)}$$

This behavior is shown as the FAC=1.0 curve in Figs. D.4 to D.7, which present transient temperature responses for various models, and corresponding to conditions of the CWI-S experiments of Arihara. Although the precise shape of the curve of lumped temperature vs. time on semi-logarithmic graph paper is fixed by the exponential function, it can be translated to the left or right by modifying the thermal capacitance

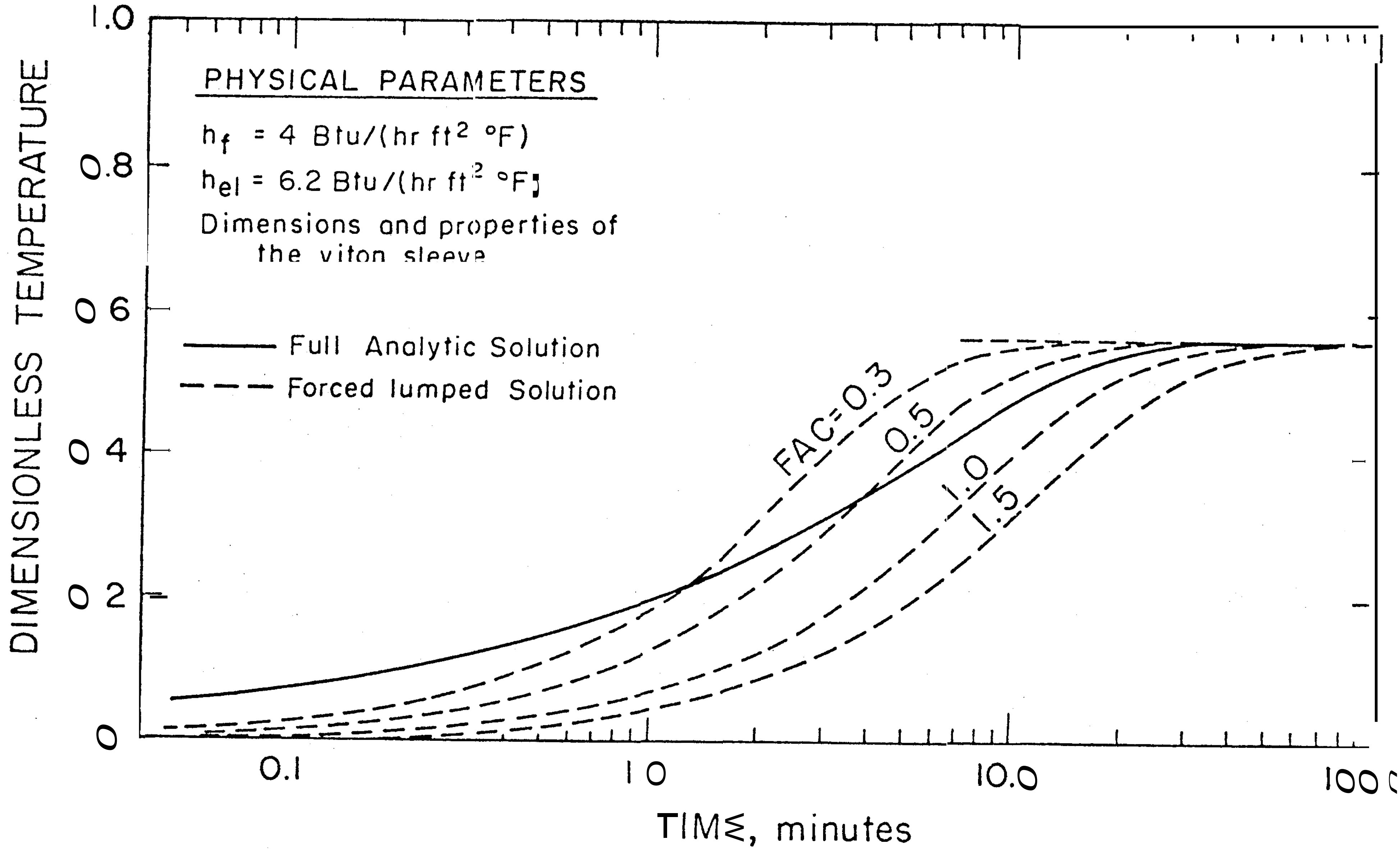

FIGURE D.4. TEMPERATURE RESPONSE OF THE LUMPED PARAMETER MODEL WITH A FORCED LONG TIME FIT, AND OF THE FULL ANALYTIC MODEL FOR CONDITIONS OF EXPERIMENT CWI-S-1 O ARIHARA

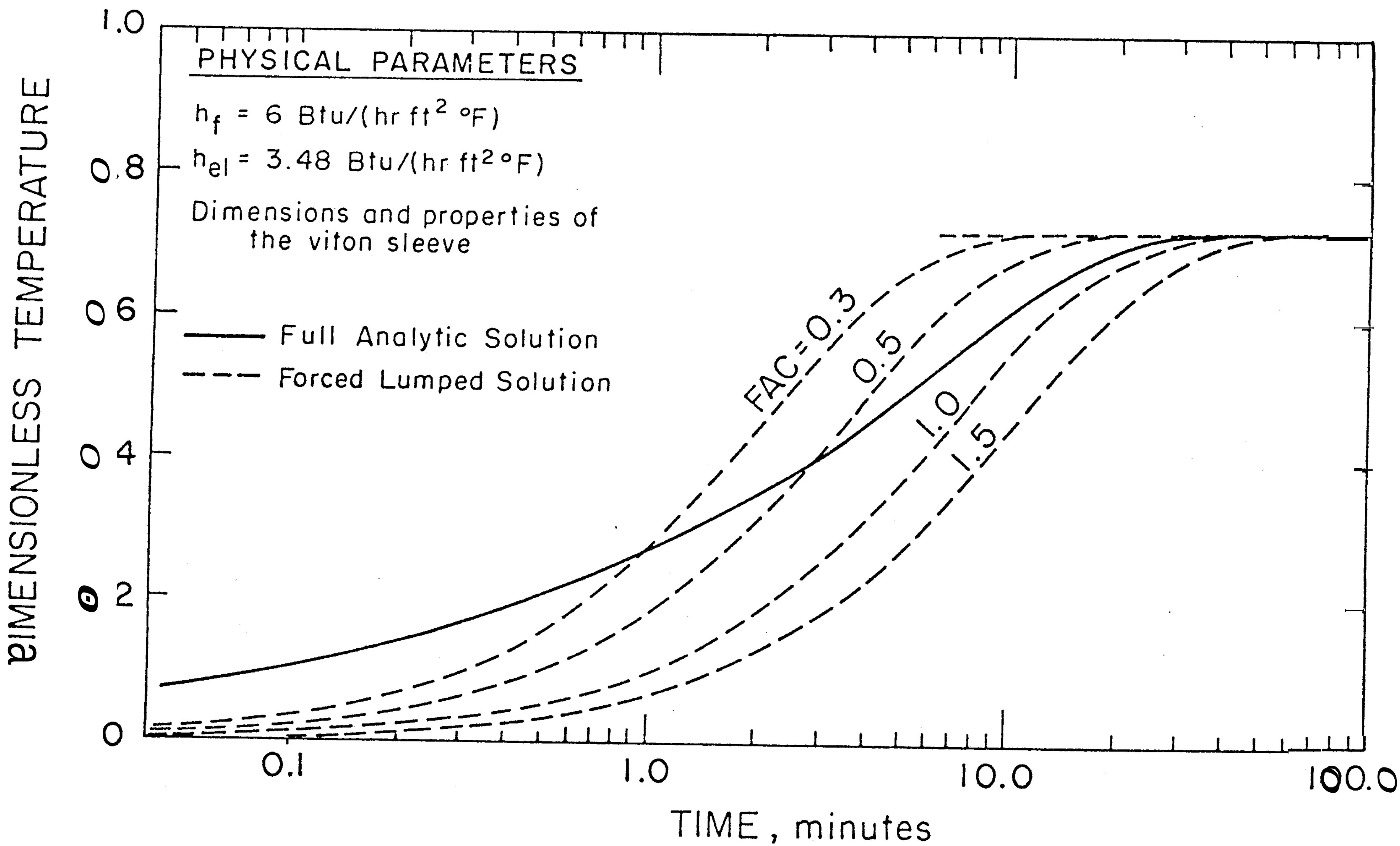

FIGURE D.5. TEMPERATURE RESPONSE OF THE LUMPED PARAMETER MODEL WITH A FORCED LONG TIME FIT, AND OF THE FULL ANALYTIC MODEL FOR CONDITIONS OF EXPERIMENT CWI-S-2 OF ARIHARA

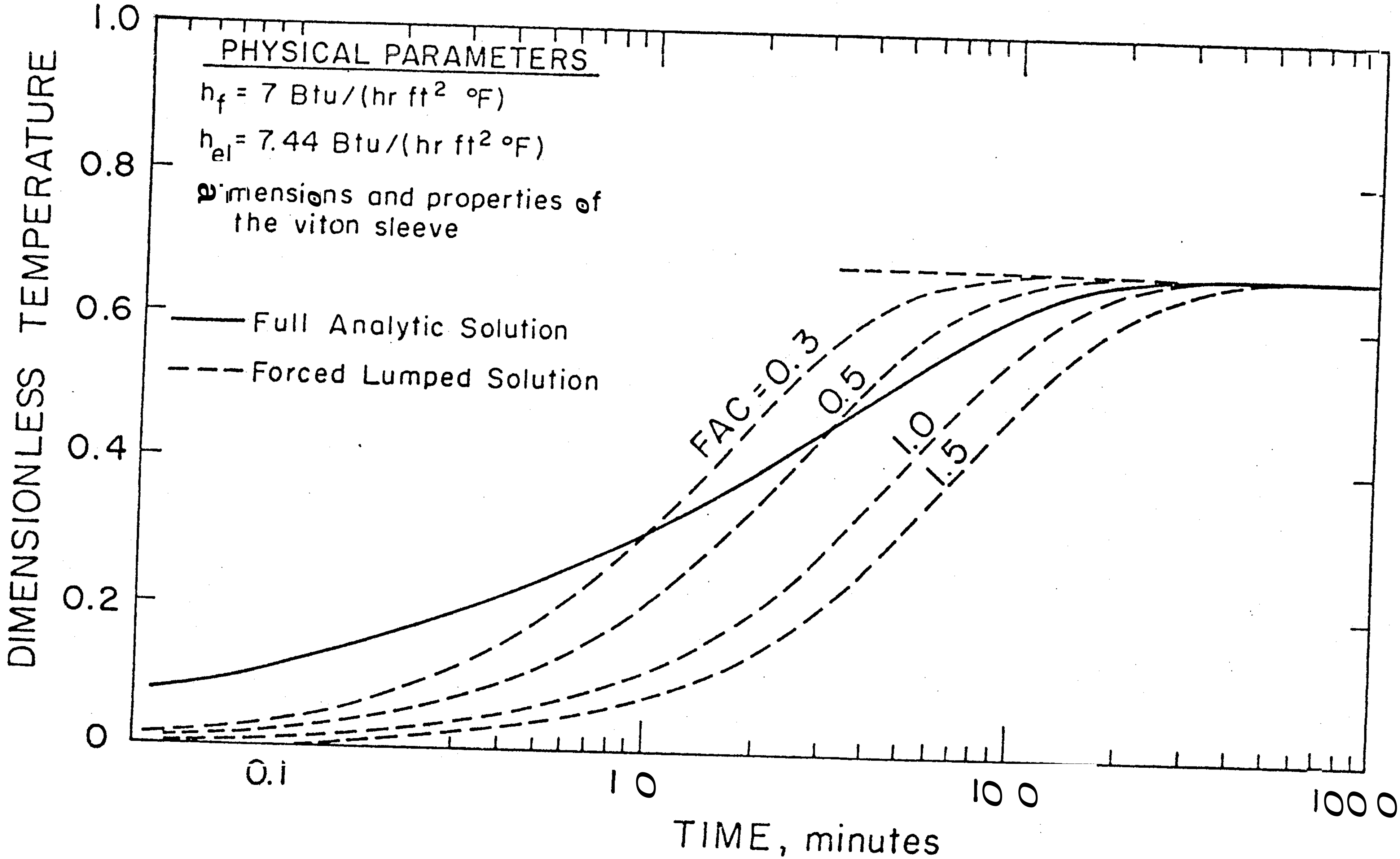

FIGURE D.6. TEMPERATURE RESPONSE OF THE LUMPED PARAMETER MODEL WITH A FORCED LONG TIME FIT, AND OF THE FULL ANALYTIC MODEL FOR CONDITIONS OF EXPERIMENT CWI-S-3 OF ARIHARA

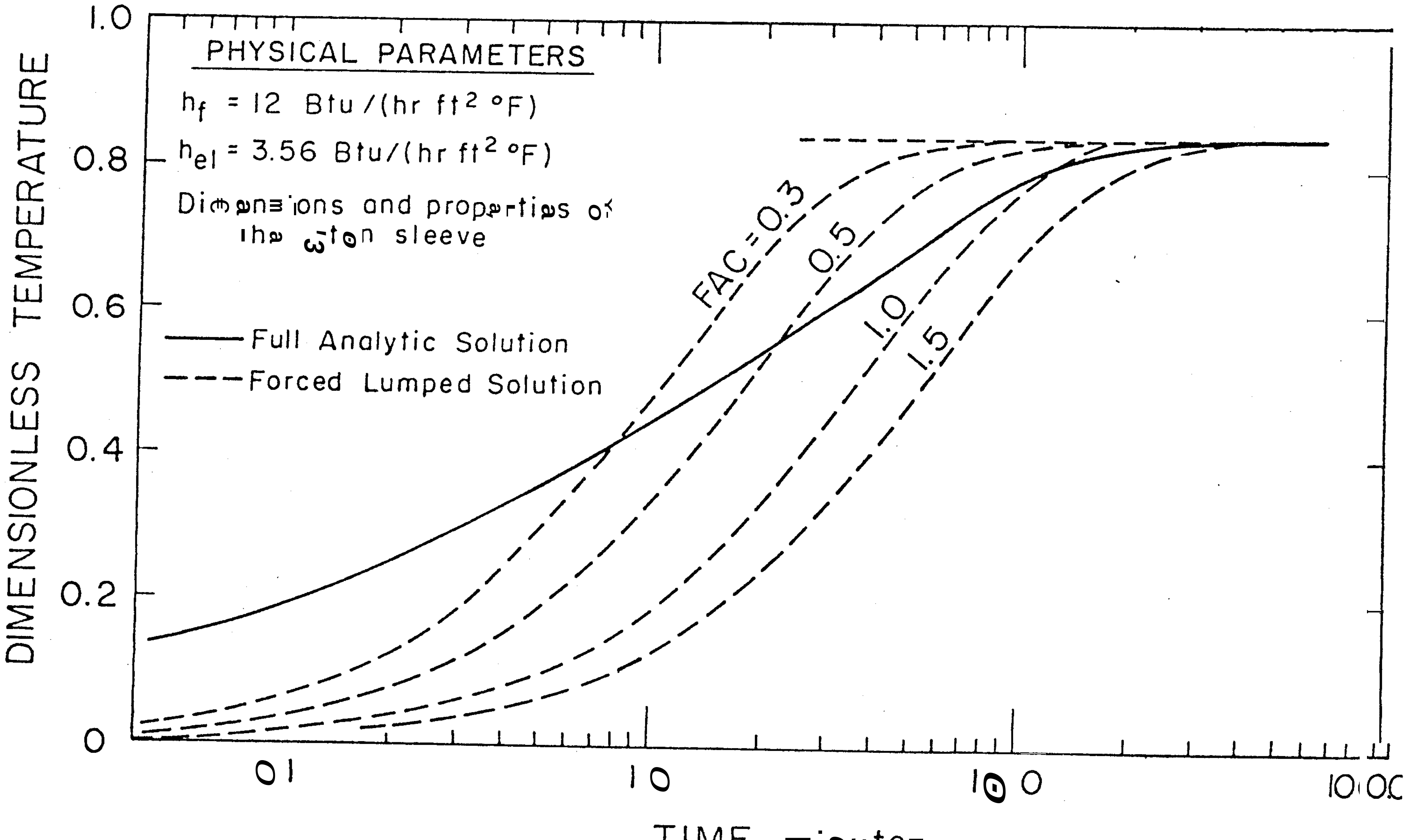

FIGURE D.7. TEMPERATURE RESPONSE OF THE LUMPED PARAMETER MODEL WITH A FORCED LONG TIME FIT, AND OF THE FULL ANALYTIC MODEL FOR CONDITIONS OF EXPERIMENT CWI-S-4 OF ARIHARA

term, $(\rho_v C_v D)$, by a factor FAC. This has the effect of causing behavior corresponding to a greater or lesser thermal capacitance, and will slow down or speed up the lumped temperature response.

Thus, using: (1) a correct value of $h_{f\ell} = h_f$; (2) a value of $h_{e\ell} = h_e\ (1/\gamma - 1)$; and (3) a modified thermal capacitance, $(FAC)\cdot(\rho_v C_v D)$; the lumped model will have the behavior:

$$v_\ell = \gamma \cdot \left[1 - \exp\left(- \frac{t\ h_f}{FAC(\rho_v C_v D)\cdot\gamma} \right) \right] \qquad (D.17)$$

The lumped parameter response for various values of the modifying factor, FAC, is compared to the fully-analytic response for various combinations of h_f and h_e in Figs. D.4 to D.7.

APPENDIX E

ANALYTIC SOLUTION TO THE PSEUDO TWO-DIMENSIONAL MATHEMATICAL MODEL USING THE LAPLACE TRANSFORM METHOD

The mathematical problem in non-dimensional form is (*see* Eqs. 4.11 through 4.15):

$$\frac{\partial v}{\partial t_D} + v = \zeta u, \quad x_D>0, \quad t_D>0 \tag{E.1}$$

$$\frac{\partial u}{\partial t_D} \quad \frac{\partial u}{\partial x_D} + \omega (u-v) = 0, \quad x_D>0, \quad t_D>0 \tag{E.2}$$

$$u\,(0,t_D) = 1, \quad t_D>0 \tag{E.3}$$

$$\frac{\partial u}{\partial x_D}(\infty,t_D) = \frac{\partial v}{\partial x_D}(\infty,t_D) = 0, \quad t_D>0 \tag{E.4}$$

$$u\,(x_D,0) = v\,(x_D,0) = 0; \quad x_D>0 \tag{E.5}$$

Applying the Laplace transformation to Eqs. E.1 to E.5, with the definitions:

$$L\,\{u\,(x_D,t_D)\} \triangleq \bar{u}\,(x_D,s)$$

$$L\,\{v\,(x_D,t_D)\} = \bar{v}\,(x_D,s)$$

we obtain:

$$s \bar{v} + \bar{v} = \zeta \bar{u} \tag{E.6}$$

$$s \bar{u} + \frac{\partial \bar{u}}{\partial x_D} + \omega (\bar{u} - \bar{v}) = 0 \tag{E.7}$$

$$u (0,s) = \frac{1}{s} \tag{E.8}$$

$$\frac{\partial \bar{u}}{\partial x_D} (\infty, s) = \frac{\partial \bar{v}}{\partial x_D} (\infty, s) = 0 \tag{E.9}$$

The solution for $\bar{u} (x_D, s)$ can be obtained from Eqs. E.6 to E.8.

$$\bar{u} (x_D, s) = e^{-\omega x} \cdot \frac{1}{s} \cdot e^{-s x_D} \cdot \exp \left\{ \frac{\omega \zeta x_D}{s+1} \right\} \tag{E. 10}$$

Although Eq. E.9 is not needed to obtain the solution E.10, this solution does satisfy the condition E.9. Eq. E.10 can be inverted as follows:

$$L^{-1} \{\bar{u} (x_D, s)\} = e^{-\omega x} \cdot L^{-1} \{\frac{1}{s} \cdot e^{-sx} \cdot e^{\omega \zeta x / s+1}\}$$

$$= e^{-\omega x_D} \cdot e^{-t_D} \cdot L^{-1} \{\frac{1}{s-1} \cdot e^{-(s-1) x_D} \cdot e^{\omega \zeta x_D / s}\}$$

$$= e^{-\omega x_D} \cdot e^{-(t_D - x_D)} \cdot H (t_D - x_D) \cdot F (t_D - x_D) \tag{E.11}$$

where $F (t_D) = L^{-1} \{\frac{\sqrt{s}}{s-1} \cdot \frac{e^{\omega \zeta x_D / s}}{\sqrt{s}}\}$

$$= L^{-1} \{f_1(s) \cdot f_2 (s)\}$$

$$= \int_0^{t_D} F_1(\lambda) \cdot F_2(t_D - \lambda)\, d\lambda \qquad \text{(E.12)}$$

$$= \int_0^{T_D} F_1(t_D - \lambda) \cdot F_2(\lambda)\, d\lambda \qquad \text{(E.13)}$$

$F_1(t_D)$ is given in Churchill (1958, Appendix 3) as No. 38:

$$L^{-1}\left\{\frac{\sqrt{s}}{s-1}\right\} = \frac{1}{\sqrt{\pi t_D}} + e^{t_D} \cdot \text{erf}\,(\sqrt{t}) \qquad \text{(E.14)}$$

and $F_2(t_D)$ is given as No. 77:

$$L^{-1}\left\{\frac{\exp(\omega\zeta x_D/s)}{\sqrt{s}}\right\} = \frac{1}{\sqrt{\pi t}} \cdot \cosh\,\{2\sqrt{\omega\zeta x_D}\} \qquad \text{(E.15)}$$

The solution for $\bar{v}(x_D, s)$, and hence $v(x_D, t_D)$ could be obtained in a similar fashion using Eqs. E-6, E-9, and E-10.